(Radiation Laboratory Report No. 010748-2-T)

April 1972

NUMERICAL INVESTIGATION OF WAVEFORMS RADIATED BY A PULSE EXCITED RESISTIVELY LOADED LINEAR ANTENNA

Yu-Ping Liu, Dipak L. Sengupta and Chen-To Tai

The University of Michigan Radiation Laboratory
Department of Electrical Engineering
Ann Arbor, Michigan 48105

ABSTRACT

The waveforms of the radiation field produced by non-uniformly resistance-loaded finite linear antenna excited by pulse signals are investigated by numerical means. The antenna model considered is a thin cylinder loaded symmetrically and continuously with resistance and is assumed to be excited symmetrically by a slice generator supplying a time dependent signal of arbitrary shape.

Current distributions and the transfer functions of the antenna are obtained as functions of frequency for different values of the loading. Spectral density of the radiated waveform produced by the antenna is obtained as a function of frequency for two different types of input pulse and for different values of loading and widths of input pulse. Finally the radiated waveforms produced by the antenna for the particular input pulse are obtained by using Fast Fourier inversion technique. Far field waveforms are obtained in $\theta = \pi/2$, $\pi/3$, $\pi/4$, $\pi/6$ directions and for different values of the loading. Three selected values of the ratio of the input pulse width to the transit time on the antenna have been used for a Gaussian pulse, while one specific ratio value has been used for a Gamma pulse. pulse.

1. INTRODUCTION

The waveforms of the radiation field produced by non-uniformly resistance-loaded finite linear antennas excited by pulse signals are investigated in the present technical note. The antenna model considered is a thin cylinder loaded symmetrically and continuously with resistance. Emphasis is given to a specific type of loading in which the amount of loading increases continuously towards the antenna end-points. The antenna is excited symmetrically by a slice generator supplying short pulse type time dependent signals.

Analytical solution of such a boundary value problem is extremely difficult. A similar problem with step input excitation has been analyzed by Baum[1] from the transmission line point of view. Analytic results for both unloaded and uniform resistively loaded antennas with step excitations are given by Latham and Lee[2, 3] only for cases when the antenna lengths are infinite. Bennett and Auckenthaler[4] reported some results for uniformly loaded finite linear antennas obtained by applying numerical technique directly in the time domain. By applying the moment methods in the time domain Sayre[5] obtained results for unloaded and uniformly loaded linear antennas of finite length. Taylor and his group[6, 7] obtained some results of limited application by numerical means for the case of discretely loaded linear antennas.

Analytic solution of the Gaussian pulse excited non-uniformly loaded linear antenna of special kind will be discussed in a separate note[8]. In the present technical note our approach to the problem has been numerical. At first the radiation field produced by the antenna excited by harmonically time dependent slice generators are obtained numerically as a function of frequency. The far field waveforms produced by the pulse excited antenna are then obtained numerically with the help of Fast Fourier Inversion technique.

2. METHODS OF ANALYSIS

In this section we give a brief discussion of the method of analysis and also define a few terms that will be used throughout. Let us assume that the linear antenna of length 2L be aligned along the z-axis of a rectangular coordinate system with origin located at the center of the antenna and that it is excited by a slice generator located at the origin. In the harmonically time dependent case the voltage signal supplied to the antenna by the unit strength slice generator may be represented by $e^{j\omega t}$ volts, where ω is the radian frequency. Let the current distribution on the antenna due to this source be $I(z, \omega)e^{j\omega t}$. The far electric field produced by the antenna under such conditions, will have only a θ-component and may be written formally as follows:

$$F = \tilde{F}_{\theta}(r, \omega)\, e^{j\omega t} \quad , \tag{1}$$

where,

$$\tilde{F}_{\theta}(r, \omega) = \frac{j\eta_o \omega \sin\theta}{c\, 4\pi} \frac{e^{-jkr}}{r} \int_{-L}^{L} I(z', \omega)\, e^{jkz' \cos\theta}\, dz' \quad . \tag{2}$$

where,

$\eta_o = \sqrt{\dfrac{\mu_o}{\epsilon_o}}$ = intrinsic impedance of free space,

$c = \dfrac{1}{\sqrt{\mu_o \epsilon_o}}$ = velocity of light in free space,

$k = \dfrac{\omega}{c}$ = propagation constant in free space,

(r, θ, ϕ) = the spherical coordinates.

Let the slice generators have arbitrary time dependence such that the input signal voltage envelope in time is represented by $V(t)$. It is now assumed that $V(t)$ is Fourier transformable i.e.

$$V(t) \longleftrightarrow \tilde{V}(\omega) \tag{3}$$

which means that the following relations are true,

$$\tilde{V}(\omega) = \int_{-\infty}^{\infty} V(t)\, e^{-j\omega t}\, dt \quad , \tag{4}$$

$$V(t) = \frac{1}{2\pi} \int_{-\infty}^{\infty} \tilde{V}(\omega)\, e^{j\omega t}\, d\omega \quad . \tag{5}$$

Assuming the linearity of the entire system and using the superposition theorem, it can be shown that the far field produced by the antenna when excited by a slice generator having arbitrary time dependence is given by the following expression:

$$E_\theta\left(r,\ t - \frac{r}{c}\right) = \frac{1}{2\pi} \int_{-\infty}^{\infty} \tilde{F}_\theta(r, \omega)\, \tilde{V}(\omega)\, e^{j\omega t}\, d\omega \quad . \tag{6}$$

Notice that E_θ, as given by Eq. (6) is dependent on the parameter r, and also that it is delayed in time with respect to the input by $\frac{r}{c}$ which is the retarded time taken by the signal to reach the far field point from the antenna. It is found convenient sometimes to remove both of these effects from the final result. This can be done as follows.

Let us define a quantity $\tilde{f}_\theta$ which is related to $\tilde{F}_\theta$ in the following manner:

$$\tilde{f}_\theta(\theta, \omega) = r\, \tilde{F}_\theta(r, \omega)\, e^{+j\frac{\omega}{c}r}$$

$$= \frac{j\eta_o \omega \sin\theta}{c\ 4\pi} \int_{-L}^{L} I(z', \omega)\, e^{jkz'\cos\theta}\, dz' \,. \tag{7}$$

Similarly we can remove the dependence of r and $\frac{r}{c}$ from Eq. (6) and define the following modified field quantity produced by the antenna excited by arbitrary

time dependent input signals:

$$e_\theta(\theta, t) = \frac{1}{2\pi} \int_{-\infty}^{\infty} r \tilde{F}_\theta(r, \omega)\, e^{j\frac{\omega}{c} r}\, \tilde{V}(\omega)\, e^{j\omega t}\, d\omega$$

$$= \frac{1}{2\pi} \int_{-\infty}^{\infty} \tilde{f}_\theta(\theta, \omega) \tilde{V}(\omega)\, e^{j\omega t}\, d\omega \quad . \tag{8}$$

Thus, formally if the field $\tilde{f}_\theta(\theta, \omega)$ produced by harmonically time dependent excitation of unit strength is known, then the field produced by any other time dependent signal can be obtained with the help of Eq. (8). Of course, it is assumed that the time dependent signal must have a Fourier transform.

From the analogy with signal transmission through linear system, we shall call $\tilde{f}_\theta(\theta, \omega)$ given by Eq. (7) as the frequency response or the transfer function of the antenna and $\tilde{e}_\theta(\theta, \omega) = \tilde{f}_\theta(\theta, \omega) \tilde{V}(\omega)$ as the spectral density function of the radiated signal for arbitrary time dependent input signal. Note that according to this definition $e_\theta(\theta, t)$ and $\tilde{e}_\theta(\theta, \omega)$ constitute a Fourier transform pair, i.e.

$$e_\theta(\theta, t) \leftrightarrow \tilde{e}_\theta(\theta, \omega) \tag{9}$$

3. BRIEF OUTLINE OF THE REPORT

It can be seen from Eq. (8) that the knowledge of the transfer function of the antenna under consideration is necessary for obtaining the waveform radiated by the antenna for arbitrary signal input. Equation (7) indicates that the current distribution $I(z, \omega)$ on the antenna for the harmonic time dependent excitation must be known so that $\tilde{f}_\theta(\theta, \omega)$ may be evaluated. In the following sections we at first determine the current distribution $I(z, \omega)$. This is done by numerically solving a modified form of Hallen's integral equation appropriate for the antenna

under consideration. The transfer function $\tilde{f}_\theta(\theta, \omega)$ is then obtained by numerically evaluating Eq. (7). The spectral density function $\tilde{e}_\theta(\theta, \omega)$ is obtained by multiplying the transfer function by the Fourier spectrum of the input signal. Finally the waveform of the radiated signal is obtained by numerically evaluating Eq. (8) with the help of Fast Fourier Inversion technique. Two input waveforms have been assumed in this work. They are the Gaussian and gamma pulse represented by

$$V_1(t) = e^{-t^2/2\sigma^2} \tag{10 A}$$

$$V_2(t) = t\, e^{-dt} U(t) \tag{10 B}$$

where the constants parameter σ and $1/d$ are proportional to the width of the input pulse and $U(t)$ is the unit step function. The Fourier spectra corresponding to the signals given above are, respectively,

$$\tilde{V}_1(\omega) = \sqrt{2\pi}\ \sigma\, e^{-\omega^2\sigma^2/2} \tag{11 A}$$

$$\tilde{V}_2(\omega) = \frac{1}{(j\omega + d)^2} \tag{11 B}$$

4. INTEGRAL EQUATION FOR THE CURRENT DISTRIBUTION $I(z, \omega)$.

In this section we discuss briefly the integral equation for the current distributions on thin cylindrical antennas continuously loaded with resistance. As before we consider a linear antenna of length $2L$ oriented along the z-axis of the Cartesian coordinate system such that $z = 0$ is at the center of the antenna. Assuming azimuthally independent excitation, Hallen's integral equation for the current distribution on a linear antenna excited by harmonically time dependent slice generator of unit strength is given by:

$$\int_{-L}^{L} I(z', \omega)\, G(z, z')\, dz' = B \cos kz - j/\eta_o \int_0^z E_{sz}(\xi) \sin k(z-\xi)\, d\xi \tag{12}$$

where, E_{sz} is the electric field on the surface of the antenna due to the induced currents. $G(z, z')$ is the free space Green's function and B is a constant to be determined from the end condition $I(\pm L) = 0$, a is the radius of the antenna element and ϵ_o is the free space permittivity. Since the dipole is electrically thin, i.e., $\frac{a}{\lambda} < 0.01$, we can assume the current to be located at the axis of the antenna. This implies that the Green's function is approximately given by:

$$G(z, z') = \frac{e^{-jk\left[(z-z')^2 + a^2\right]^{1/2}}}{4\pi\left[(z-z')^2 + a^2\right]^{1/2}} \tag{13}$$

If the antenna is loaded with distributed resistance $R_s(z)$ ohms/meter, then the total tangential electrical field on the surface of the antenna is given by:

$$E_z(z) = I(z, \omega) R_s(z) = E_{oz}(z) + E_{sz}(z) \tag{14}$$

where $E_{oz}(z)$ is the field due to the externally impressed source. In the present case the external source is assumed to be a unit slice generator with harmonic time dependence, i.e.,

$E_{oz}(z) = \delta(z)$, where $\delta(z)$ is the Dirac delta function.

Under these conditions, the integral equation for the current distribution on a symmetrically loaded linear antenna is given by:

$$\int_{-L}^{L} I(z', \omega) \frac{e^{-jk\left[(z-z')^2 + a^2\right]^{1/2}}}{4\pi\left[(z-z')^2 + a^2\right]^{1/2}} dz'$$

$$= B \cos kz - \frac{j}{2\eta_o} \sin k|z| +$$

$$+ j\frac{1}{\eta_o}\int_0^z I(\xi,\omega)\, R_s(\xi) \sin k(z-\xi)\, d\xi \qquad (15)$$

Eq. (15) is the desired integral equation for the current distribution on the loaded antenna when excited by slice generator of unit strength having harmonic time dependence $e^{j\omega t}$.

In the next section Eq. (15) will be solved numerically for some assumed values of $R_s(z)$. The loading function of special importance to us is of the form:

$$R_s(z) = \frac{C}{L - |z|} \qquad (16)$$

For some special value of C, the above loading gives rise to a pure outward traveling wave of current at a specific frequency on the antenna as discussed by Wu and King[9]. For this reason the antenna with this special loading is sometimes referred to as the reflectionless antenna. Baum[1] arrived at the same conclusion from his transmission line model analysis of this antenna. We shall consider in detail the effects of the loading of the type given by Eq. (16) for various values of C including the value corresponding to the reflectionless case.

5. EVALUATION OF THE CURRENT DISTRIBUTION $I(z, \omega)$.

Standard numerical technique[10] is used to solve Eq. (15) for $I(z, \omega)$. For this purpose the integral equation is reduced by moments method to the following set of N simultaneous algebraic equations:

$$\sum_{n=1}^{N} \int_{\Delta z_n} I(z', \omega)\, G(z_j, z')\, dz'$$

$$= B \cos k z_j - \frac{j}{2\eta_o} \sin k|z_j|$$

$$+ j/\eta_o \sum_n{}' \int_{\Delta z_n} I(z', \omega) R_s(z') \sin k(z_j - z') dz'$$

$$j = 1, 2, \ldots, N \qquad (17)$$

where the summation on the r.h.s. of Eq. (17) is interpreted as:

$$\sum_n{}' = - \sum_{n=j}^{N/2} \quad , \quad \text{for } j \leq N/2$$

$$= \sum_{n = N/2 + 1}^{j} \quad \text{for } j > N/2 \qquad (18)$$

and it is assumed that N is an even number and $z' \in \Delta z_n$. Eq. (17) implies that the antenna of length 2L is divided into N sections, the numbering of the sections increasing from 1 to N along the antenna length from -L to L as shown in Fig. 1.

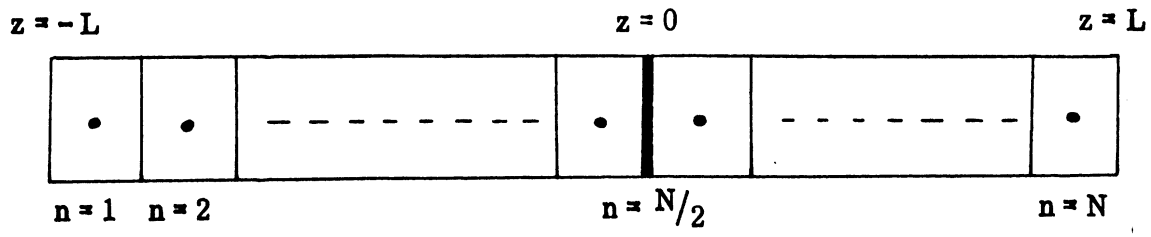

FIG. 1: Division of the antenna into N-sections.

It remains now to make an appropriate approximation to the current distribution $I(z')$ in each of the sections Δz_n. When the antenna length is small

electrically the usual pulse approximation[11] to the current in each section provides sufficient accuracy. Since our preliminary results have been obtained by this method we give here a brief discussion of the appropriate expressions used in this method.

Pulse Approximation Expressions

In this method the unknown current in each section is assumed to be a rectangular pulse, i.e.,

$$\begin{aligned} I(z') &= I_n \qquad z' \in \Delta z_n \qquad n = 1, 2, \ldots, N \\ &= 0 \qquad \text{elsewhere} \end{aligned} \tag{19}$$

Using Eq. (19) it can be shown that the general integral equation given by Eq. (15) can be transformed into the following N simultaneous equations:

$$\sum_{n=1}^{N} I_n \int_{\Delta z_n} G(z_j, z')\, dz' = B \cos k z_j - \frac{j}{2\eta_o} \sin k(z_j) + \frac{j}{\eta_o} \sum_{n}{}' I_n \int_{\Delta z_n} R_s(\xi) \sin k(z_j - \xi)\, d\xi \,, \tag{20}$$

$$j = 1, 2, \ldots, N$$

where the meaning the summation $\sum_{n}{}'$ is as explained before. In general the unknown current $I(z)$ and the unknown constant B are complex quantities. Let us assume:

$$\left.\begin{aligned} I(z) &= I_R(z) + jI_C(z) \\ B &= B_R + jB_C \end{aligned}\right\} \tag{21}$$

Separating Eq. (20) into real and imaginary parts we obtain:

$$\sum_{n=1}^{N} I_{R_n} \int_{\Delta z_n} \frac{\cos k\left[(z_j - z')^2 + a^2\right]^{1/2}}{4\pi\left[(z_j - z')^2 + a^2\right]^{1/2}} dz' - B_R \cos k z_j$$

$$\mp {}^{1}/_{\eta_o} \sum_{n} I_{C_n} \int_{\Delta z_n} R_s(\xi) \sin k(z_j - \xi)\, d\xi$$

$$+ \sum_{n=1}^{N} I_{C_n} \int_{\Delta z_n} \frac{\sin k\left[(z_j - z')^2 + a^2\right]^{1/2}}{4\pi\left[(z_j - z')^2 + a^2\right]^{1/2}} dz' = 0 \qquad (22)$$

$$\sum_{n=1}^{N} I_{C_n} \int_{\Delta z_n} \frac{\cos k\left[(z_j - z')^2 + a^2\right]^{1/2}}{4\pi\left[(z_j - z')^2 + a^2\right]^{1/2}} dz' - B_C \cos k z_j$$

$$\pm {}^{1}/_{\eta_o} \sum_{n} I_{R_n} \int_{\Delta z_n} R_s(\xi) \sin k(z_j - \xi)\, d\xi$$

$$- \sum_{n=1}^{N} I_{R_n} \int_{\Delta z_n} \frac{\sin k\left[(z_j - z')^2 + a^2\right]^{1/2}}{4\pi\left[(z_j - z')^2 + a^2\right]^{1/2}} dz'$$

$$= -\frac{1}{2\eta_o} \sin k|z_j| \quad , \qquad (23)$$

where the upper (lower) sign is used for $j \leq N/2$ $(j > N/2)$ respectively. The above sets of equations along with the end conditions have been solved numerically for the unknown currents. The results will be discussed later. Pulse approximation method provides farily accurate results for small antenna lengths. However, if the antenna length is long electrically, to obtain sufficiently accurate results, N must be chosen very large. Hence to obtain accurate results without taxing the computer capability a different type of approximation should be used. In the next section we discuss such a method.

Quadratic Approximation Expressions

As mentioned before, when the antenna length is large, the computer capability makes it inappropriate to use the pulse approximation method. For the present problem of resistively loaded linear antenna, it is known from theoretical considerations[1, 9] that the current amplitude decreases linearly towards the ends of the antenna.

For this reason, we make the following quadratic approximation to the unknown current in each section:

$$\begin{aligned} I(z') &= A_n + B_n(z'-z_n) + C_n(z'-z_n)^2 \quad , \qquad \text{for } z' \in \Delta z_n \\ &= 0 \, , \qquad\qquad\qquad \text{otherwise,} \end{aligned} \tag{24}$$

where A_n, B_n, C_n are three unknown constants. These constants are determined by requiring that the continuation of $I(z')$ expressions given by Eq. (24) into the centers of the adjacent sections give the appropriate current values there. Thus we obtain the following:

$$\left.\begin{aligned} I(z_n) &= I_n = A_n \\ I(z_{n-1}) &= I_{n-1} = A_n + B_n(z_{n-1}-z_n) + C_n(z_{n-1}-z_n)^2 \\ I(z_{n+1}) &= I_{n+1} = A_n + B_n(z_{n+1}-z_n) + C_n(z_{n+1}-z_n)^2 \end{aligned}\right\} \tag{25}$$

After eliminating A_n, B_n, C_n from Eq. (5) with the help of the relations given by Eq. (6) we obtain the following recurrence relation for the current in each section:

$$I(z') = I_{n-1} X_n(z') + I_n Y_n(z') + I_{n+1} Z_n(z') \quad , \quad \text{for } z' \epsilon \Delta z_n \tag{26}$$

where

$$X_n(z') = -\frac{z' - z_n}{2\Delta z} + \frac{(z' - z_n)^2}{2\Delta z^2} \quad , \quad z' \epsilon \Delta z_n \tag{27}$$

$$Y_n(z') = 1 - \frac{(z' - z_n)^2}{\Delta z^2} \quad , \quad z' \epsilon \Delta z_n \tag{28}$$

$$Z_n(z') = \frac{z' - z_n}{2\Delta z} + \frac{(z' - z_n)^2}{2\Delta z^2} \quad , \quad z' \epsilon \Delta z_n \quad . \tag{29}$$

where it has been assumed that each subsection is of equal length Δz. In view of the fact that in Eq. (26) the value of the current in section Δz_n is related to the currents I_{n+1}, I_{n-1} in the centers of the adjacent sections Δz_{n+1} and Δz_{n-1} respectively, the current values at the center and hence the entire two end sections Δz_1 and Δz_N should be treated separately. For this purpose we make use of the two sets of current coefficients I_{-L}, I_1, I_2 and I_{N-1}, I_N, I_L for obtaining the currents in the sections Δz_1 and Δz_N respectively. Using these two sets of current coefficients we obtain the following from Eq. (24) to determine the currents in the two end sections:

$$I(z') = I_1 Y_1'(z') + I_2 Z_1'(z') \quad , \quad \text{for } z' \epsilon \Delta z_1 \tag{30}$$

$$I(z') = I_N Y_N'(z') + I_{N-1} X_N'(z') \quad , \quad \text{for } z' \epsilon \Delta z_N \quad , \tag{31}$$

where,

$$Y_1'(z') = 1 + \frac{(z'-z_1)}{\Delta z} - 2\frac{(z'-z_1)^2}{\Delta z^2} \quad , \quad z' \epsilon \Delta z_1 \quad , \qquad (32)$$

$$Z_1'(z') = \frac{(z'-z_1)}{3\Delta z} + \frac{2(z'-z_1)^2}{3\Delta z^2} \quad , \quad z' \epsilon \Delta z_1 \quad , \qquad (33)$$

$$Y_N'(z') = 1 - \frac{z'-z_N}{\Delta z} - \frac{2(z'-z_N)^2}{\Delta z^2} \quad , \quad z' \epsilon \Delta z_N \quad , \qquad (34)$$

$$X_N'(z') = -\frac{(z'-z_N)}{3\Delta z} + \frac{2(z'-z_N)^2}{3\Delta z^2} \quad , \quad z' \epsilon \Delta z_N \quad . \qquad (35)$$

After substituting Eqs. (26) - (35) into Eq. (17) the following set of N simultaneous equations are obtained:

$$I_1\left[\int_{\Delta z_1} Y_1'(z')G(z', z_j)\,dz' + \int_{\Delta z_2} X_2(z')G(z', z_j)\,dz'\right]$$

$$+ I_2\left[\int_{\Delta z_1} Z_1'(z')G(z', z_j)\,dz' + \int_{\Delta z_2} Y_2(z')G(z', z_j)\,dz' + \int_{\Delta z_3} X_3(z')G(z', z_j)\,dz'\right]$$

$$+ \sum_{n=3}^{N-2} I_n\left[\int_{\Delta z_{n-1}} Z_{n-1}(z')G(z', z_j)dz' + \int_{\Delta z_n} Y_n(z')G(z', z_j)dz' + \int_{\Delta z_{n+1}} X_{n+1}(z')G(z', z_j)d\right.$$

$$+ I_{N-1}\left[\int_{\Delta z_{N-2}} Z_{N-2}(z')G(z', z_j)\,dz' + \int_{\Delta z_{N-1}} Y_{N-1}(z')G(z', z_j)\,dz' + \right.$$

$$\left. + \int_{\Delta z_N} X_N'(z')G(z', z_j)\,dz'\right] +$$

$$+ I_N \left[\int_{\Delta z_N} Y'_N(z')G(z', z_j)dz' + \int_{\Delta z_{N-1}} Z_{N-1}(z')G(z', z_j)\,dz' \right]$$

$$= B \cos k z_j - \frac{j V_o}{2\eta_o} \sin k|z_j| + \frac{j\omega\epsilon}{k} \left\{ H_{1,j} I_1 \left[\int_{\Delta z_1} Y'_1(z')F(z')dz' + \int_{\Delta z_2} X_2(z')F(z')dz' \right] \right.$$

$$+ H_{2j} I_2 \left[\int_{\Delta z_1} Z'_1(z')F(z')dz' + \int_{\Delta z_2} Y_2(z')F(z')dz' + \int_{\Delta z_3} X_3(z')F(z')dz' \right]$$

$$+ \sum_{n=3}^{N/2} H_{n,j} I_n \left[\int_{\Delta z_{n-1}} Z_{n-1}(z')F(z')dz' + \int_{\Delta z_n} Y_n(z')F(z')dz' \right.$$

$$\left. \left. + \int_{\Delta z_{n+1}} X_{n+1}(z')F(z')dz' \right] \right\}, \quad \text{for } j \leq N/2$$

$$+ {}^{j}/_{\eta_o} \left\{ \sum_{n=\frac{N}{2}+1}^{j} H_{n,j} I_n \left[\int_{\Delta z_{n-1}} Z_{n-1}(z')F(z')dz' + \int_{\Delta z_n} Y_{n+1}(z')F(z')dz' + \int_{\Delta z_{n+1}} X_{n+1}(z')F(z')dz' \right] \right.$$

$$+ H_{N-1,j} I_{N-1} \left[\int_{\Delta z_{N-2}} Z_{N-2}(z')F(z')dz' + \int_{\Delta z_{N-1}} Y_{N-1}(z')F(z')dz' \right.$$

$$\left. + \int_{\Delta z_N} X'_N(z')F(z')dz' \right]$$

$$\left. + H_{N,j} I_N \left[\int_{\Delta z_{N-1}} Z_{N-1}(z')F(z')dz' + \int_{\Delta z_N} Y'_N(z')F(z')dz' \right] \right\}, \quad (36)$$

for $j > N/2$,

j (as the subscript) = $1, 2, 3, \ldots, N$

where

$$H_{m,j} \begin{cases} 1, & \text{for } j \geq m \\ 0, & \text{for } j < m \end{cases}$$

$$F(z') = \frac{C}{L-|z'|} \sin k(z_j - z') \quad . \tag{37}$$

The above is a set of N algebraic equations involving the N unknown current coefficients $I_1, I_2, \ldots, I_N$ and the extra unknown constant B which is to be determined by applying the end condition $I(-L) = 0$. By using Taylor's expansion for the currents at the centers of the first three sections we obtain the following:

$$I(z_1) = I_1 = (z_1+L)I'(-L) + \frac{(z_1+L)^2}{2} I''(-L) \quad , \tag{38}$$

$$I(z_2) = I_2 = (z_2+L)I'(-L) + \frac{(z_2+L)^2}{2} I''(-L) \quad , \tag{39}$$

$$I(z_3) = I_3 = (z_3+L)I'(-L) + \frac{(z_3+L)^2}{2} I''(-L) \quad , \tag{40}$$

where we have already used the fact $I(-L) = 0$. The derivative terms in (38), (39), (40) can be eliminated and we obtain the following extra equation:

$$3I_3 - 10I_2 + 15I_1 = 0 \quad . \tag{41}$$

Thus Eqs. (36) and (41) constitute a set of N+1 equations for the N+1 unknowns (i.e., $I_1, I_2, \ldots, I_N$, B). The system can now be solved by standard means.

If the end condition is applied at the other end of the antenna, i.e. $I(+L) = 0$, then the following equations should be used instead of Eq. (41):

$$15I_N - 10I_{N-1} + 3I_{N-2} = 0 \quad . \tag{42}$$

Eqs. (41) or (42) will be referred to as the 3-point end condition formula. In order to estimate the accuracy of the results, computation has also been done by using 4-point and 2-point end condition expressions. These have been obtained by applying the end condition $I(+L) = 0$ and retaining 4 and 2 terms in the Taylor's expansion respectively. The relevant expressions for these two cases are:

$$-5I_{N-3} + 21I_{N-2} - 35I_{N-1} + 35I_N = 0 \quad , \tag{43}$$

$$3I_N - I_{N-1} = 0 \quad . \tag{44}$$

The above completes the theoretical discussion on the numerical procedure to be followed in the determination of the current distribution for the loaded linear antenna.

6. EVALUATION OF THE TRANSFER FUNCTION $\tilde{f}_\theta(\theta, \omega)$

In the previous section we discussed the numerical method of obtaining the current distribution $I(z, \omega)$ on the antenna for the harmonic time dependence case. After introducing the sampled values of $I(z, \omega)$ in Eq. (7), $f_\theta(\theta, \omega)$ is obtained numerically with the help of the following equation:

$$\tilde{f}_\theta(\theta, \omega) = j\frac{\omega\eta_o}{c}\frac{\sin\theta}{4\pi}\sum_n I_n e^{j\frac{\omega}{c}z_n\cos\theta}\Delta z_n \quad , \tag{45}$$

where we have used the notation $I(z_n) = I_n$ and $z' = z_n$ is the coordinate at the center of the section Δz_n. The pulse approximation is good for transfer function calculation because the current distribution is linear as mentioned before.

7. PRELIMINARY NUMERICAL RESULTS

In this section we discuss briefly some preliminary numerical results

obtained for a few simple cases. The motivation behind this section has been mainly to ascertain the correctness and accuracy of the numerical technique used for later investigation.

7.1 Uniformly Loaded Antenna $L = \lambda/2$.

For the case of uniformly loaded dipole of total length $2L = \lambda$, there is no variation of loading along the antenna, i.e., $R_s(z) = r^i$ ohms/meter. Fig. 2 shows the real and imaginary parts of the current distribution on a uniformly loaded dipole for two values of r^i. These results have been obtained by using Eqs. (21)-(23) with $N = 30$. In Fig. 2 we have used the notation $\phi_i = 2\lambda r^i/\eta_o$ where λ is the wavelength and η_o is the intrinsic impedance of free space. The results shown here compare very well with those of King, et. al.[12]. Thus it proves the correctness of the computation followed here.

7.2 Non-Reflecting Loaded Case $L = \lambda$.

Here consider a one wavelength long linear antenna non-uniformly loaded according to Eq. (16). The radius a of the antenna element is chosen such that $\Omega = 2\ell n\frac{2L}{a} = 11.5$. This value of Ω is chosen so that our results may be compared with some available published results. Wu and King[9] predicted from theoretical considerations that a purely outgoing traveling wave of current is sustained on the antenna loaded according to Eq. (16) provided the constant C is chosen to be equal to $60\,\psi\alpha$ with $\psi\alpha = 5.3$. In other words the antenna considered in this section is loaded as follows:

$$R_s(z) = \frac{60\,\psi\alpha}{L-|z|} \quad , \tag{46}$$

with $\psi\alpha = 5.3$. The $\psi\alpha$ notation is used here to correspond to that used in Wu and King[9]. Fig. 3 gives the amplitude of the current distribution on the antenna as obtained by numerical computation using pulse approximation with $N = 30$. The current distributions obtained for the same antenna by Taylor[13] and Shen[14] are also shown in Fig. 3 for comparison. The results of Shen have been

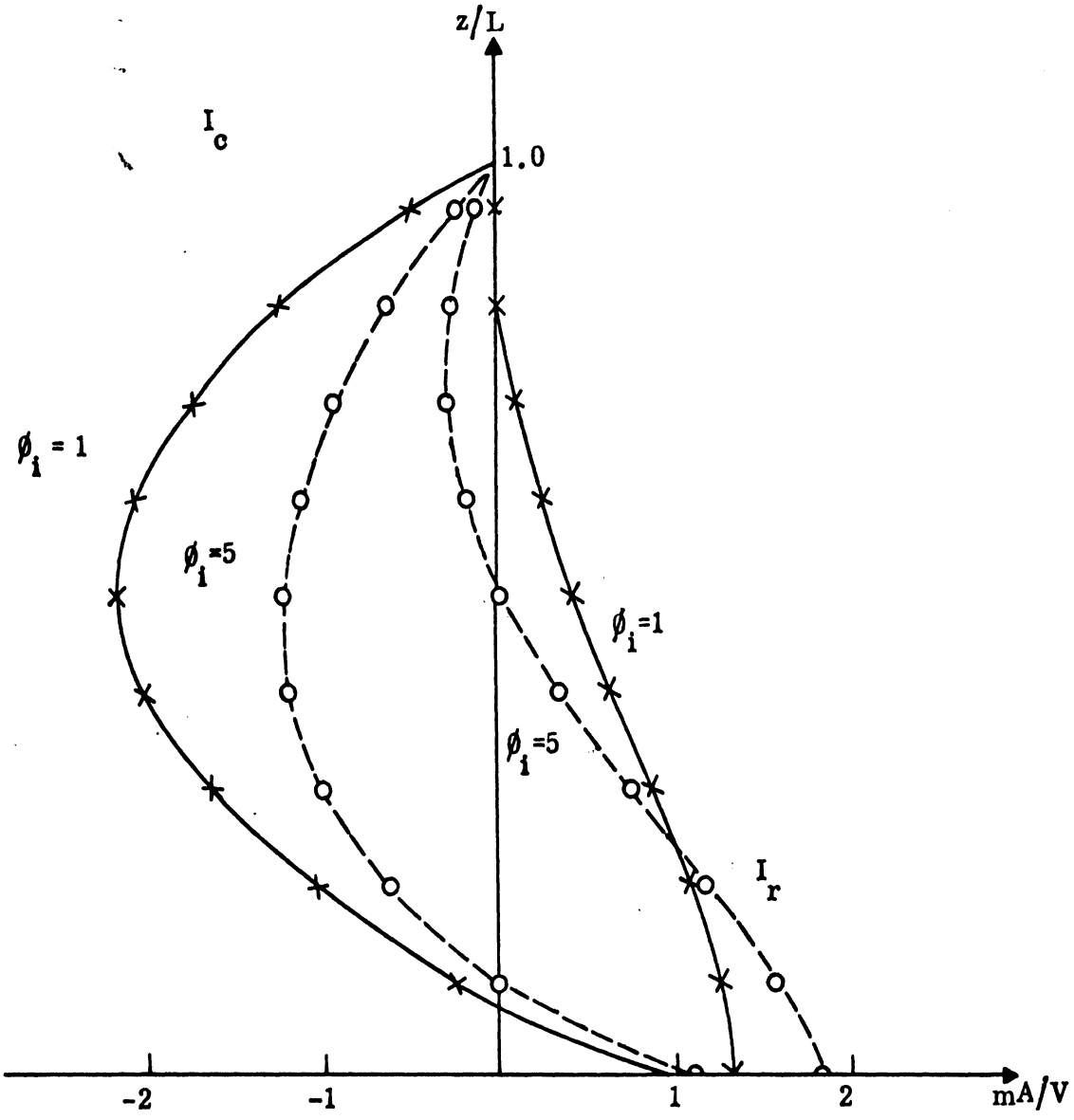

FIG. 2: Real (I_r) and imaginary (I_c) parts of the current distribution on uniformly loaded dipole. $L=\pi/2$, $\Omega=9.92$, $\phi_i = 2\lambda r^i/\eta_0$.

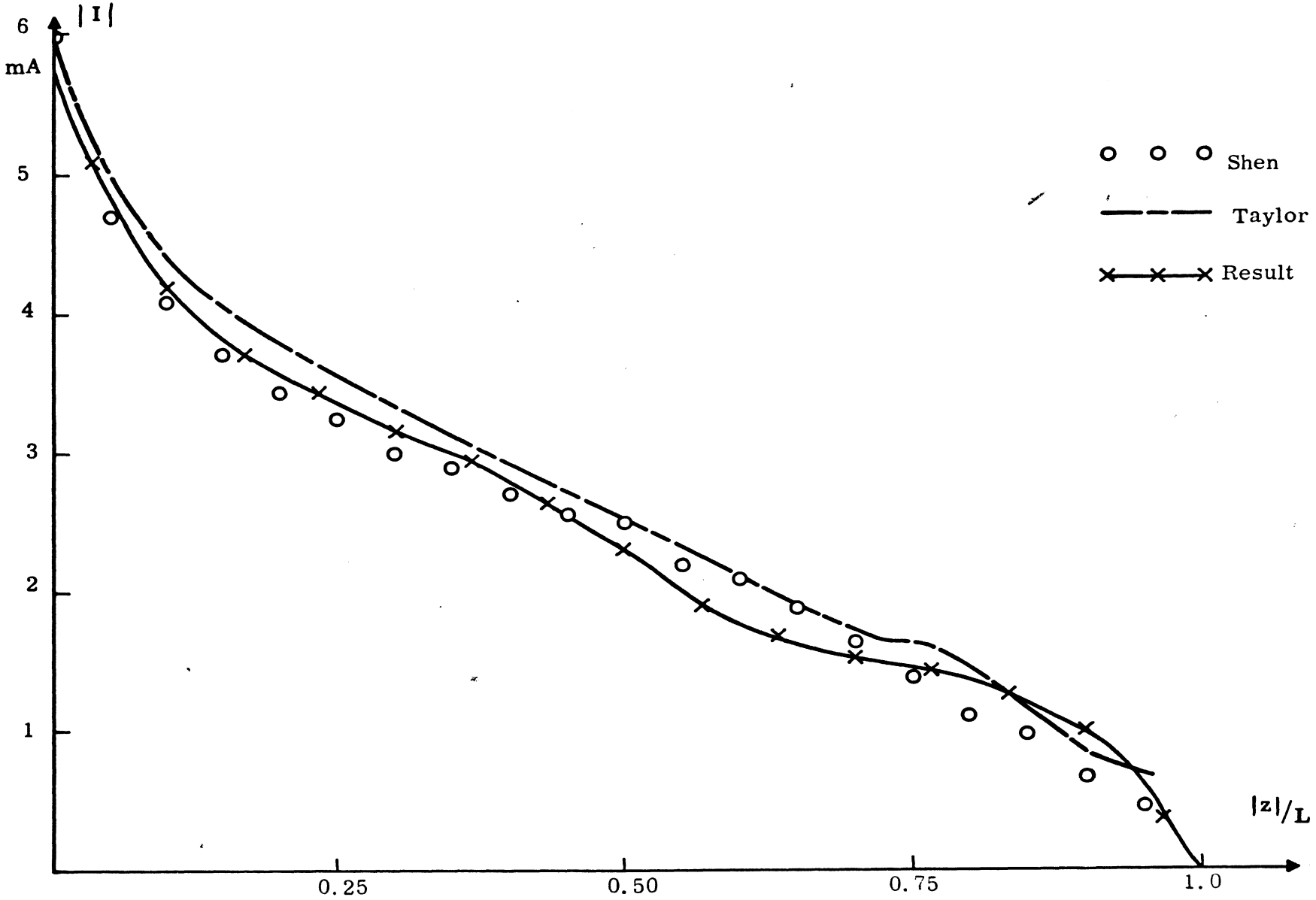

FIG. 3: Current distribution on non-reflectively loaded monopole. $\Omega = 11.5$, $\omega L/c = 2\pi$, $\psi\alpha = 5.3$.

obtained experimentally and those of Taylor have been obtained by numerical solution of Pocklington integral equation for the current distribution. Fig. 3 indicates that our computed results agree fairly well with Shen's experimental values.

7.3 Exponentially Loaded Case

Fig. 4 shows the current distributions on a one wavelength long monopole loaded exponentially. The loading function used is

$$R_s(z) = c' e^{\alpha|z|} , \qquad (47)$$

where c' is a constant and α is another constant which determines the rate of loading. In order to compare the results of Fig. 4 with those of Fig. 3 the constant c' is chosen to be $c' = 604\alpha = 60 \times 5.3$. Fig. 4 shows the current distributions obtained numerically with the help of Eqs. (21)-(23) with $N = 30$ for two cases with $\alpha = 2.2$ and $\alpha = -2.2$. The case with $\alpha = 2.2$ corresponds approximately to Shen's[14] and it clearly shows the existence of a traveling wave type of current distribution. For $\alpha = -2.2$, the loading decreases towards the end and the current distribution obtained is of standing wave nature.

7.4 Phase Distribution of the Current

Fig. 5 shows the phase variations of the current along the length of the antenna for the different non-uniformly loaded cases considered above. The progressive linear variations of phase for the non-reflecting case indicates the existence of a pure traveling wave of current in the antenna. It is interesting to observe from Fig. 4 that for the exponentially loaded case with $c' = 60 \times 5.3$, $\alpha = 2.2$ the antenna may be considered to be approximately non-reflecting. This observation may have significant implications for theoretical analysis of such antennas. No such conclusion can be made from the phase variation for the exponentially loaded antenna with $\alpha = -2.2$.

7.5 Results for a Long Antenna $2L = 5\lambda$

In the previous sections numerical results have been given for an antenna

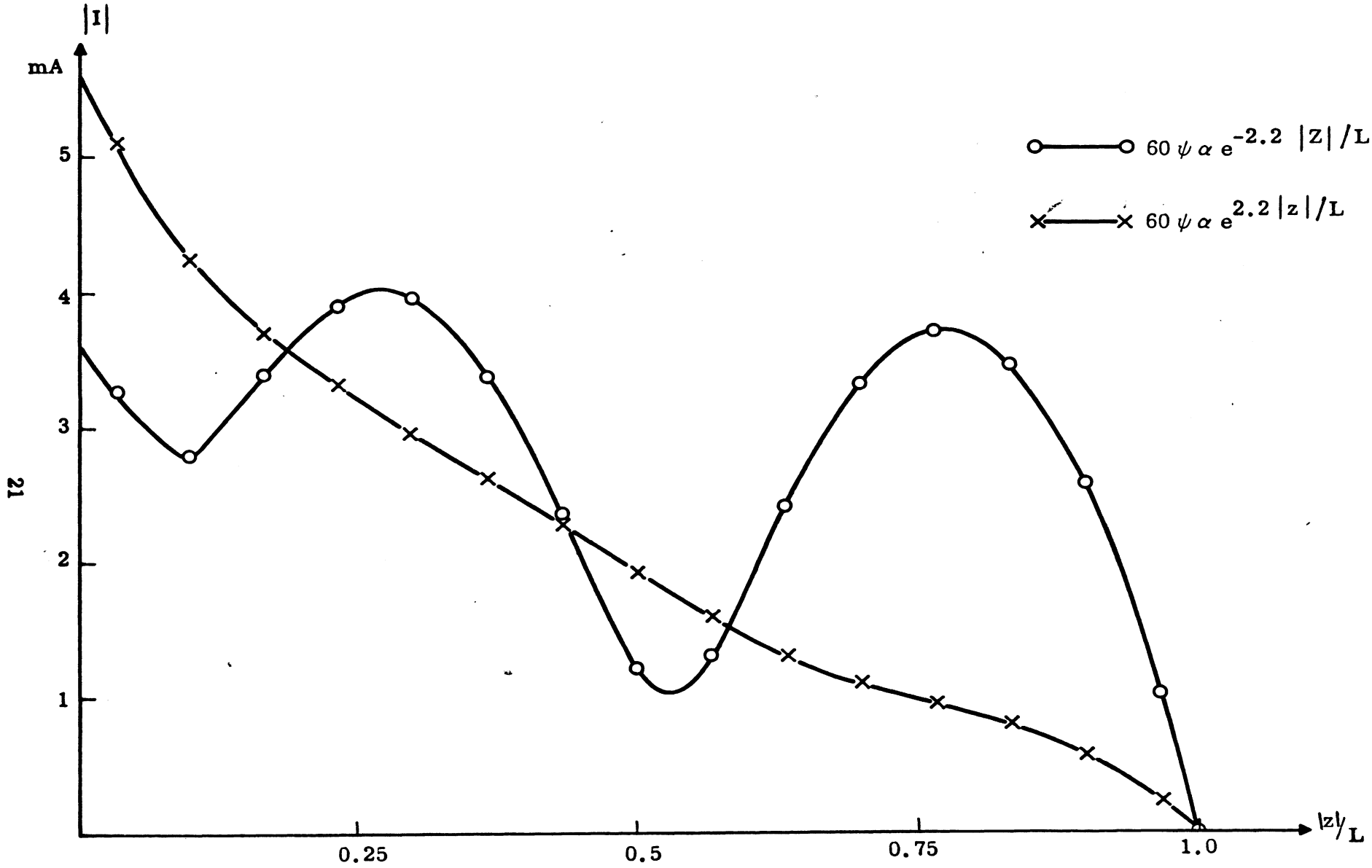

FIG. 4: Current distribution on exponentially loaded monopole. $\Omega = 11.5$, $\psi\alpha = 5.3$, $\omega L/c = 2\pi$.

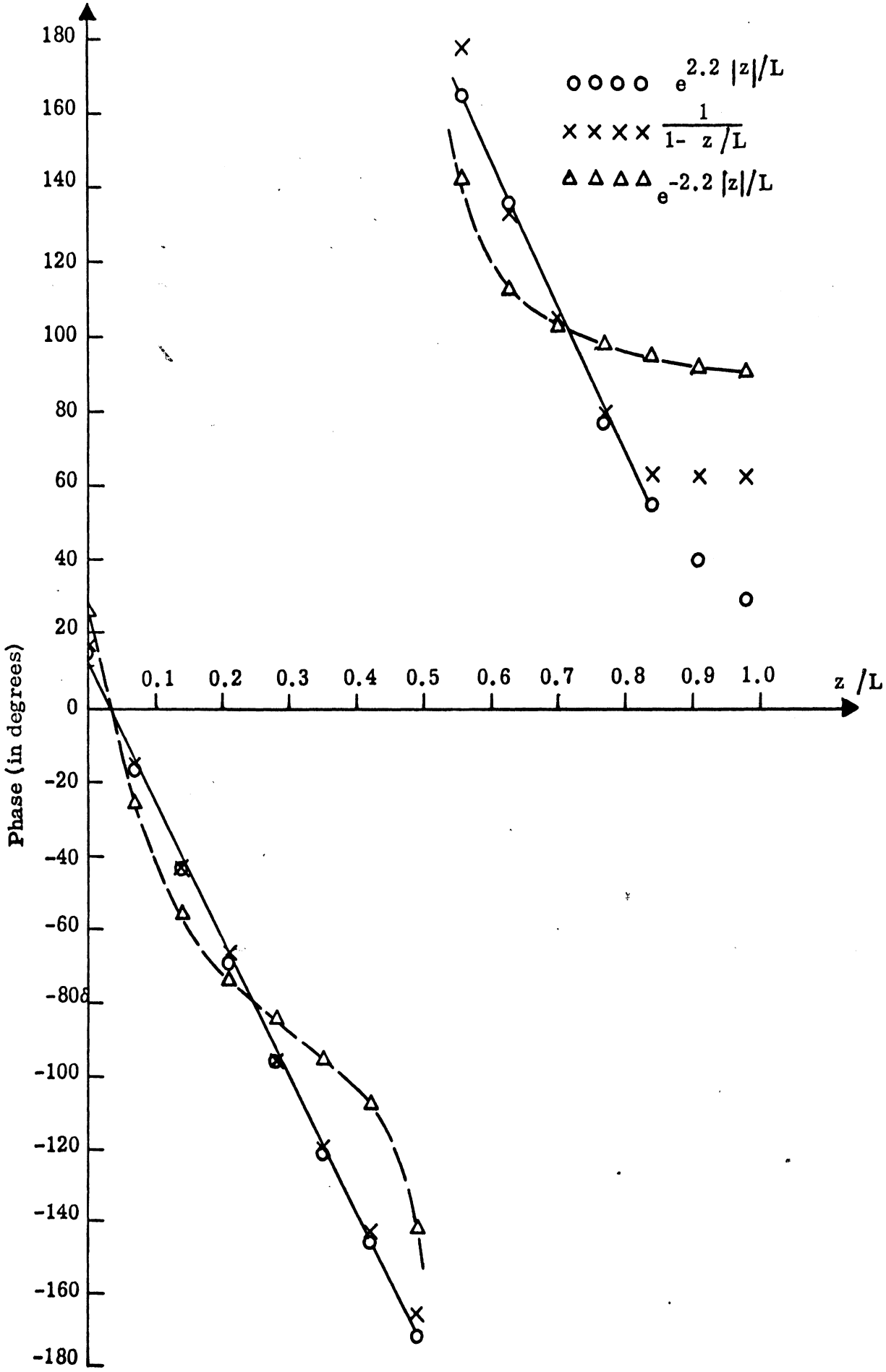

FIG. 5: Phase variation of the current along the antenna.

having total length $2L = 2\lambda$. During the process of obtaining the transfer function of the antenna as a function of frequency, the effective length of the antenna becomes very large at the high frequency end. The computer capacity as well as the accuracy of the numerical results restrict the highest frequency for which the transfer function can be evaluated. For long antennas, the computer program should be modified for retaining satisfactory accuracy of the results without taxing the computer. For small antenna length the usual pulse approximation for the current in each section Δz_n provides sufficient accuracy as has been found in the previous sections. As discussed in Section 4, for long antennas we use the quadratic approximation to the current during the numerical evaluation of the current. We study the accuracy of this procedure in this section. In addition to this we also investigate the use of 4-, 3- and 2-point end conditions for the long antenna case. The results of a sample computation done for the case with $2L = 5\lambda$ with different values of the loading parameter in Eq. (16) are discussed in the present section.

Figs. 6, 7 and 8 show the current amplitude distribution, the current phase distribution and the transfer function respectively of the non-reflecting loaded linear antenna of length $2L = 5\lambda$ with the loading parameter $C = 60 \times 5.3$. All these curves have been obtained by using Eqs. (36) with $N = 30$. In each case the results obtained by using 4-, 3- and 2-point end condition expressions are also shown in Figs. 5-7. It can be seen from Figs. 5-7 that the results are not appreciably different among the three cases. However, near the end of the antenna the results are found to differ with each other slightly. From a study of Figs. 5 and 6, in particular, the phase variation near the end of the antenna as shown in Fig. 6 it is concluded that the 4-point end condition expression given by Eq. (43) is more accurate and hence should be used during the numerical computation of the transfer function of the antenna for high frequencies. Fig. 9 shows the amplitude of the current distribution on the antenna as a function of the loading parameter $C = 60\psi\alpha$ obtained by Eq. (36) with $N = 30$ and the 4-point end condition.

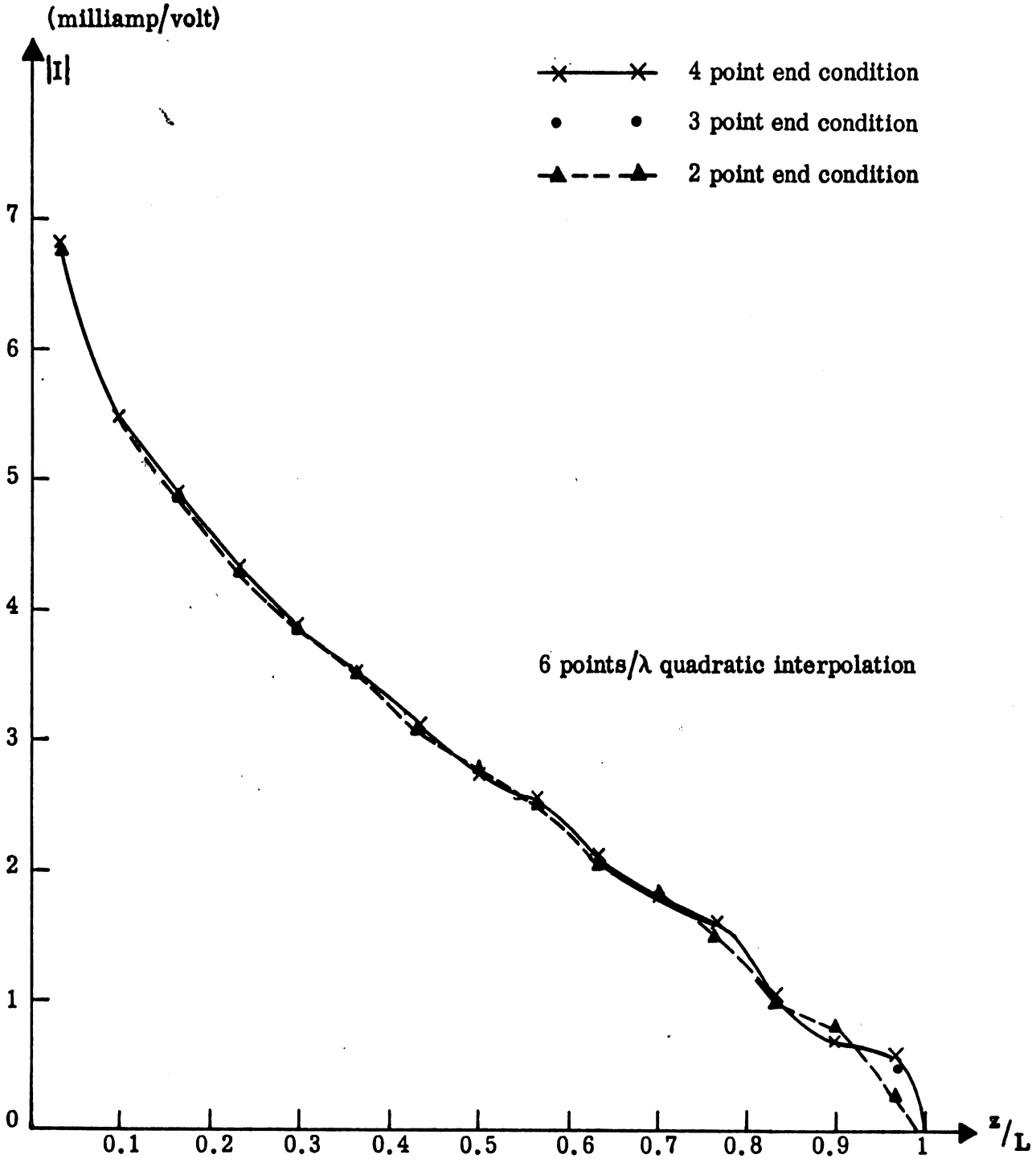

FIG. 6: Current distribution on non-reflectively loaded antenna, $\Omega = 11.5$ $kL = 5\pi$, $\psi\alpha = 5.3$, $R_s(z) = 60\,\psi\alpha/L - |z|$.

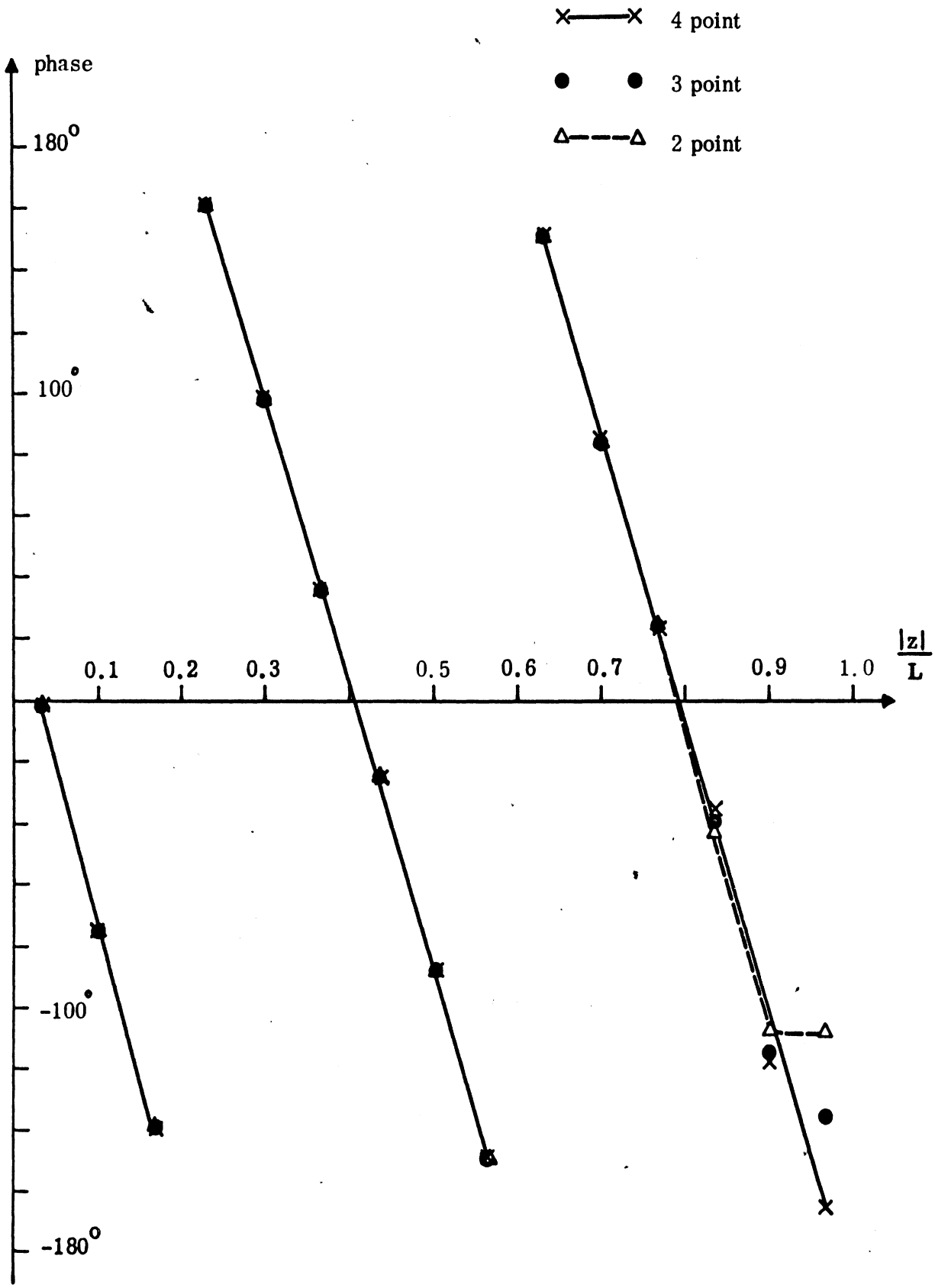

FIG. 7: Phase variation of the current along the non-reflectively loaded antenna, $\Omega = 11.5$, $kL = 5\pi$, $\psi\alpha = 5.3$, $R_s(z) = 60\psi\alpha/L - |z|$.

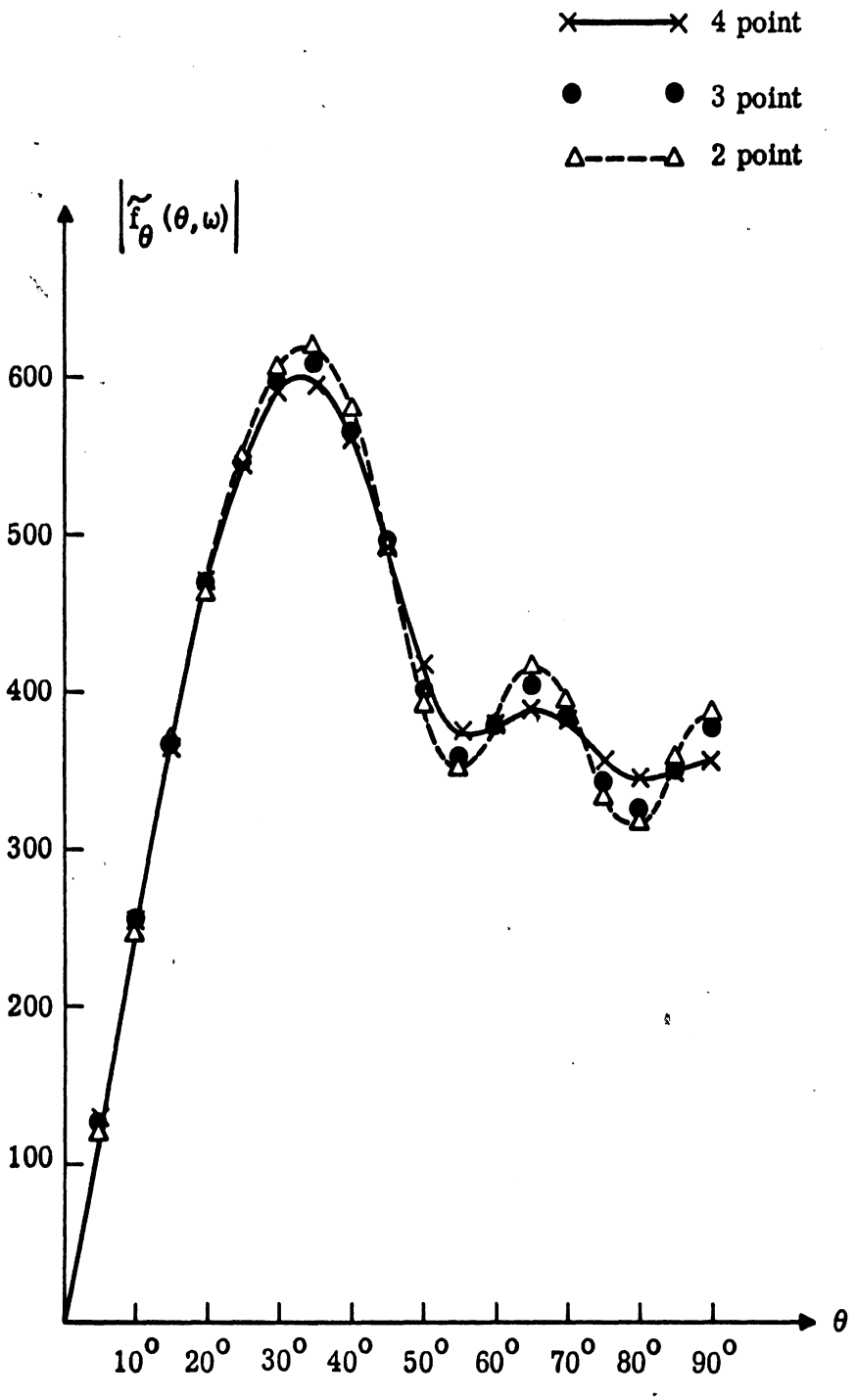

FIG. 8: Transfer function $\tilde{f}_\theta(\theta,\omega)$ of the non-reflectively loaded antenna. $\Omega = 11.5$, $kL = 5\pi$, $\psi\alpha = 5.3$, $R_s(z) = 60\psi\alpha/L - |z|$.

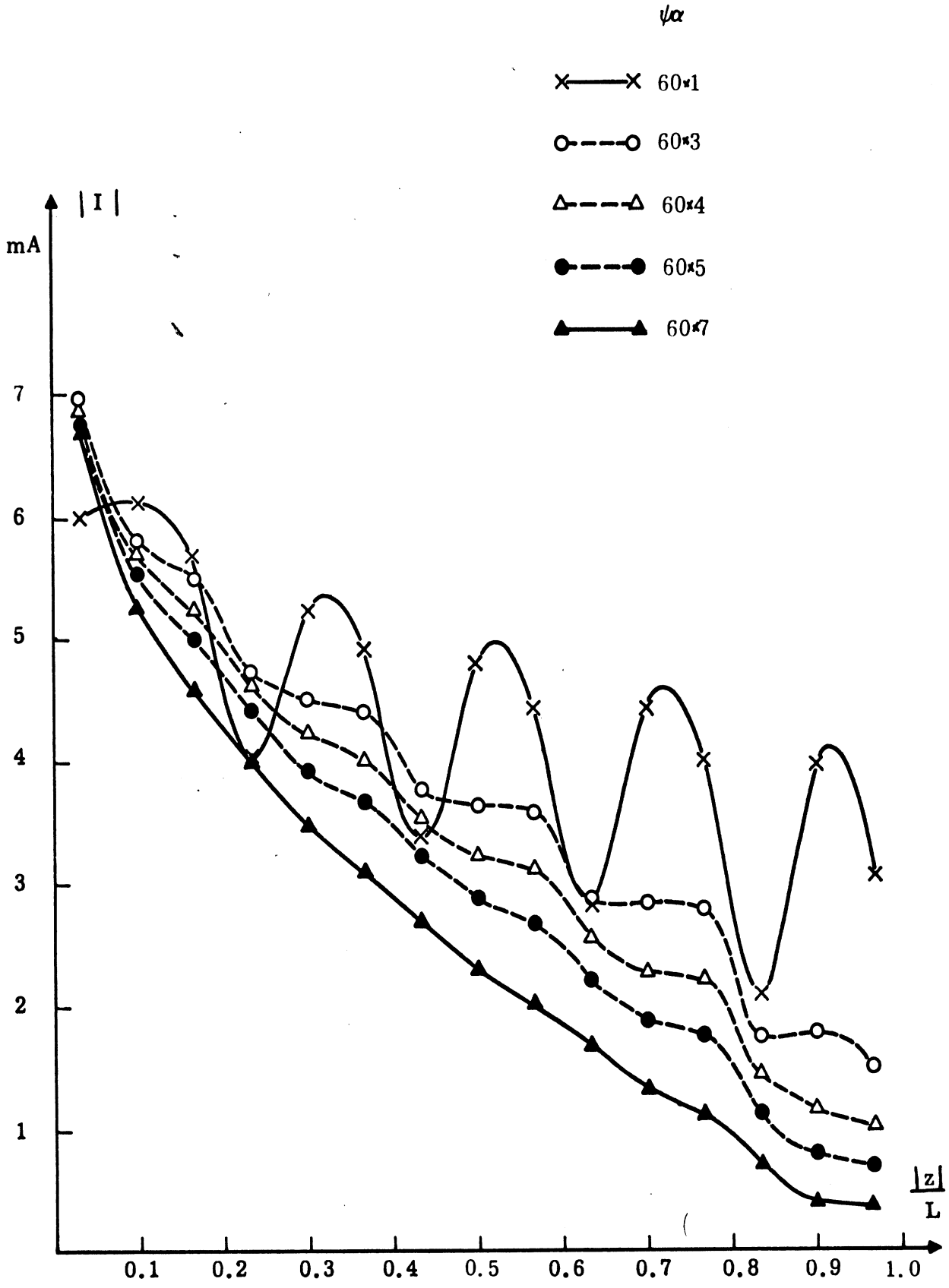

FIG. 9: Amplitude of the current distribution on resistively loaded dipole antenna as a function of loading. $\Omega = 11.5$, $kL = 5\pi$, $\psi\alpha$ variable.

It is interesting to observe here that on the basis of King's work, the expansion factor ψ is a fixed value for one particular size and frequency. That means only at this specific value of loading ($60\psi\alpha$) and specific frequency, we can have a reflectionless current wave on the antenna. For $C < 60 \times 5$, the reflection effects on the current distribution become quite appreciable as expected. While $C > 60 \times 7$, Fig. 9 tells us the nonreflection nature. The higher value of loading on the antenna supresses the small amount of reflection that occurs due to the use of a value of ψ slightly different from the specific value referred to above.

On the basis of the results given in this section, we have decided to use the 4-point end-condition expression during the numerical computation. Six subsections per wavelength to divide the antenna is required to guarantee the accuracy.

8. CURRENT DISTRIBUTION $I(z, \omega)$ ON THE LOADED ANTENNA

In this section we give the numerical results obtained for the amplitude of the current distribution $I(z, \omega)$ for the harmonically excited loaded antenna. The loading used is of the form given by Eq. (16) with C variable. Figs. 10(a)-10(d) show the amplitude of the current distribution on the antenna with antenna length as parameter for different values of the loading.

The amplitude of the current in general increases as the frequency is increased. The value of the magnitude at the same frequency is surpressed by the higher loading as expected. The current distribution is not strictly linear as those of the transmission line found by Baum. It is due to the factor ψ which is a function of the thickness ratio of the antenna and the frequency used. So it is not possible to excite a traveling current wave for all frequencies on an antenna of fixed size.

9. TRANSFER FUNCTION OF THE LOADED ANTENNA $\tilde{f}_\theta(\theta, \omega)$.

In this section the magnitude and phase of the transfer function of the antenna are given as functions of $\omega L/c$ for different values of the loading parameter C.

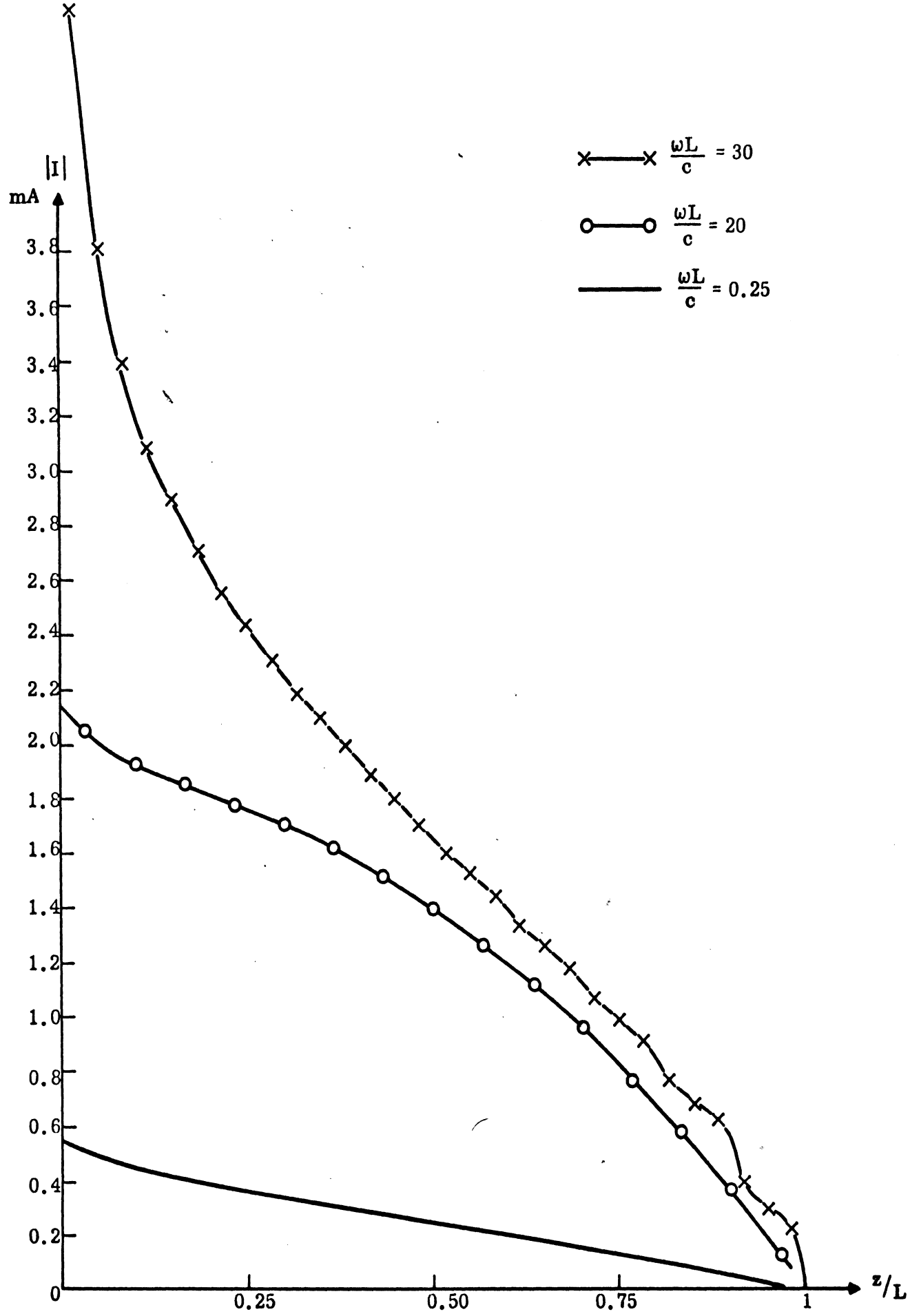

FIG. 10a: Amplitude of the current distribution $|I(z,\omega)|$ vs z/L on the loaded antenna with kL (= ωL/c), as the parameter, C = 60 x 4.

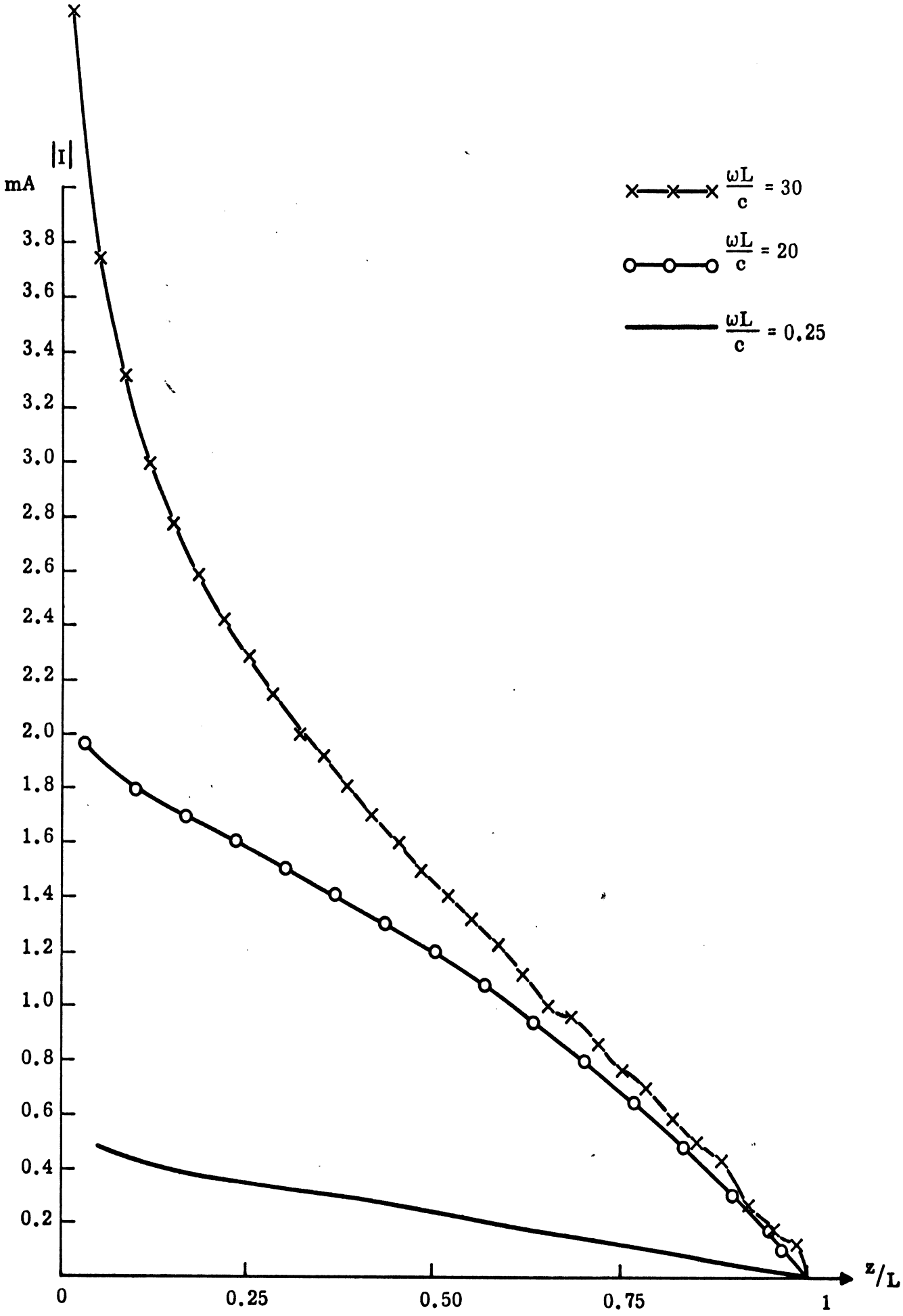

FIG. 10b: Amplitude of the current distribution $|I(z,\omega)|$ vs. z/L on the loaded antenna with $kL\ (=\omega L/c)$, as the parameter $C = 60 \times 5$.

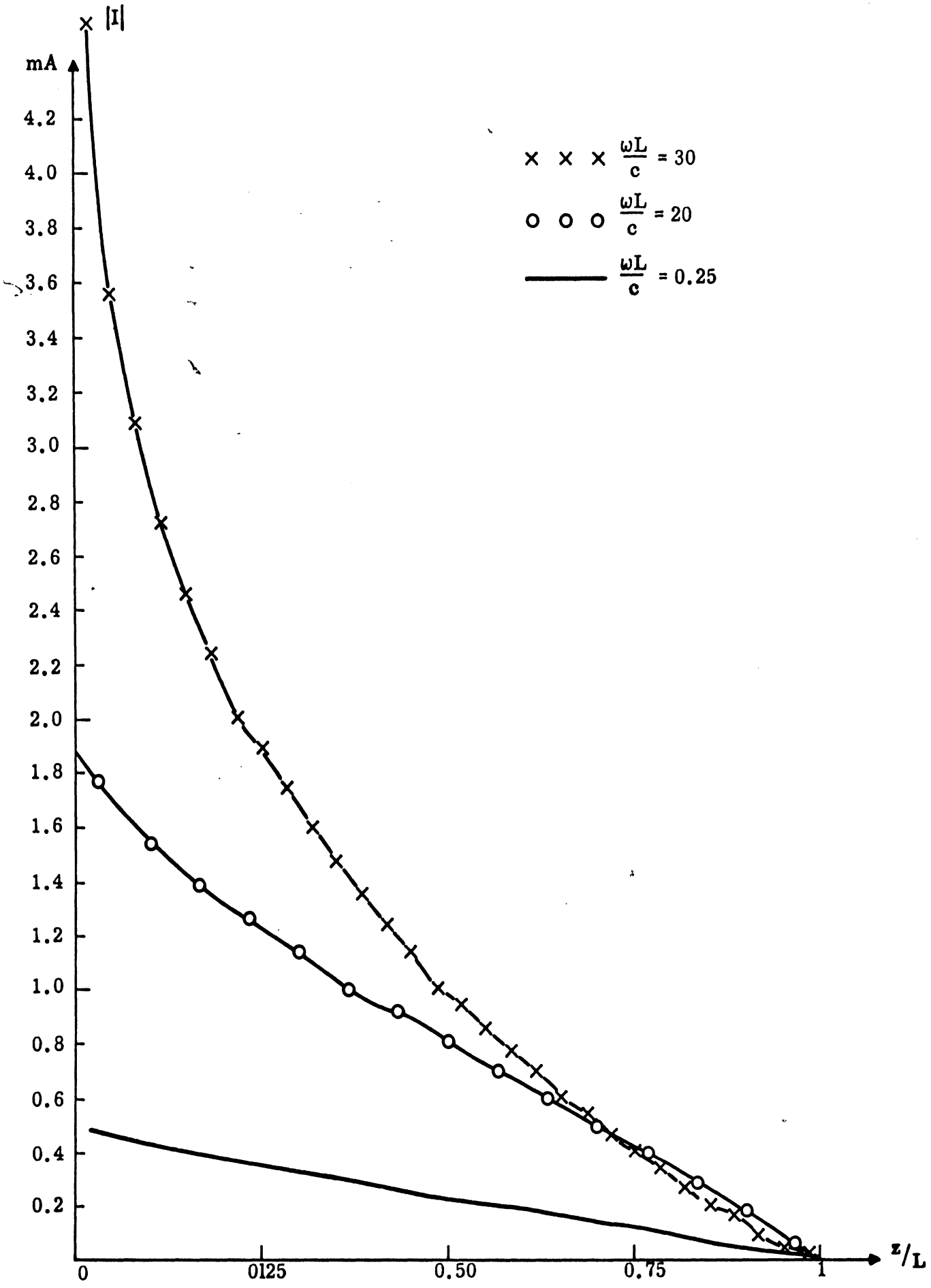

FIG. 10c: Amplitude of the current distribution $|I(z,\omega)|$ vs z/L on the loaded antenna with kL (= ωL/c), as the parameter. C = 60 x 8.

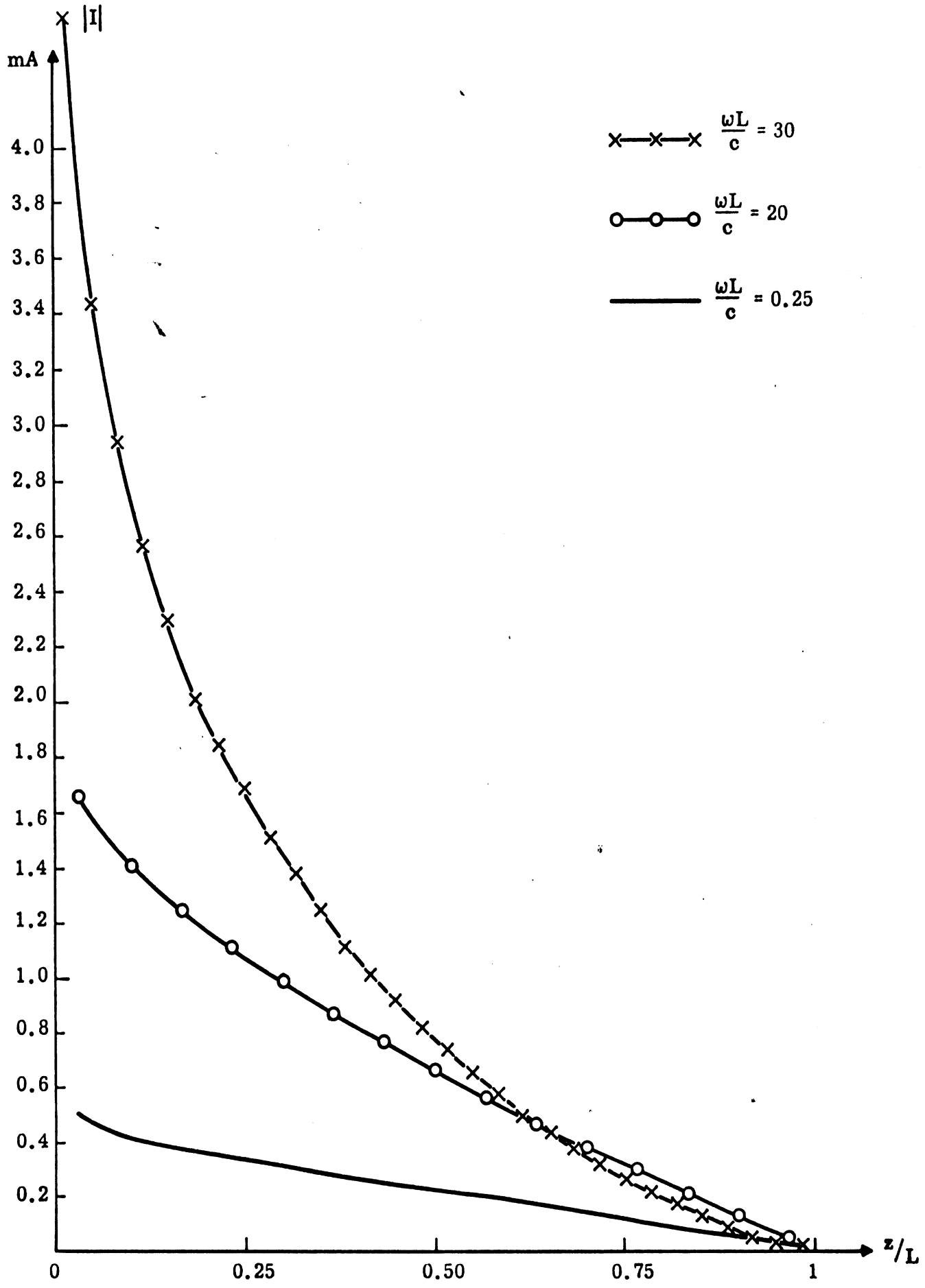

FIG. 10d: Amplitude of the current distribution $|I(z,\omega)|$ vs z/L on the loaded antenna with $kL = \omega L/c$), as the parameter. C = 60 x 10.

These have been obtained numerically with the help of equation (45) and the sampled values of the current distributions discussed in the previous section. Figs. 11(a)-11(d) give the variations of the magnitude and phase of the transfer function in the broadside direction ($\theta = \pi/2$) of the antenna and for four values of the loading parameter c. Similar results are given for $\theta = \pi/3$, $\theta = \pi/4$, $\theta = \pi/6$ in Figs. 12, 13, 14, respectively. Each figure contains four different values of the loading factor C. In all the curves shown, $|\tilde{f}_\theta(\theta, \omega)|$ approaches zero as ω approaches zero, which corresponds to the fact that there is no radiation at zero frequency. For higher frequencies, $|\tilde{f}_\theta(\theta, \omega)|$ appears to be an oscillating function and tends to decrease with increase of the frequency. The phase of $\tilde{f}_\theta(\theta, \omega)$ falls steadily to a positive constant. Wu and King[9] proved that the asympotatic value of the transfer function is a constant. However, within the range of the computations covered here the transfer function in Figs. 11-14 does not reach its asymptotic value especially for $\theta = \pi/6$. For an unloaded thin linear antenna, we know that the transfer function would be zero for $L = n\lambda$ at the broadside direction (where n is an integer) when the current is sinusoidal. Fig. 11(a) shows that the values at $kL = 2\pi, 4\pi, 6\pi, 8\pi$ are minimal. For higher values of C, the loading reduces the ringing which is due to the reflection from the end.

It is appropriate to mention here that the impulse response of the antenna may be obtained by numerically carrying out the inverse Fourier transform. However, the data for $\tilde{f}_\theta(\theta, \omega)$ obtained so far is not sufficient to get reasonably good results. Taylor[6] has shown that the transfer function reaches its asymptotic value at a certain frequency which is beyond the value $\omega L/c = 25$ considered here.

10. NUMERICAL RESULTS

In this section we discuss the numerical results for two different shapes of voltage input. Spectral density is obtained by multiplying the transfer function with the input pulse spectrum. The waveform of the radiated signal is then

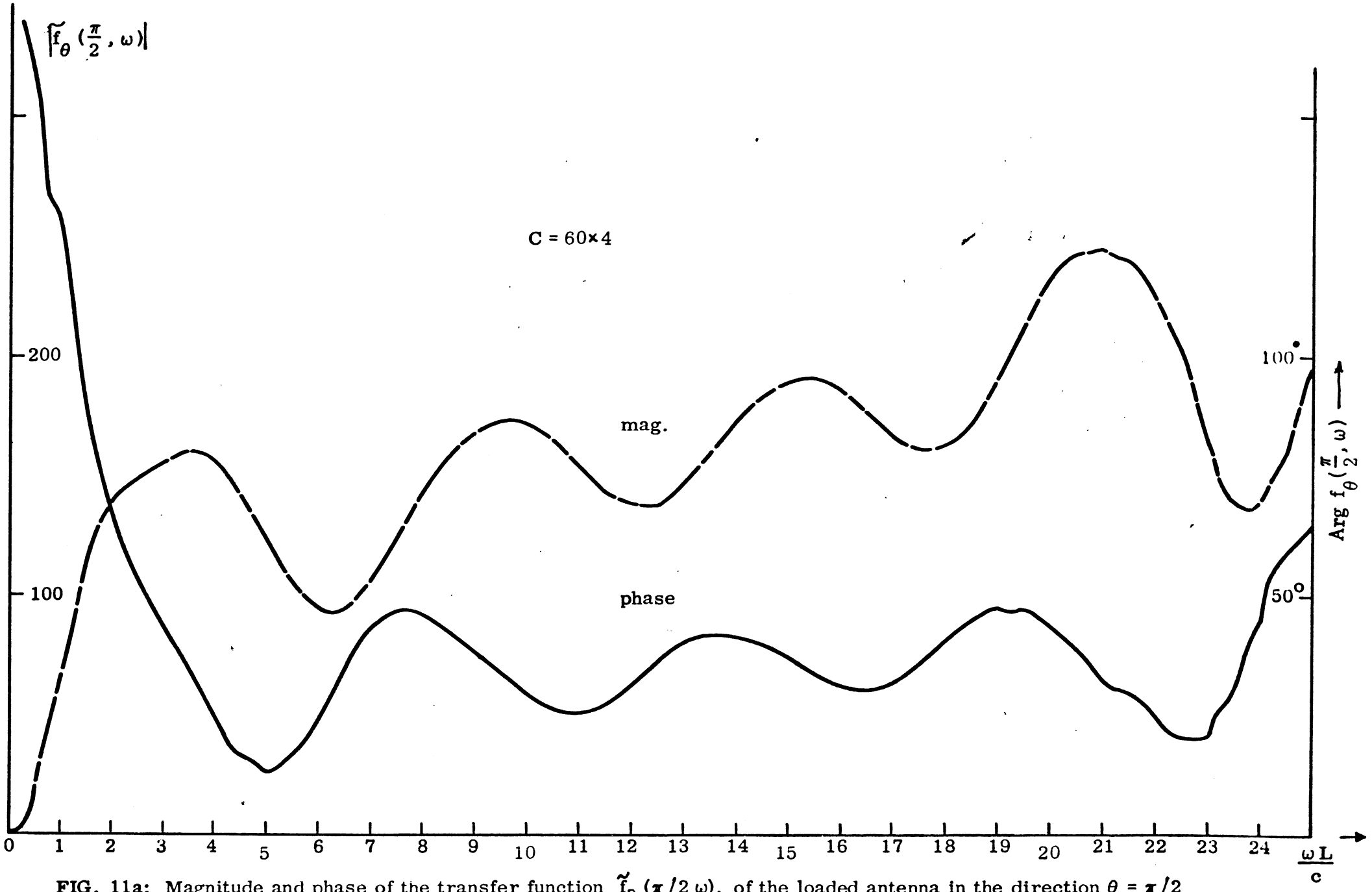

FIG. 11a: Magnitude and phase of the transfer function $\tilde{f}_\theta(\pi/2\,\omega)$, of the loaded antenna in the direction $\theta = \pi/2$ as a function of $kL = (\omega L/c)$ for different loading. C = 60 x 4.

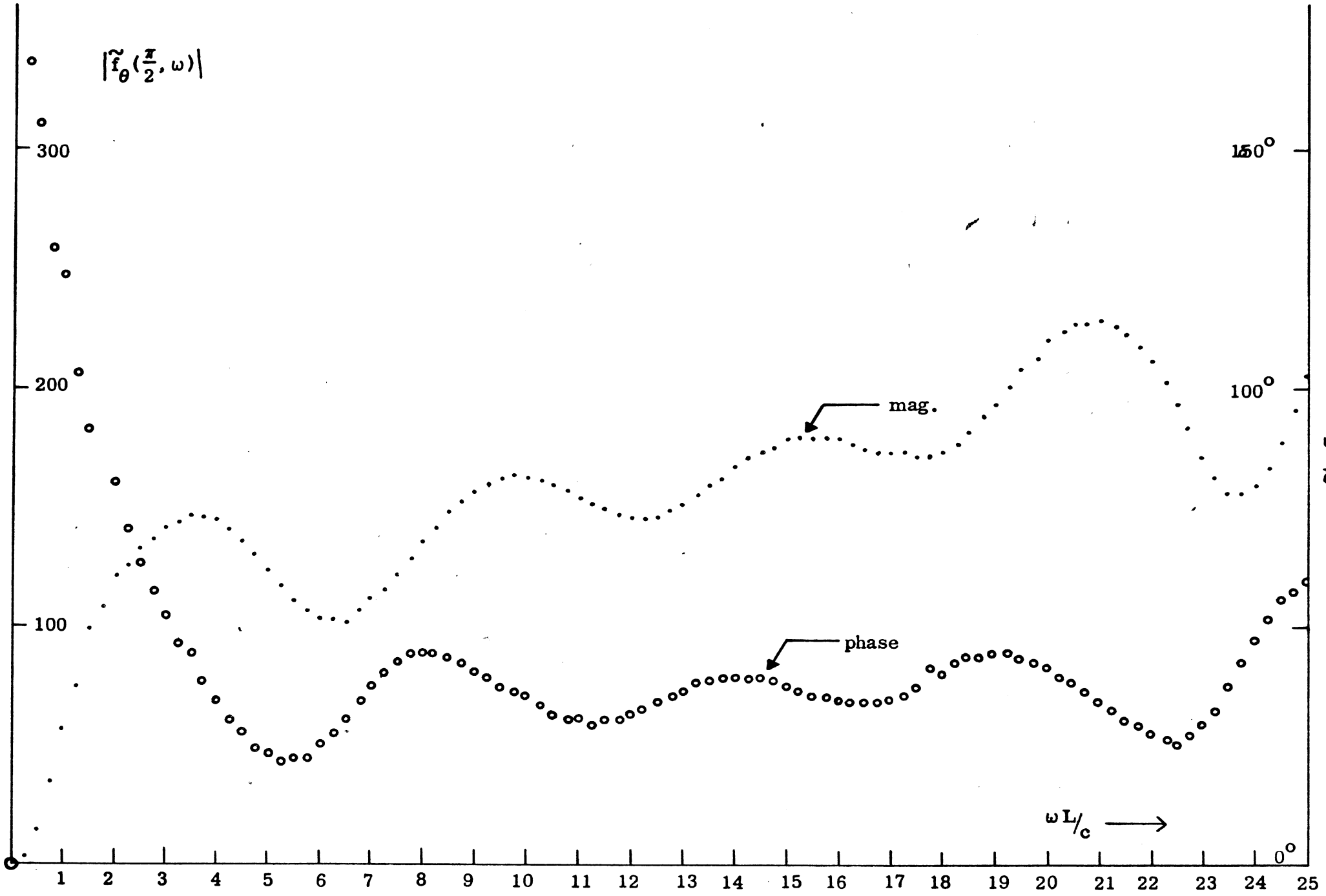

FIG. 11b: Magnitude and phase of the transfer function $\tilde{f}_\theta(\pi/2, \omega)$ of the loaded antenna in the direction $\theta = \pi/2$ as a function of kL = $(\omega l/c)$ for different loading. C = 60 x 5.

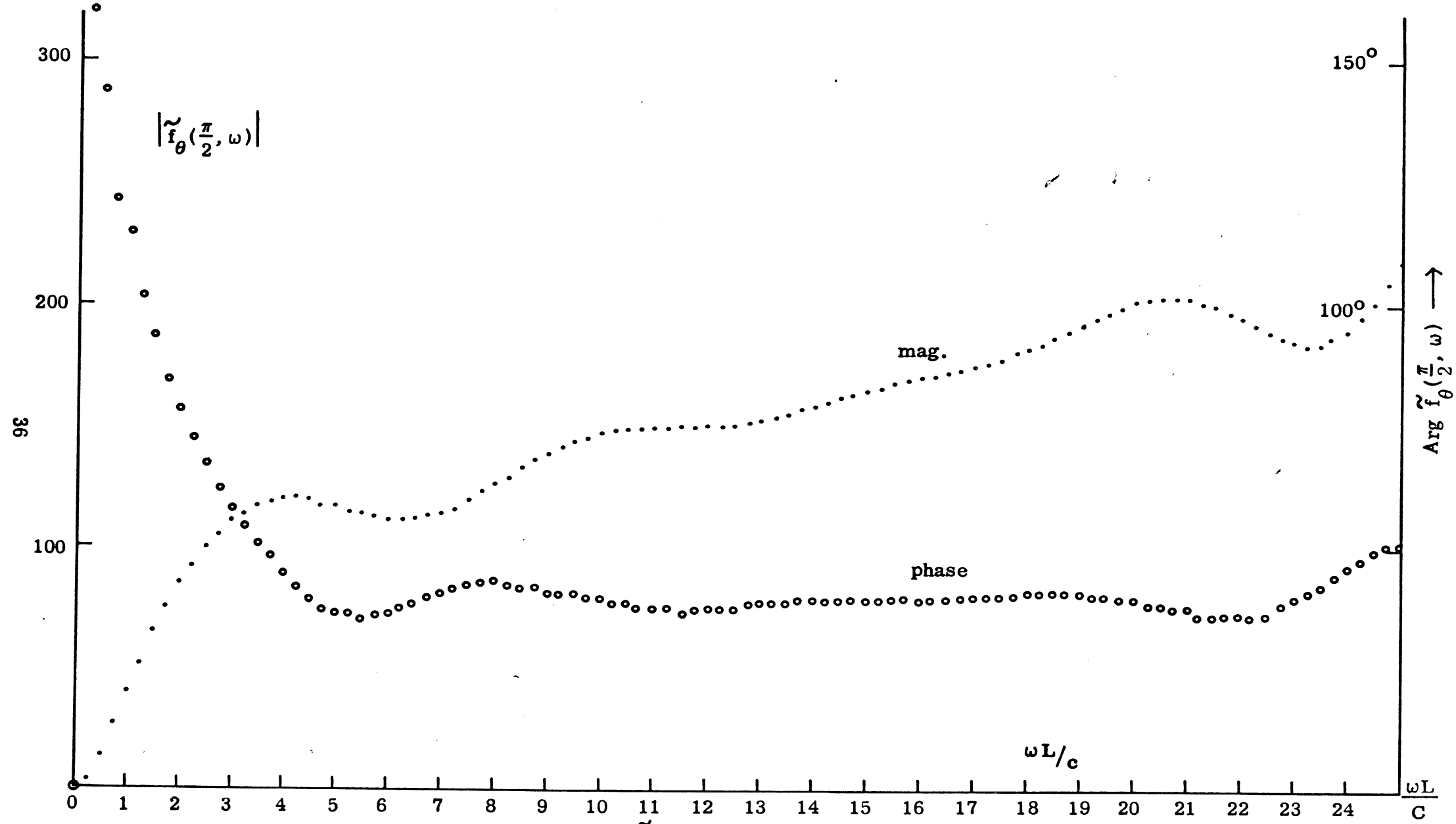

FIG. 11c: Magnitude and phase of the transfer function $\tilde{f}_\theta(\pi/2, \omega)$ of the loaded antenna in the direction $\theta = \pi/2$ as a function of $kL = (\omega L/c)$ for different loading. C = 60 x 8.

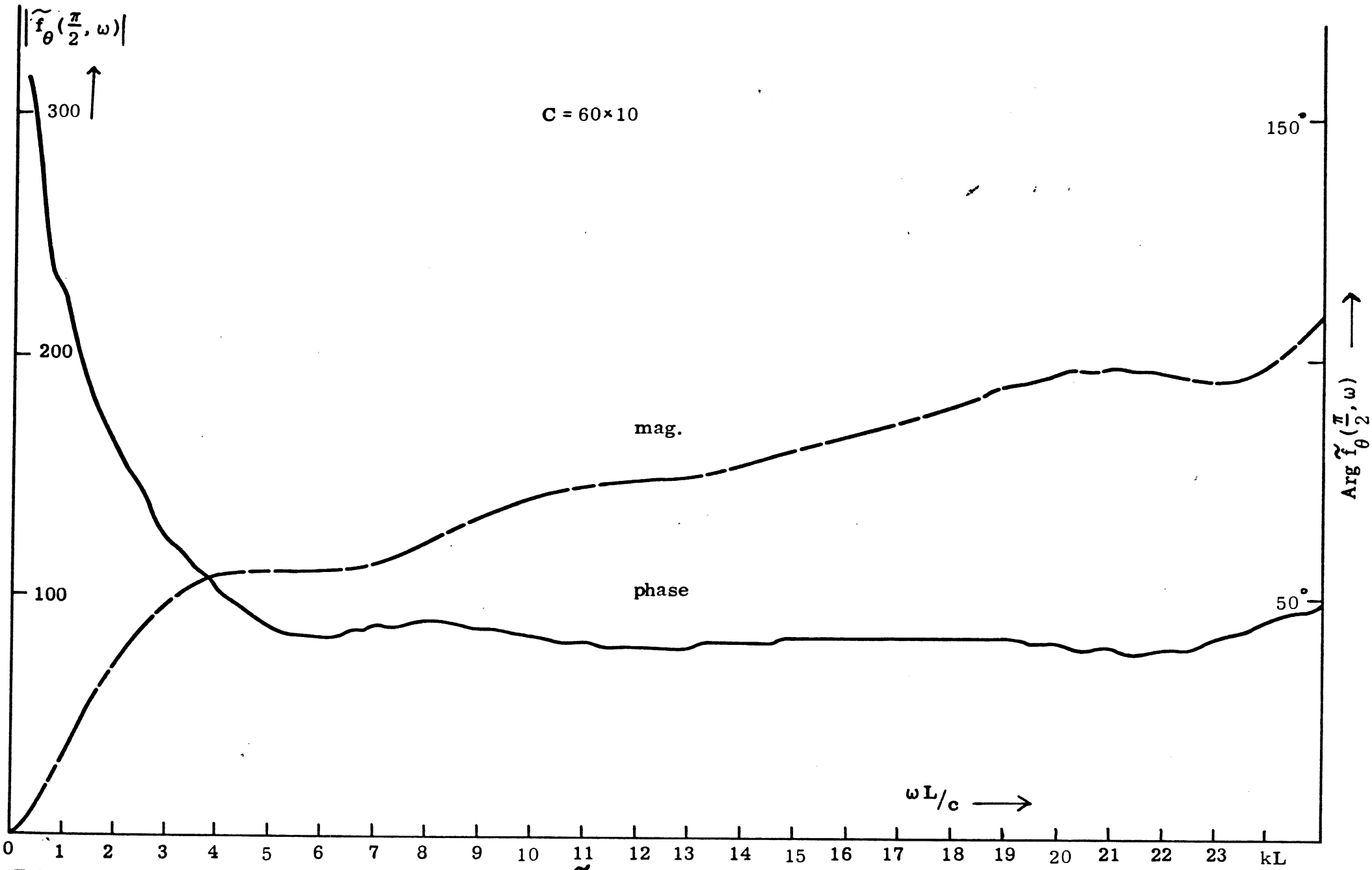

FIG. 11d: Magnitude and phase of the transfer function $\tilde{f}_\theta(\pi/2, \omega)$ of the loaded antenna in the direction $\theta = \pi/2$ as functions of kL = $(\omega L/c)$ for different loading. C = 60 x 10.

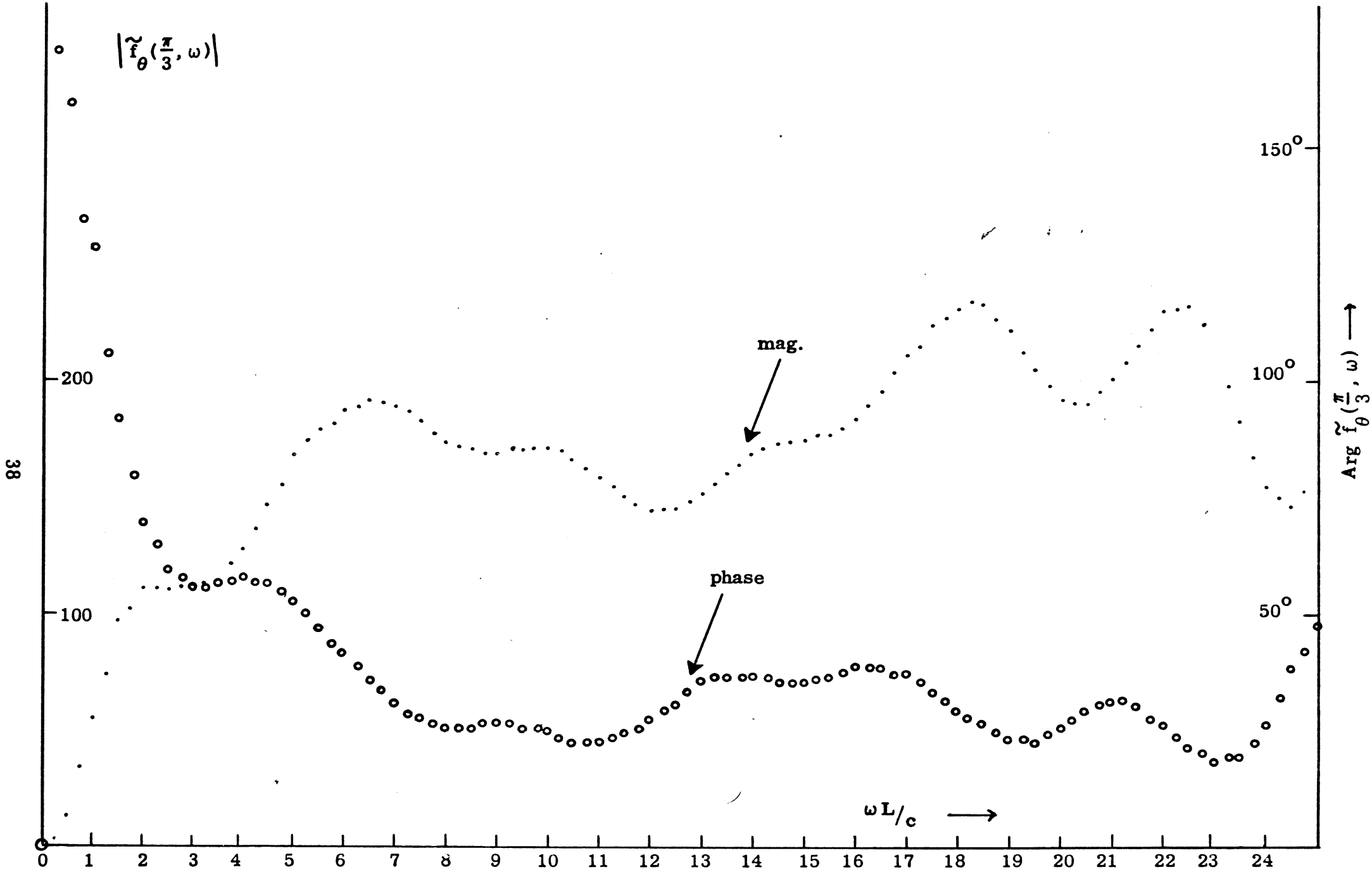

FIG. 12a: Magnitude and phase of the transfer function $\tilde{f}_\theta(\pi/3, \omega)$ of the loaded antenna in the direction $\theta = \pi/3$ as functions of kL (= $\omega L/c$) for different loading. C = 60 x 4.

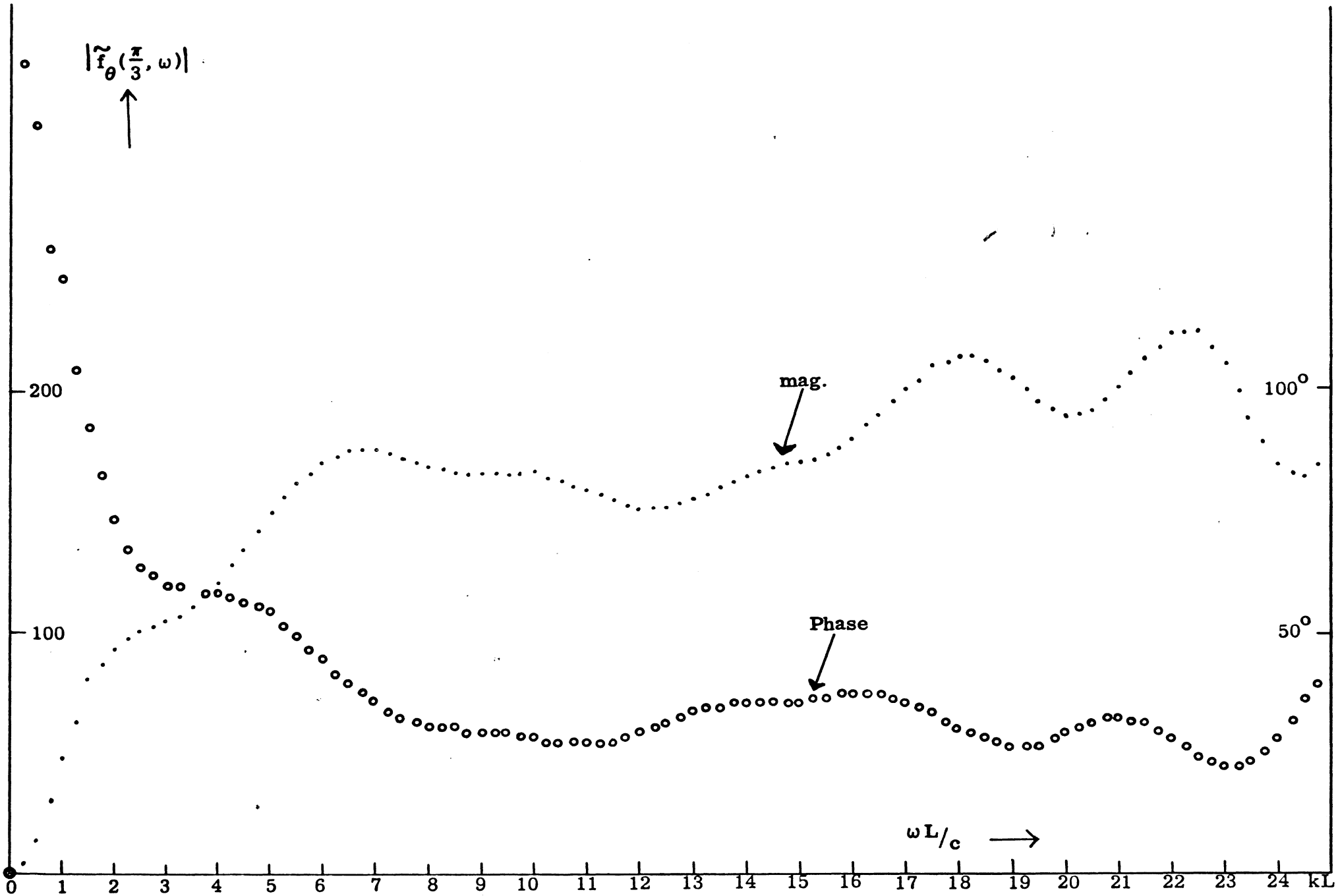

FIG. 12b: Magnitude and phase of the transfer function $\tilde{f}_\theta(\pi/3, \omega)$ of the loaded antenna in the direction $\theta = \pi/3$ as functions of kL (= $\omega L/c$) for different loading. C = 60 x 5.

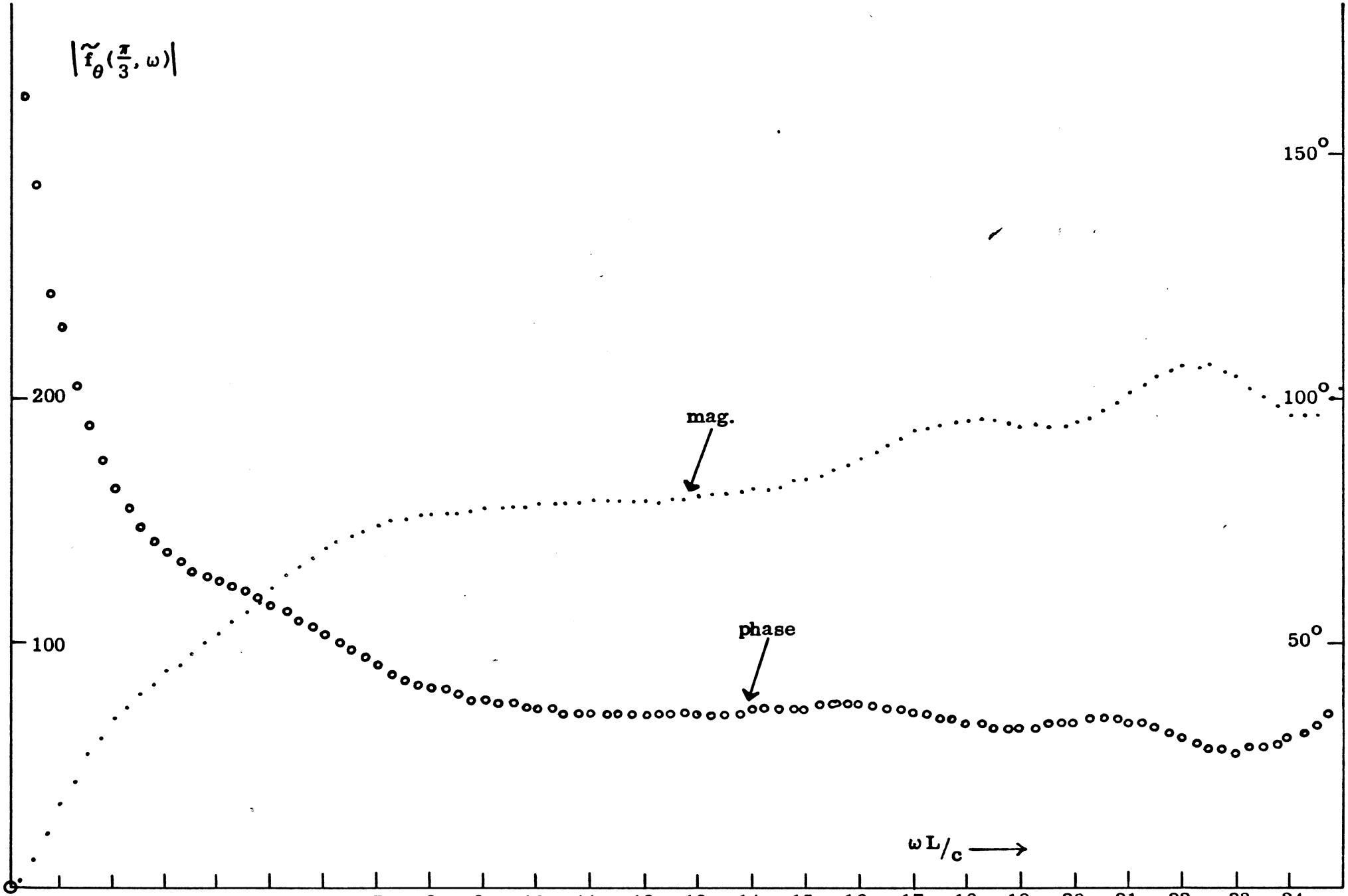

FIG. 12c: Magnitude and phase of the transfer function $\tilde{f}_\theta(\pi/3, \omega)$ of the loaded antenna in the direction $\pi = \pi/3$ as functions of kL ($= \omega L/c$) for different loading. C = 60 x 8.

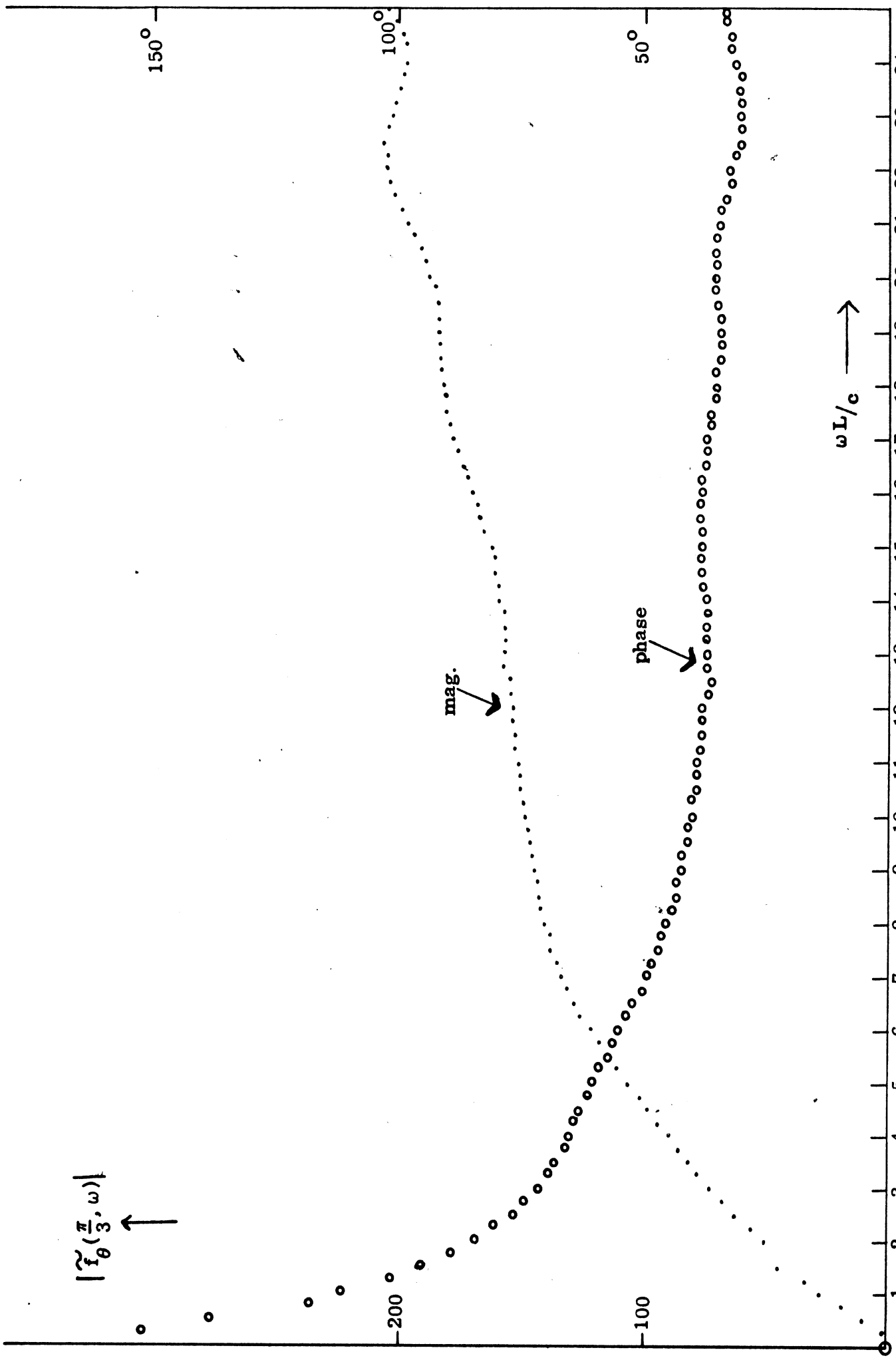

FIG. 12d: Magnitude and phase of the transfer function $\tilde{f}_\theta(\pi/3, \omega)$ of the loaded antenna in the direction $\theta = \pi/3$ as functions of $kL(= \omega L/c)$ for different loading. C = 60 x 10.

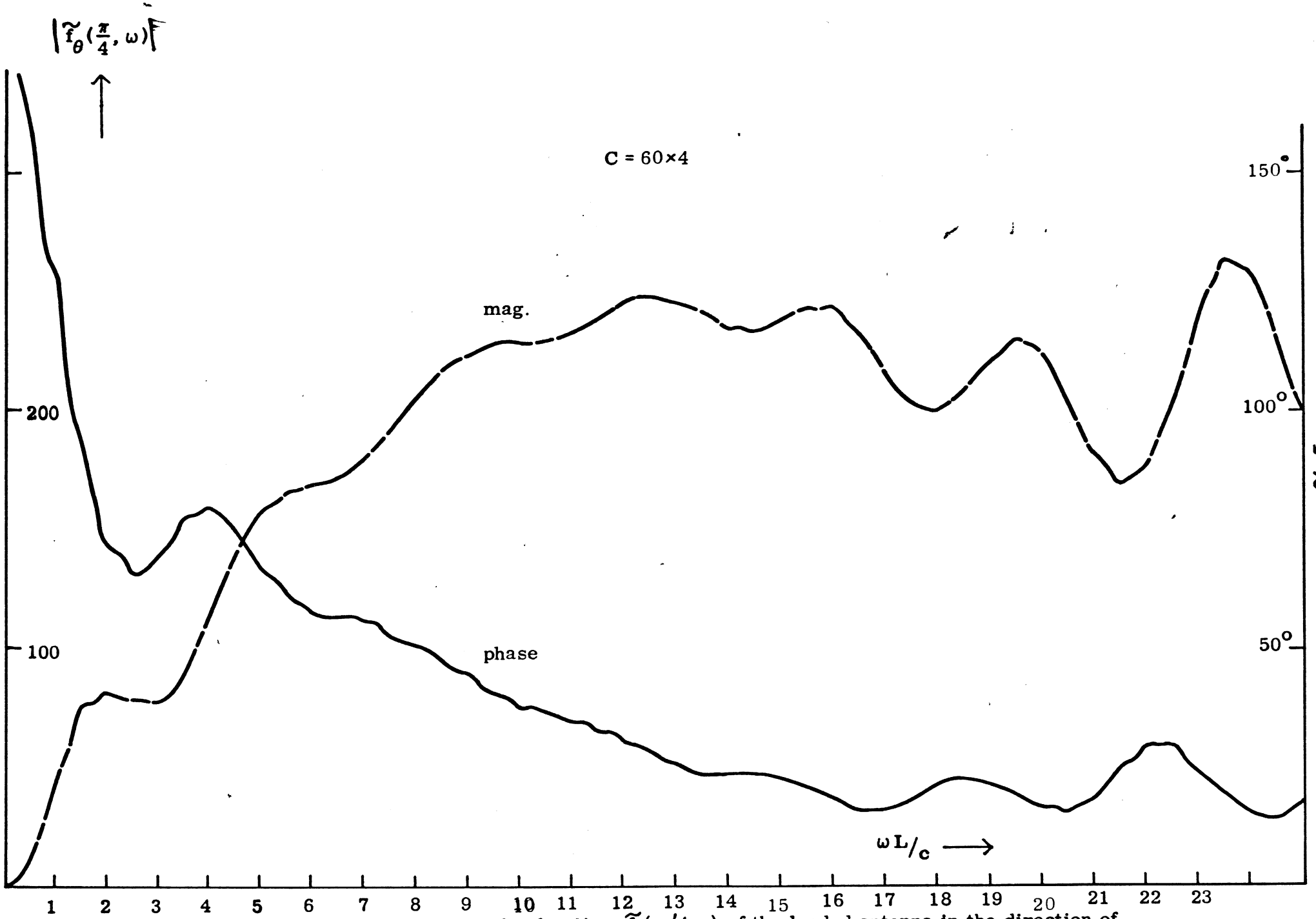

FIG. 13a: Magnitude and phase of the transfer function $\tilde{f}_\theta(\pi/4, \omega)$ of the loaded antenna in the direction of $\theta = \pi/4$ as function of kL ($= \omega L/c$) for different loading. C = 60 x 4.

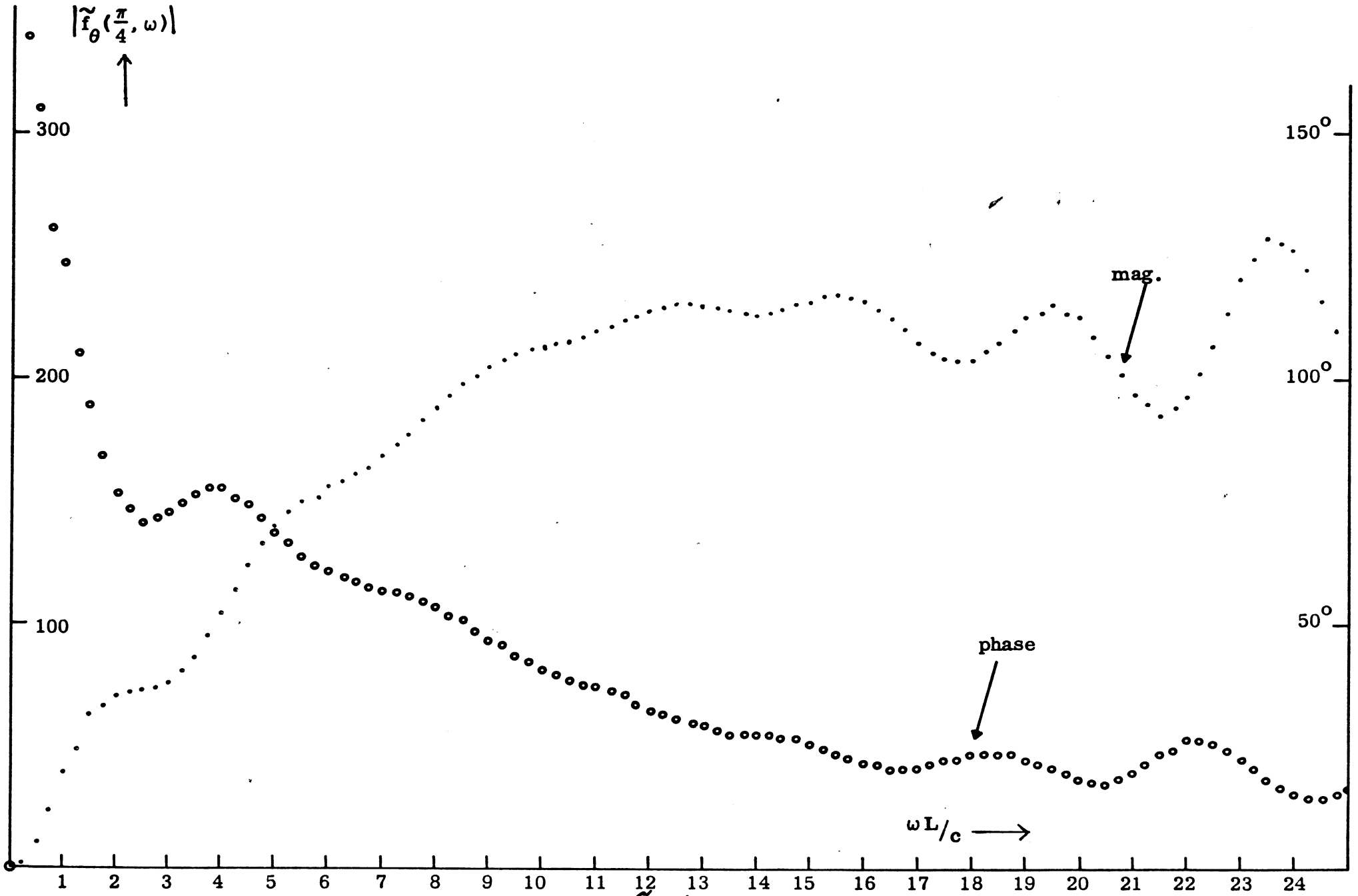

FIG. 13b: Magnitude and phase of the transfer function $\tilde{f}_\theta(\pi/4, \omega)$ of the loaded antenna in the direction $\theta = \pi/4$ as functions of kL (= $\omega L/c$) for different loading. C = 60 x 4.

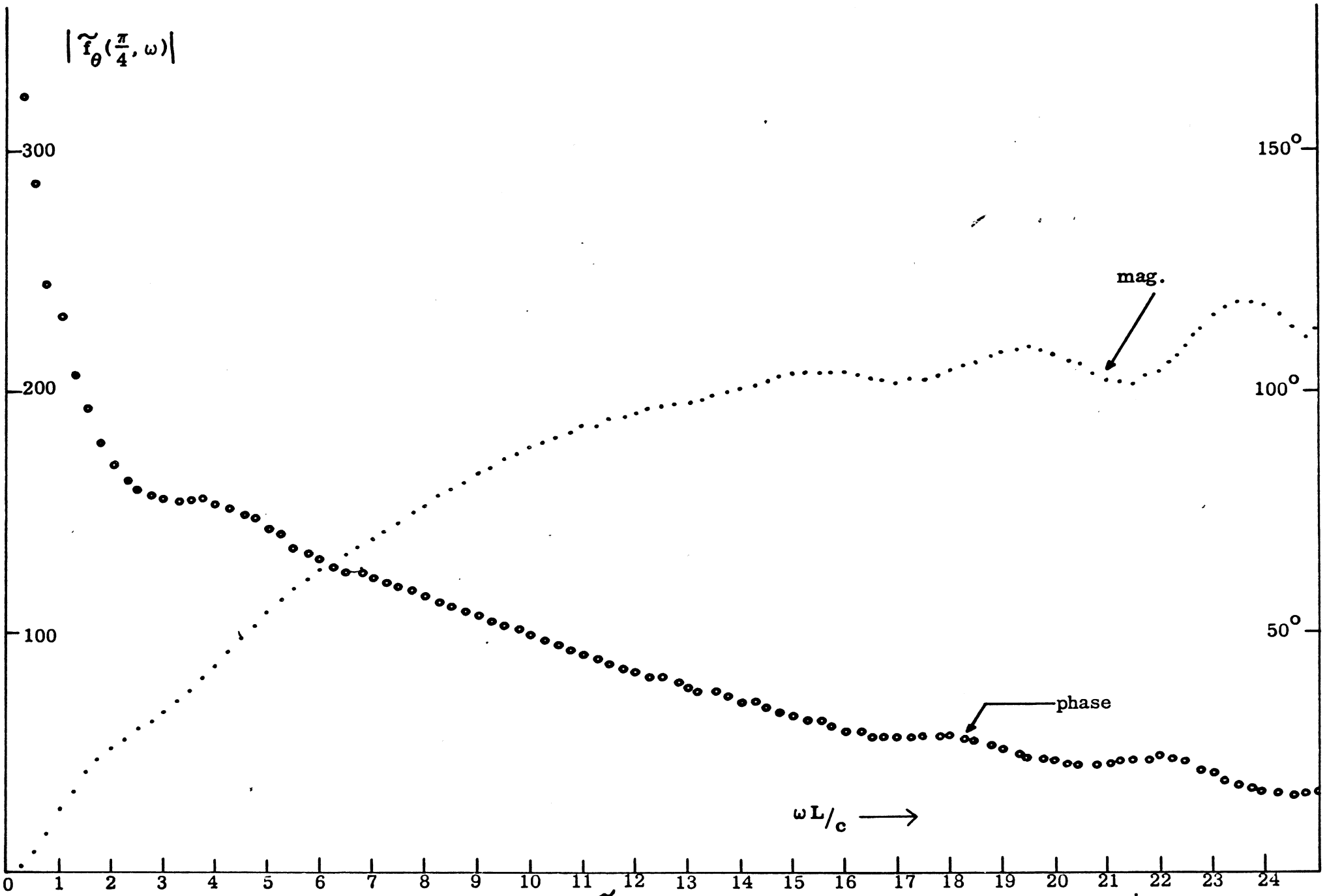

FIG. 13c: Magnitude and phase of the transfer function $\tilde{f}_\theta(\pi/4, \omega)$ of the loaded antenna in the direction $\theta = \pi/4$ as functions of kL ($= \omega L/c$) for different loading. C = 60 x 8.

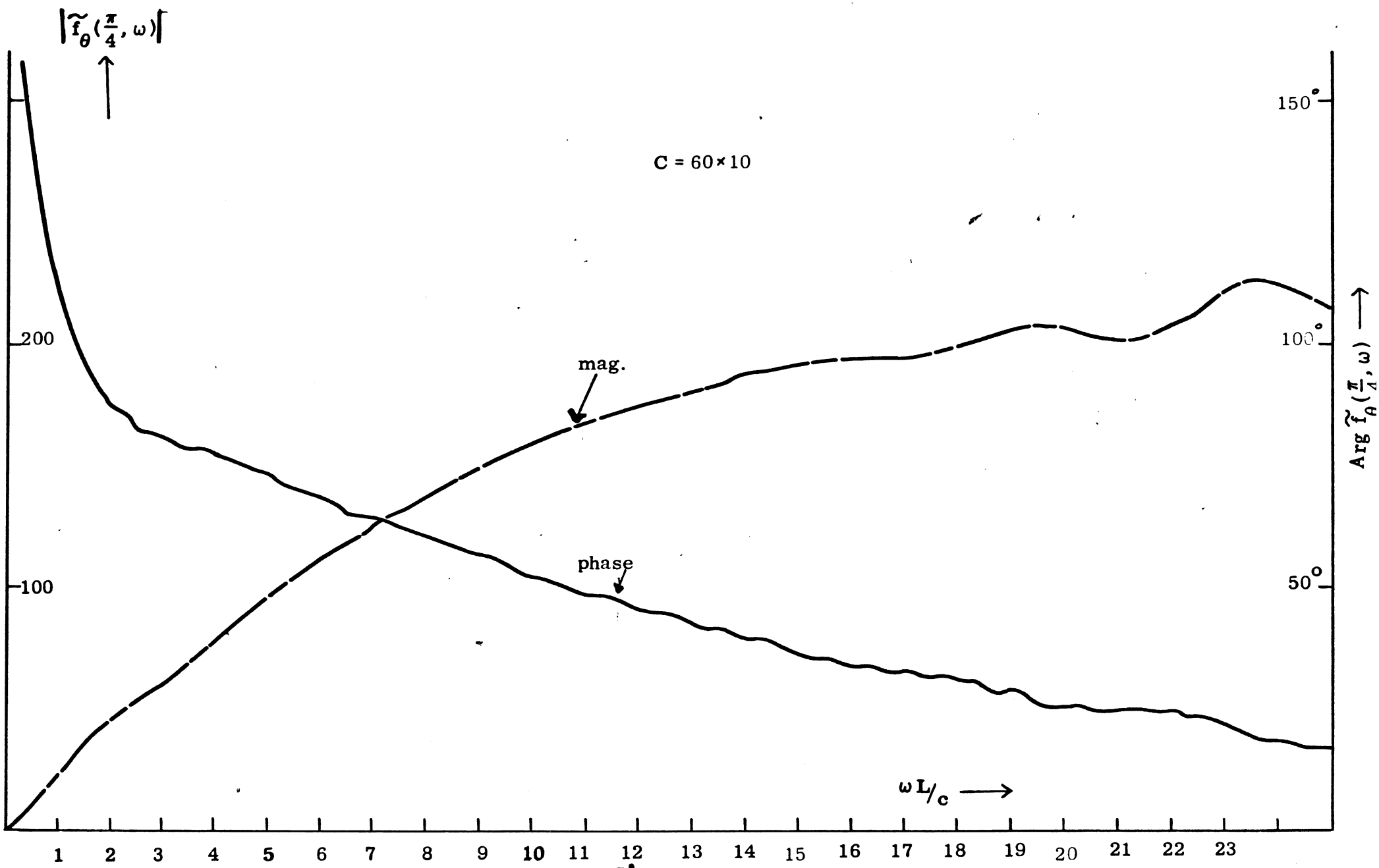

FIG. 13d: Magnitude and phase of the transfer function $\tilde{f}_\theta(\pi/4, \omega)$ of the loaded antenna in the direction $\theta = \pi/4$ as function of $kL(= \omega L/c)$ for different loading. C = 60 x 10.

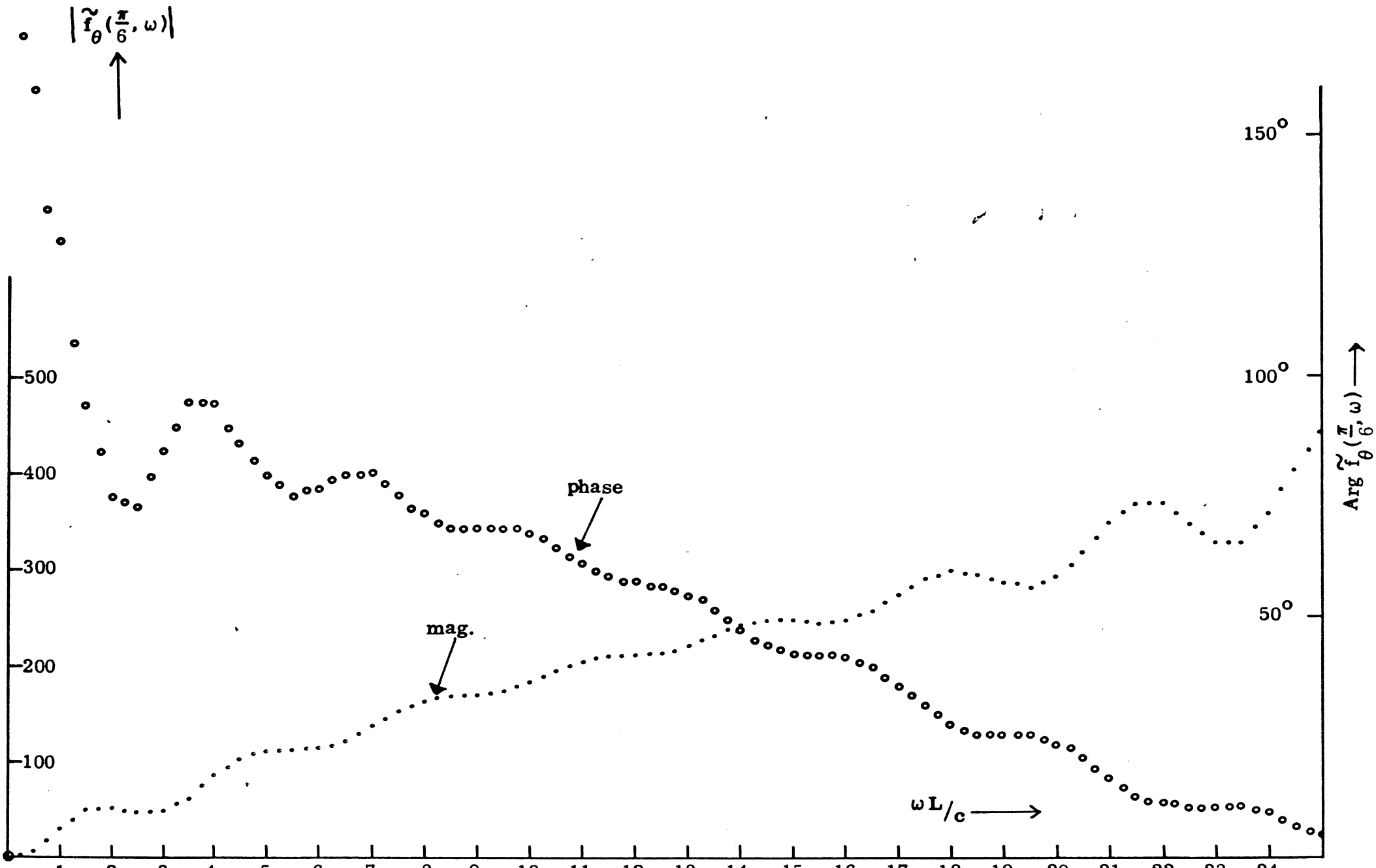

FIG. 14a: Magnitude and phase of the transfer function $\tilde{f}_\theta(\pi/6, \omega)$ of the loaded antenna in the direction $\theta = \pi/6$ as function of kL (= $\omega L/c$) for different loading. C = 60 x 4.

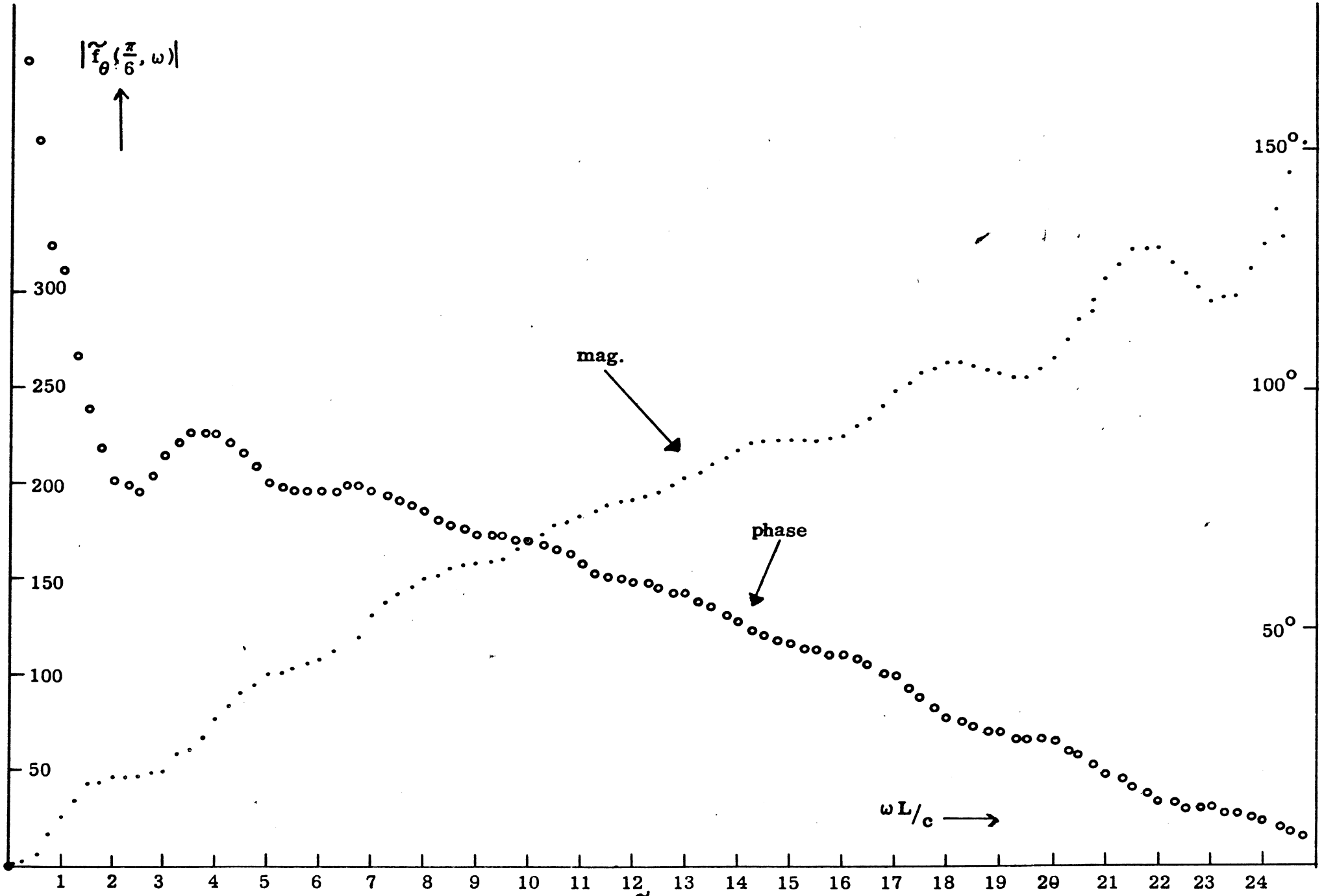

FIG. 14b: Magnitude and phase of the transfer function $\tilde{f}_\theta(\pi/6, \omega)$ of the loaded antenna in the direction $\theta = \pi/6$ as function of kL ($= \omega L/c$) for different loading. C = 60 x 5.

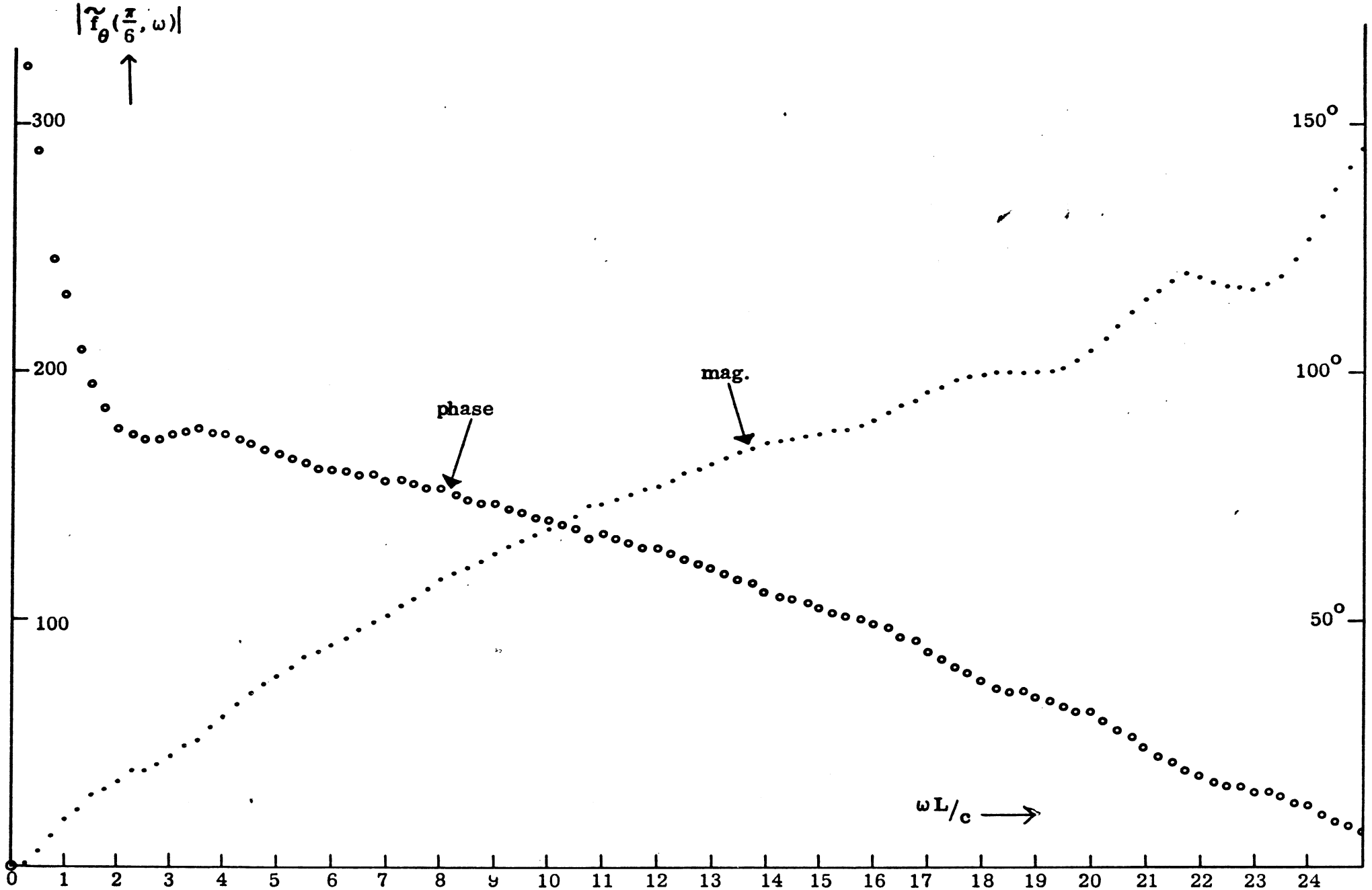

FIG. 14c: Magnitude and phase of the transfer function $\tilde{f}_\theta(\pi/6,\omega)$ of the loaded antenna in the direction $\theta = \pi/6$ as function of kL ($= \omega L/c$) for different loading. C = 60 x 8.

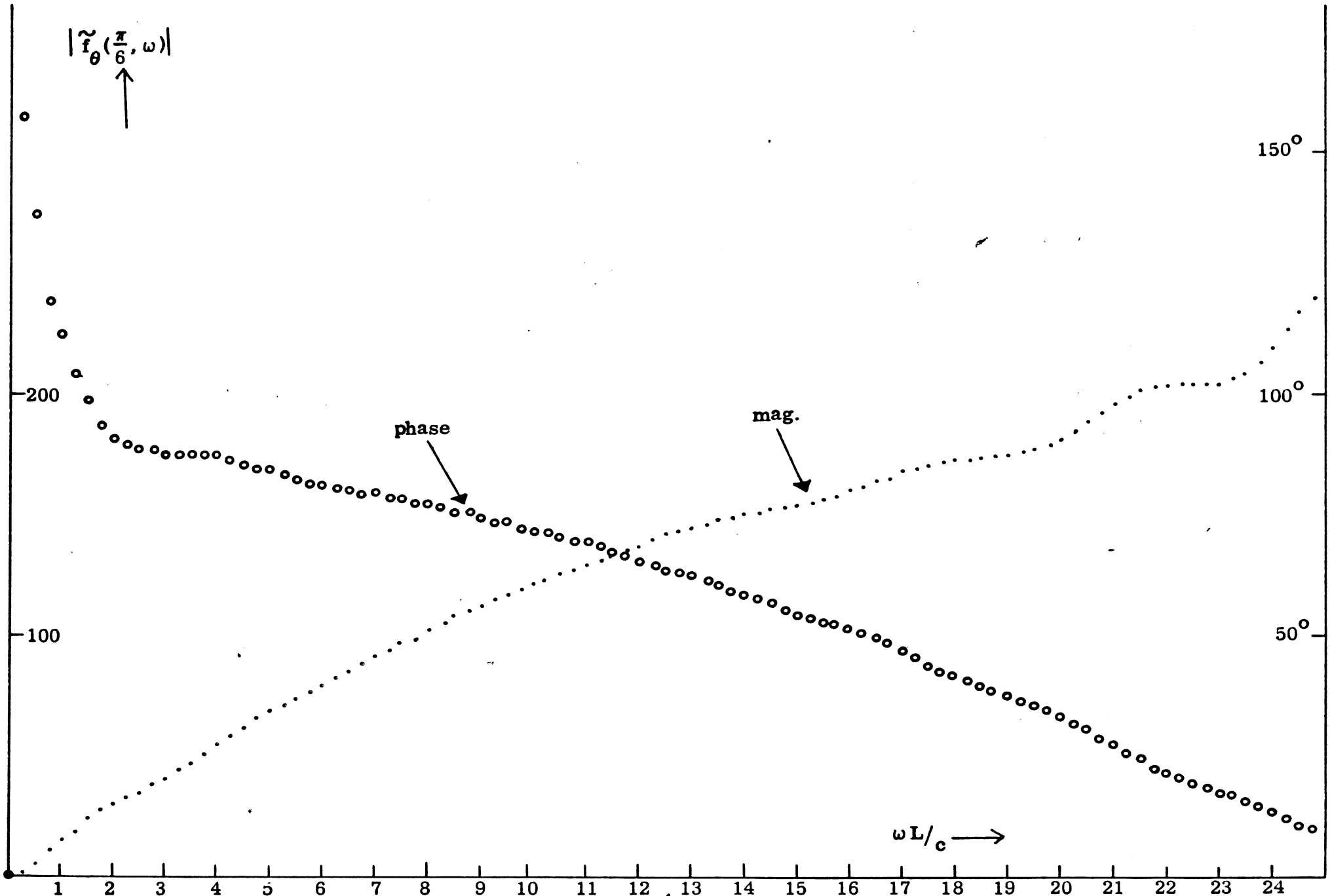

FIG. 14d: Magnitude and phase of the transfer function $\tilde{f}_\theta(\pi/6, \omega)$ of the loaded antenna in the direction $\theta = \pi/6$ as function of kL (= $\omega L/C$) for different loading. C = 60 x 10

obtained by using Fast Fourier inversion technique.

10.1 Spectral Density $\tilde{e}_\theta(\theta, \omega)$ and the Time Domain Solution $e_\theta(\theta, t)$ of the Radiated Field Excited by Gaussian Type Pulse

In this section, results are given for the spectral density $\tilde{e}_\theta(\theta, \omega)$ and the time domain solution $\tilde{e}_\theta(\theta, t)$ excited by a Gaussian pulse input. The form of the input pulse and its Fourier transform are given by Eqs. (10 A) and (11 A). For the time domain results shown here, the antenna length is taken to be $L = 1$ meter. This implies that the transit time on the antenna for centerfed case is $\tau = L/c = 3.33$ nanosecond. The radius a of the antenna element is chosen such that $\Omega = 2\,\ell n\,\frac{2L}{a} = 11.5$ in all cases.

The spectral density $\tilde{e}_\theta(\theta, \omega)$ of the radiated waveform shown here has been obtained by multiplying the transfer function of the antenna by the Fourier spectrum density function of the input signal. The waveform $e_\theta(\theta, t)$ of the radiation field produced by the antenna excited by the Gaussian signal has been obtained by numerically carrying out the integral in Eq. (8) with the aid of Fast Fourier inversion technique.

The results shown here have been calculated in the directions $\theta = \pi/2$, $\pi/3$, $\pi/4$ and $\pi/6$ from the antenna, where $\theta = \pi/2$ corresponds to the broadside direction. Three different values of the width of the Gaussian pulse have been considered for $\theta = \pi/2$, while only a narrow pulse has been obtained for the other directions. These pulses are chosen such that the spectral density will converge to zero at high frequencies. Four different values of the loading constant are used in each case. Figs. 15-17 show $|\tilde{e}(\pi/2, \omega)|$ versus kL and $e_\theta(\pi/2, t)$ versus t for these cases with $\sigma = 0.471$ n sec., 1 n sec., 3.33 n sec. respectively. From the frequency domain results, we observe that for a wider pulse only the low frequency portion of the transfer function is responsible for the overall response. For example, when $\sigma = 3.33$ n sec., we only have to consider the frequency spectrum up to $kL = 3.5$ as shown in Fig. 17. For a narrow pulse, a wider frequency domain of the antenna transfer function has to be considered. However, if the width of the pulse is too narrow, then the computing time re-

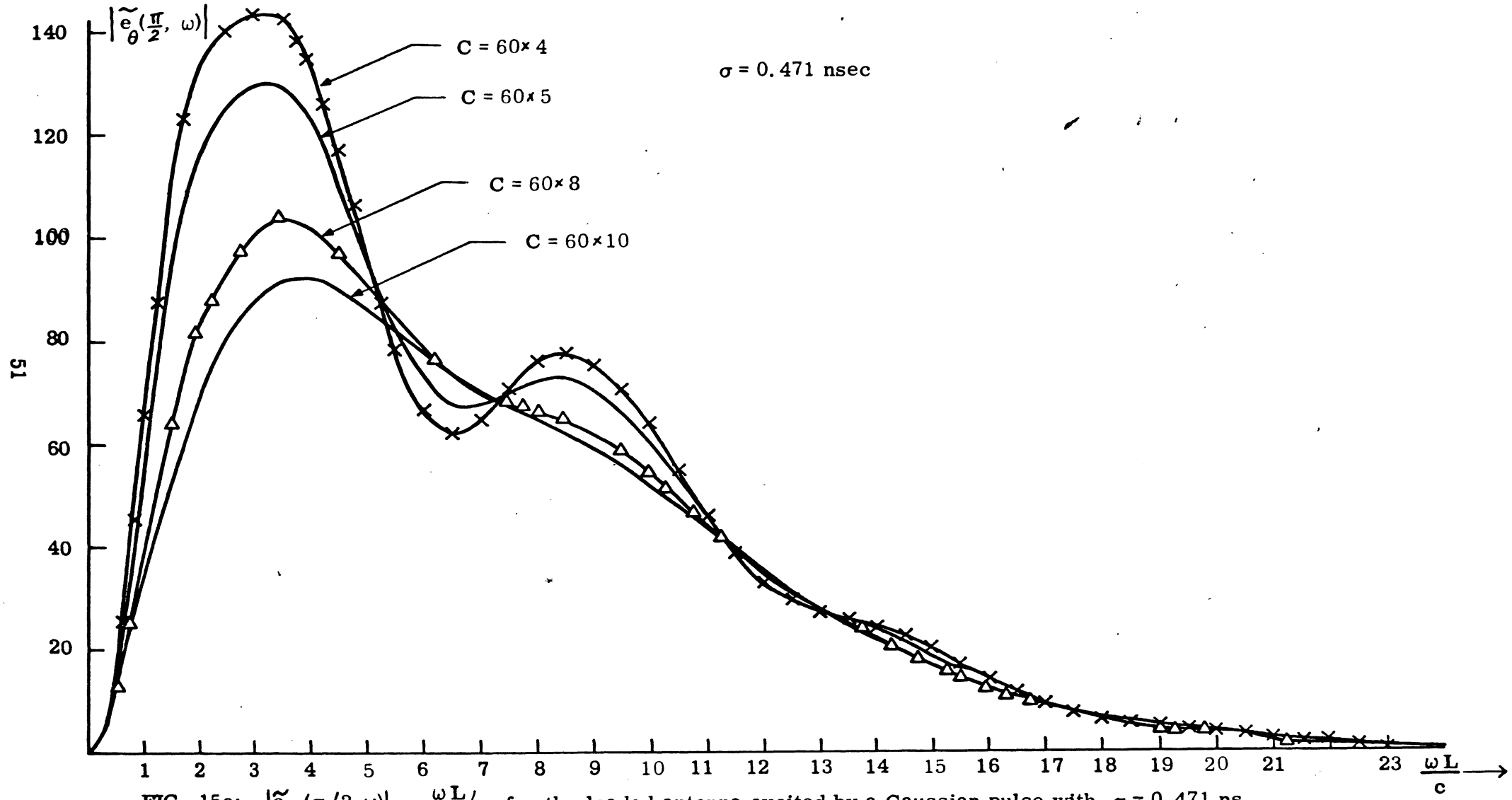

FIG. 15a: $|\tilde{e}_\theta(\pi/2, \omega)|$ vs $^{\omega L}/_{c}$ for the loaded antenna excited by a Gaussian pulse with $\sigma = 0.471$ ns.

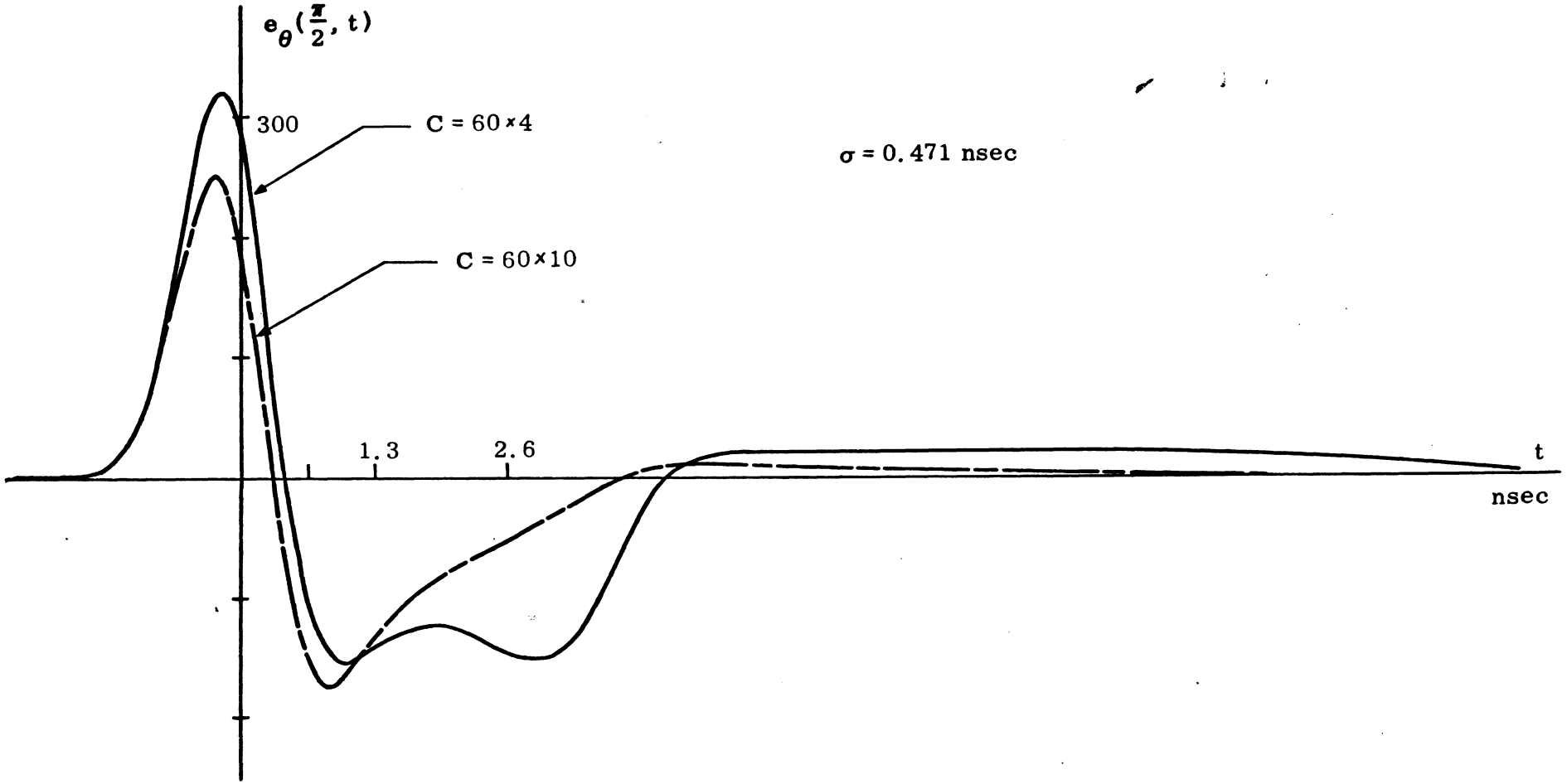

FIG. 15b: $e_\theta(\pi/2, t)$ vs t for the loaded antenna excited by a Gaussian pulse with $\sigma = 0.471$ ns.

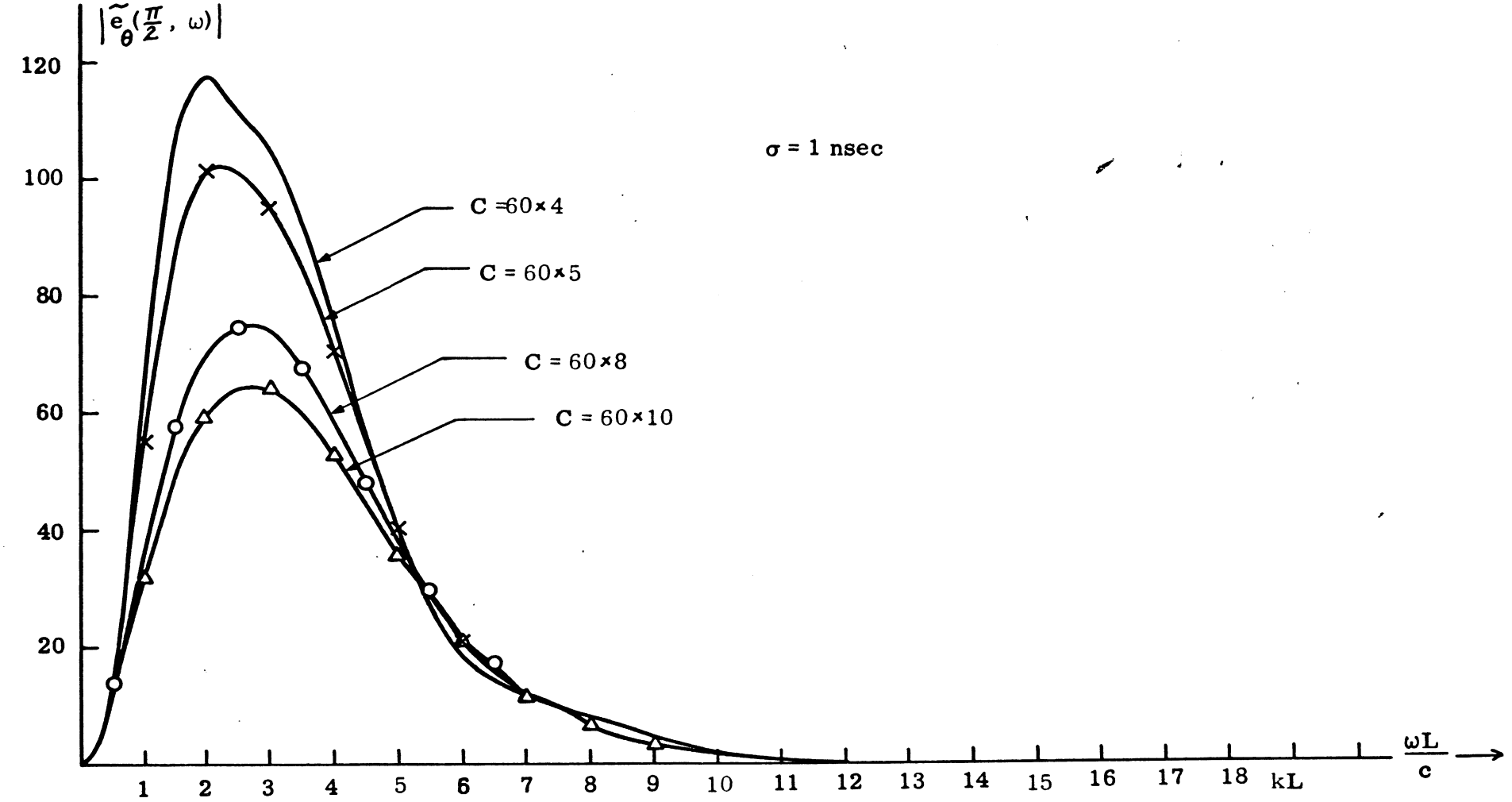

FIG. 16a: $|e_\theta(\pi/2, \omega)|$ vs $\omega L/c$ for the loaded antenna excited by a Gaussian pulse. σ = 1 ns.

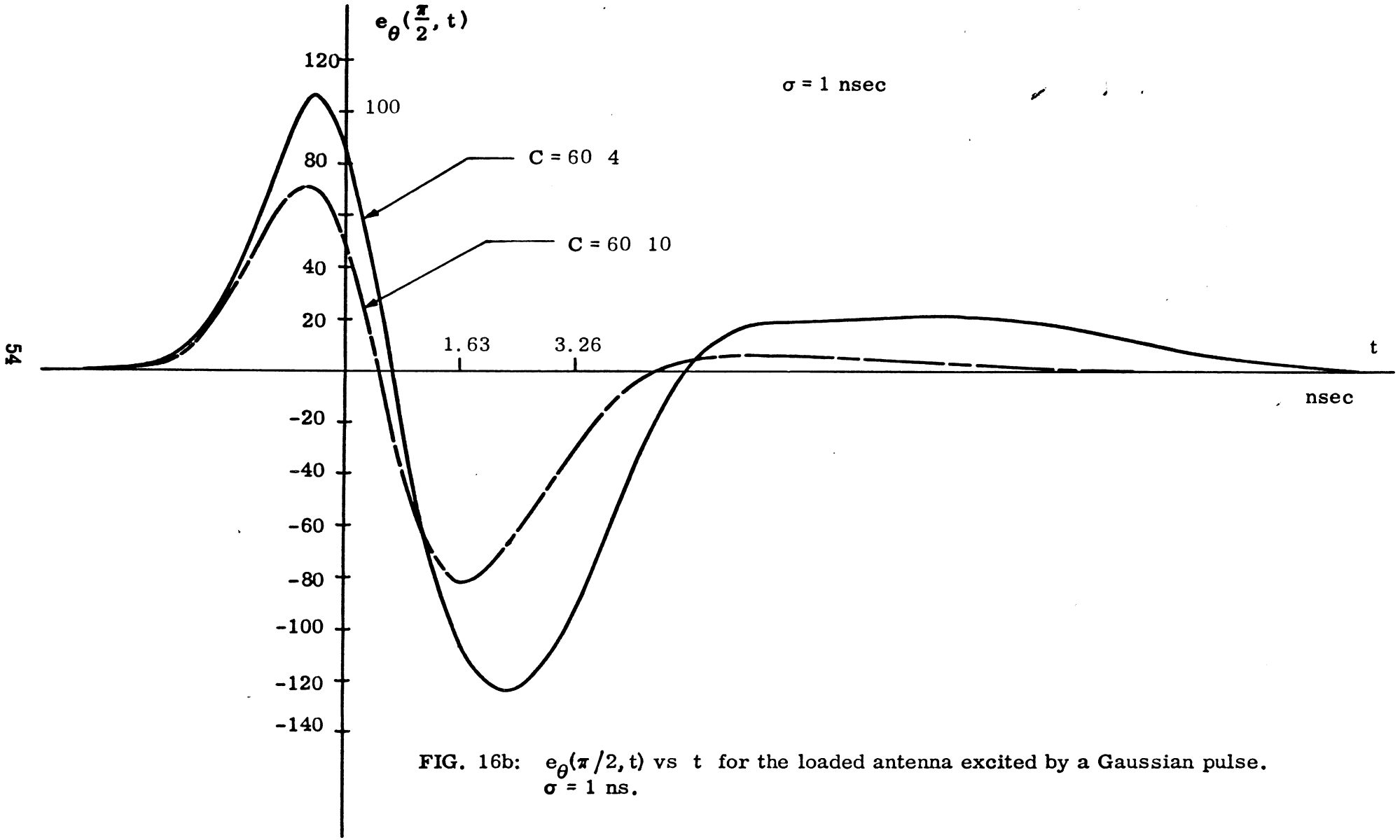

FIG. 16b: $e_\theta(\pi/2, t)$ vs t for the loaded antenna excited by a Gaussian pulse. σ = 1 ns.

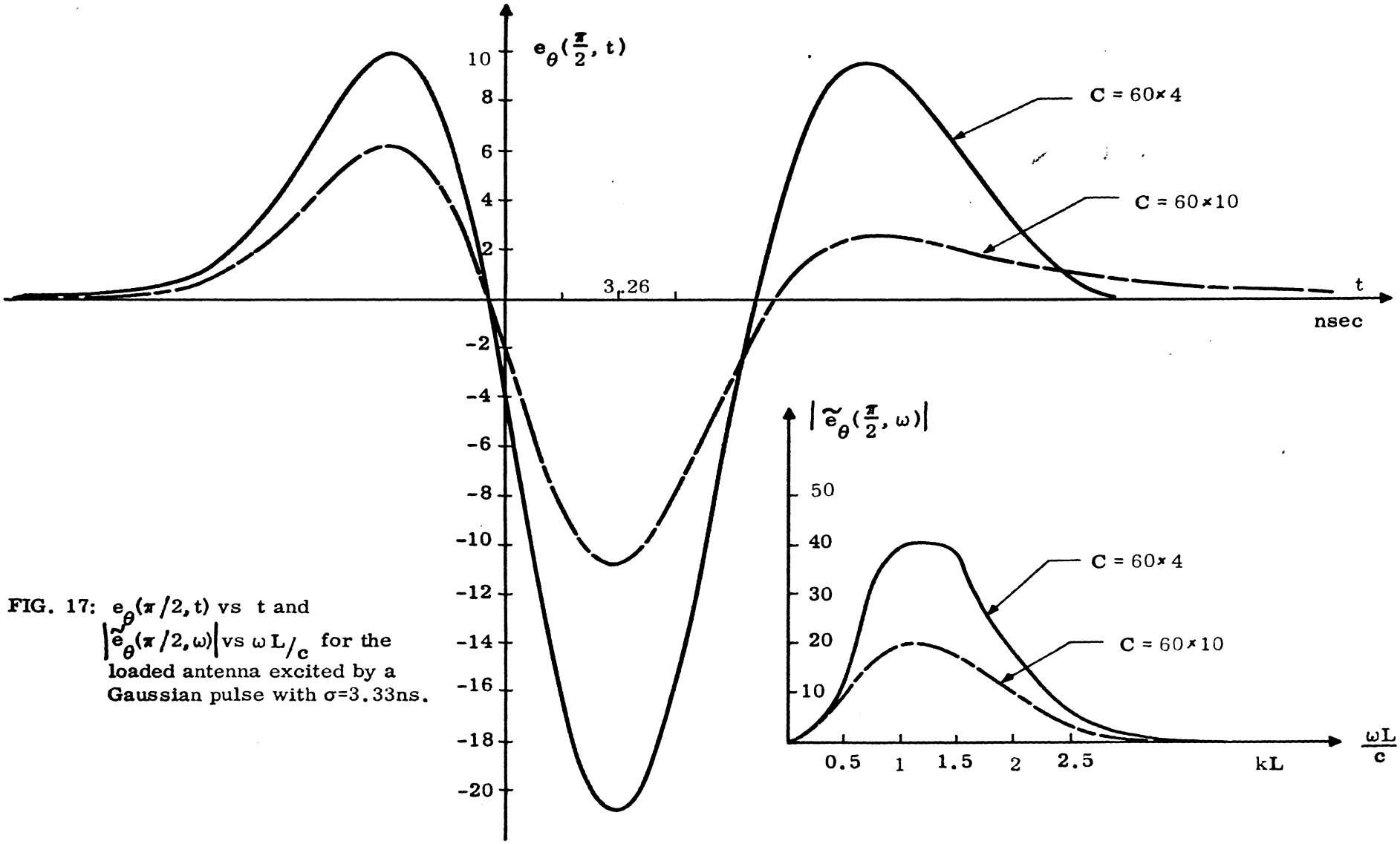

FIG. 17: $e_\theta(\pi/2, t)$ vs t and $\left|\tilde{e}_\theta(\pi/2, \omega)\right|$ vs $\omega L/c$ for the loaded antenna excited by a Gaussian pulse with σ=3.33ns.

quired becomes excessive. For practical consideration of the computing time, we we have chosen $\sigma = 0.471$ n sec. such that the upper frequency spectrum limit corresponds to $kL = 25$.

Fig. 15(a) shows $|e_\theta(\pi/2, \omega)|$ for $\sigma = 0.471$ n sec. For values of $C = 60 \times 4$ and $C = 60 \times 5$, the ringing phenomenon enters the picture. For C exceeds 60×8 the ringing disappears.

From the time domain results shown in Fig. 15(b), it appears that the initial part of the waveform represents predominantly the time derivative of the input Gaussian pulse. The general shape of the waveform depends on the radio σ/τ as expected. It is also seen that after the second zero crossing, $e(\pi/2, t)$ remains positive for all positive values of t and the magnitude decreases with the increasing C of the resistive loading.

Corresponding results are shown in Figs. 18-20 for three other directions with $\sigma = 0.471$ n sec. and for four different resistive loading. The general characteristics are similar to those discussed above. Due to the difference of the path length, the reflection occurs at different frequencies $|\tilde{e}_\theta(\theta, \omega)|$. The strength of the far field is maximum at $\theta = \pi/2$ and decreases as θ deviates from the broadside direction. In every case, the effect of loading in general reduces or eliminates the ringing.

10.2 Spectral Density $\tilde{e}_\theta(\theta, \omega)$ and the Time Domain Solution $e_\theta(\theta, t)$ of the Radiated Field Excited by a Gamma Pulse

In this section, we consider an input voltage function represented by a Gamma pulse. The equations which define this pulse and its transform are given by Eqs. (10B) and (11B). Unlike the Gaussian pulse, the Gamma pulse is defined here for positive values of t only.

The spectral density $\tilde{e}_\theta(\theta, \omega)$ shown here, again, has been obtained by multiplying the transfer function of the antenna with the Fourier Spectrum of the input signal. Then Fast Fourier inversion technique is used as before.

The results shown in Figs. 22-25, correspond to one particular pulse width

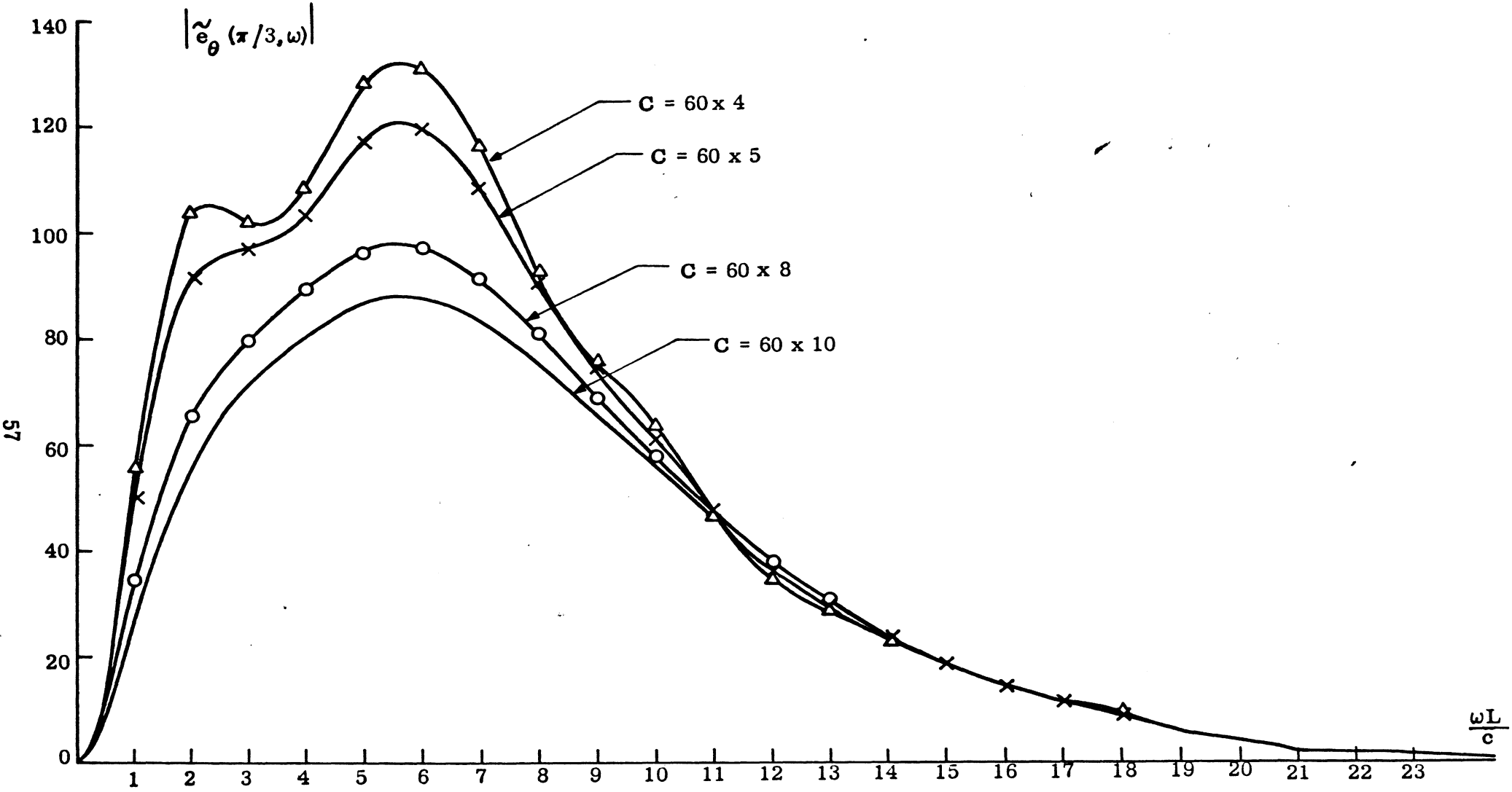

FIG. 18a: $|\tilde{e}_\theta(\pi/3,\omega)|$ vs $\omega L/c$ for the loaded antenna excited by a Gaussian pulse with $\sigma = 0.471$ ns.

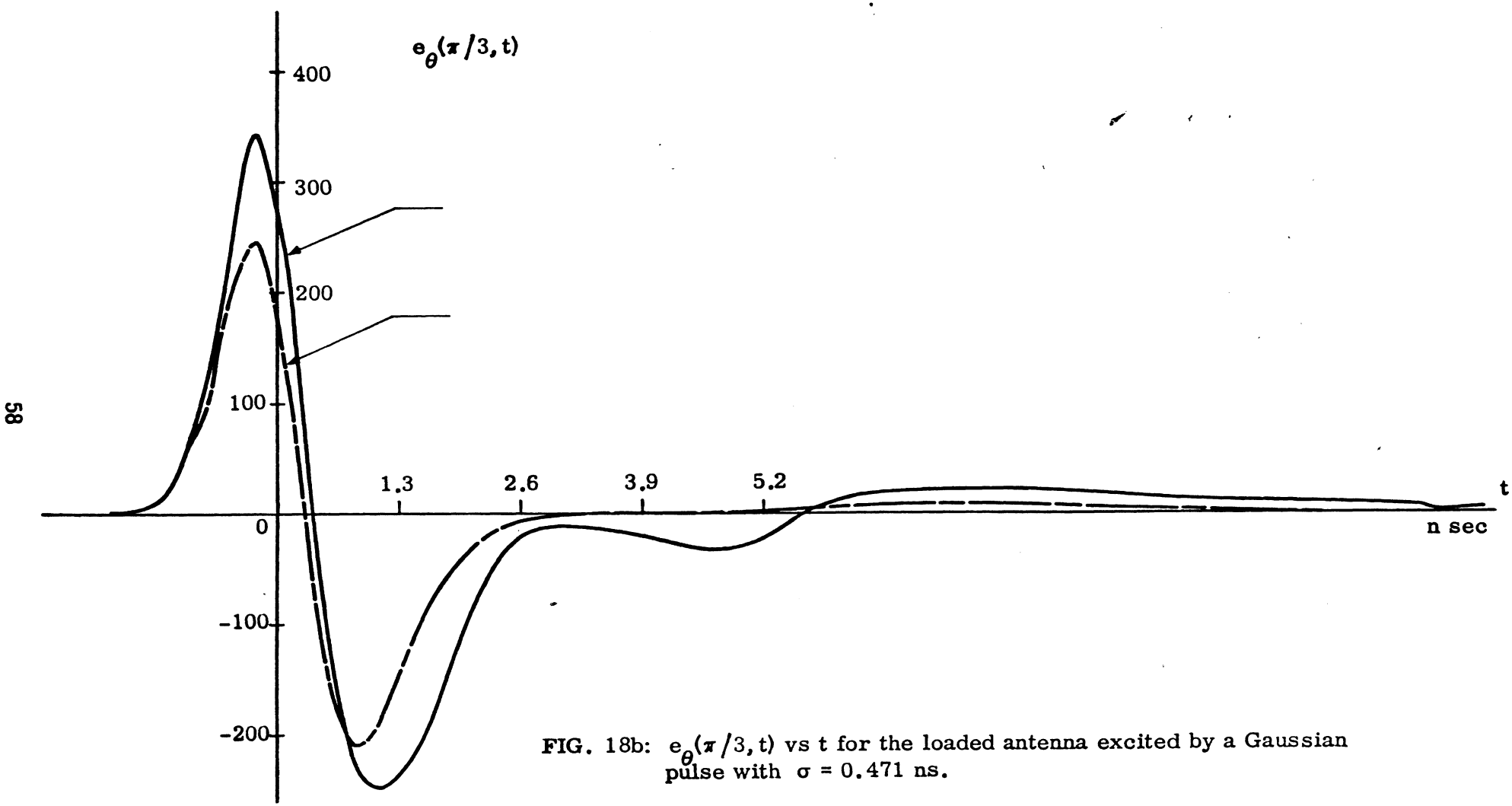

FIG. 18b: $e_\theta(\pi/3, t)$ vs t for the loaded antenna excited by a Gaussian pulse with $\sigma = 0.471$ ns.

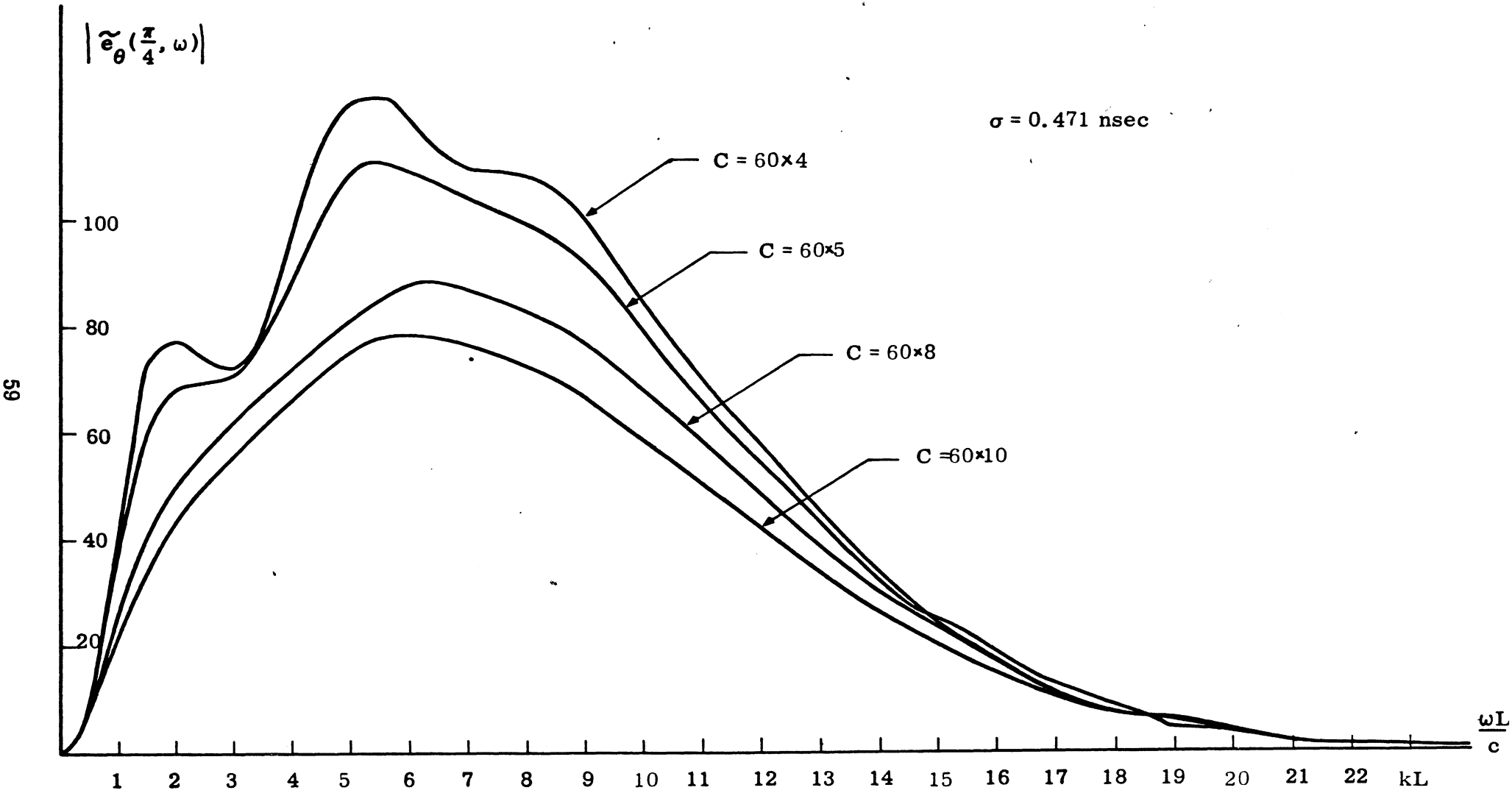

FIG. 19a: $\left|\tilde{e}_\theta(\pi/4,\omega)\right|$ vs $\omega L/c$ for the loaded antenna excited by a Gaussian pulse with $\sigma = 0.471$ ns.

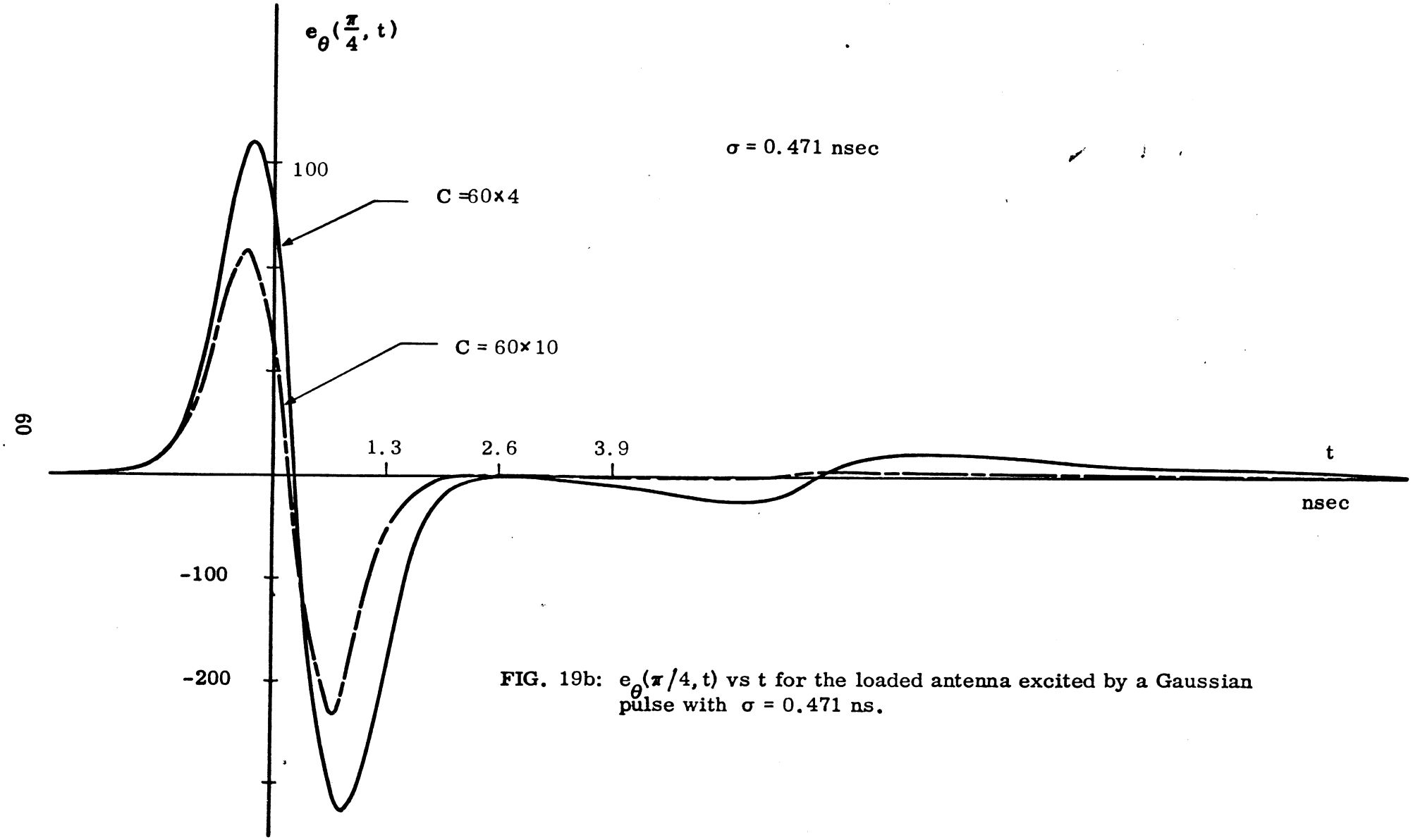

FIG. 19b: $e_\theta(\pi/4, t)$ vs t for the loaded antenna excited by a Gaussian pulse with $\sigma = 0.471$ ns.

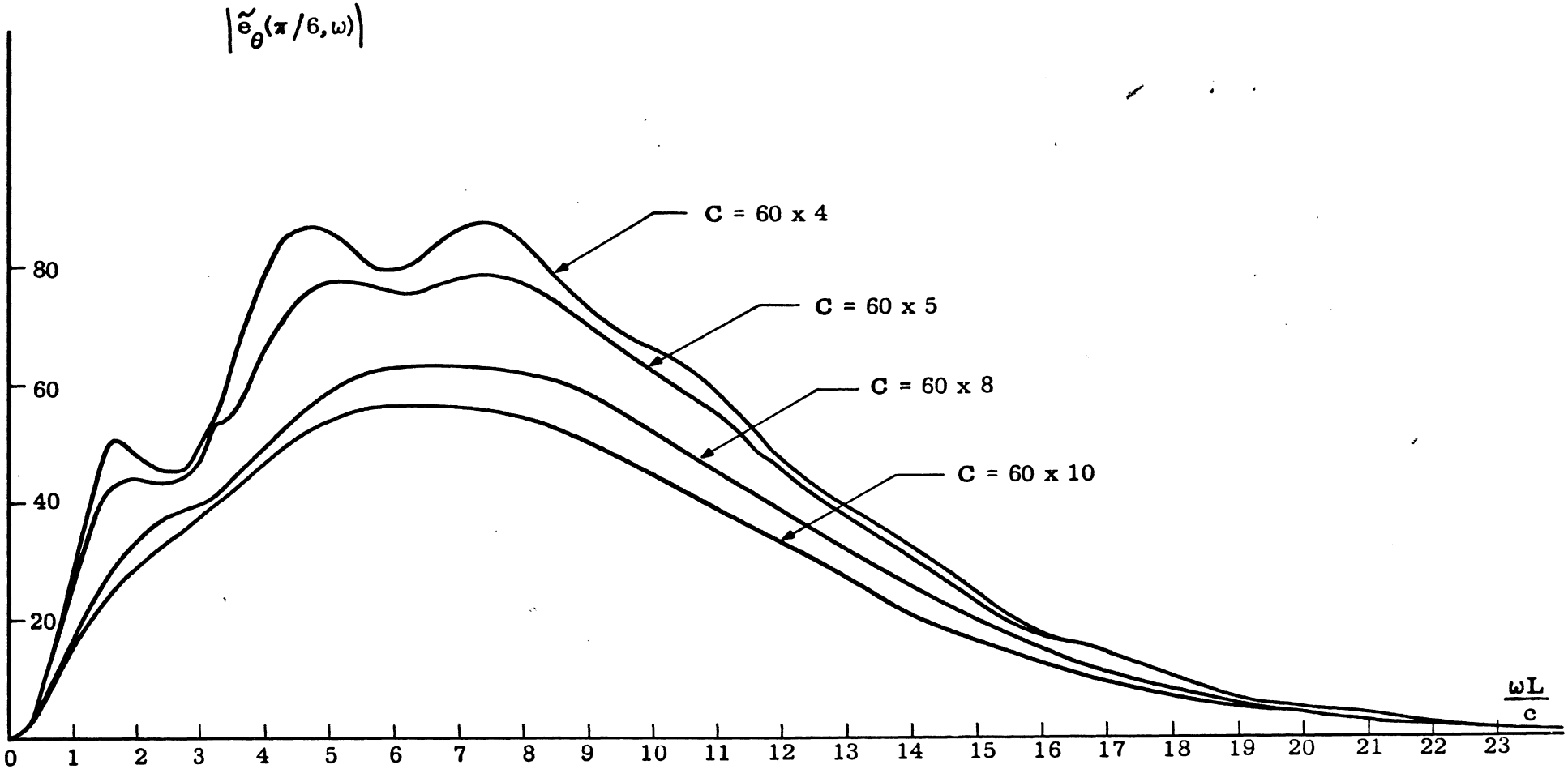

FG FIG. 20a: $|\tilde{e}_\theta(\pi/6,\omega)|$ vs $\omega L/c$ for the loaded antenna excited by a Gaussian pulse with $\sigma = 0.471$ ns.

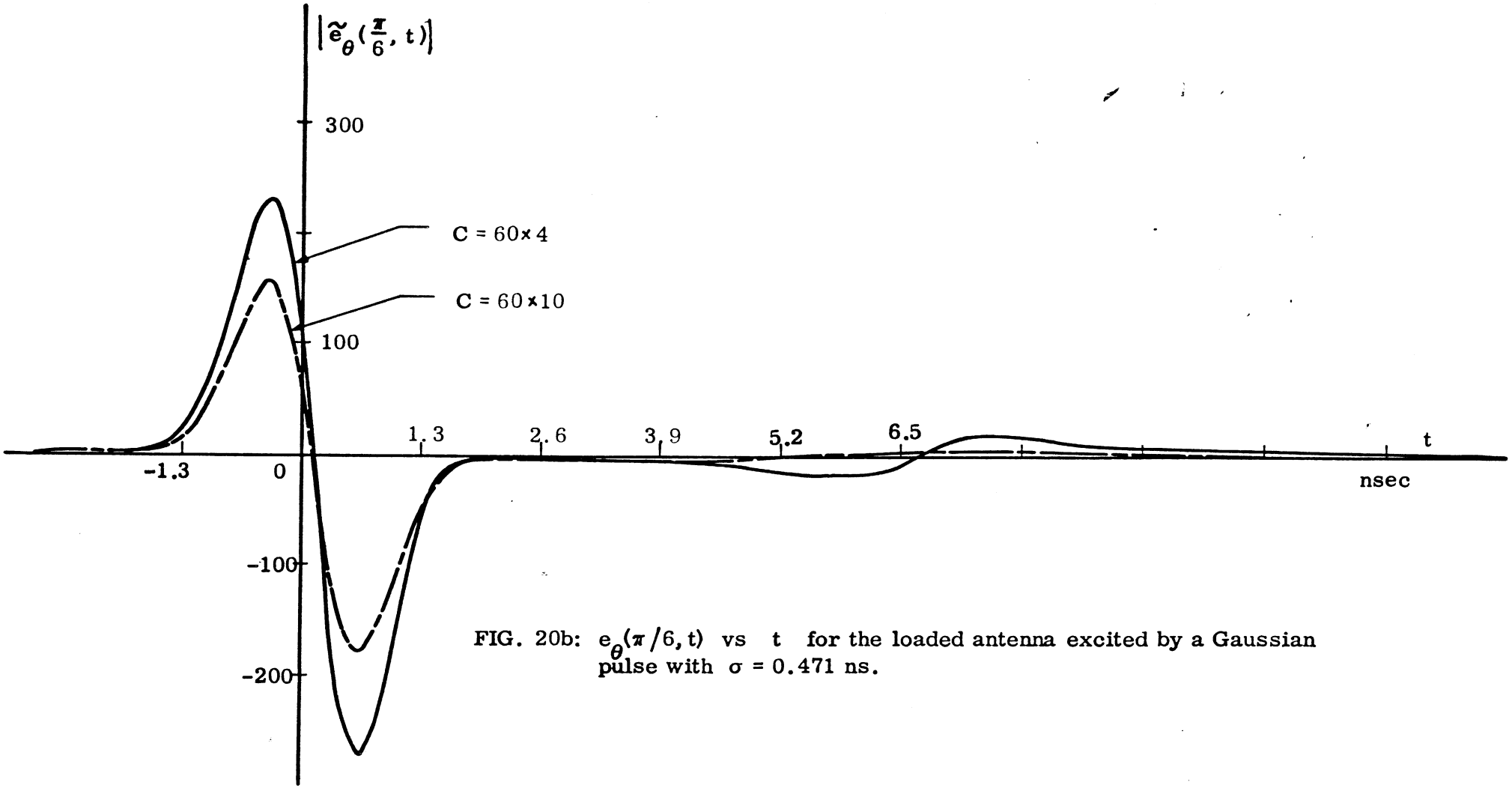

FIG. 20b: $e_\theta(\pi/6, t)$ vs t for the loaded antenna excited by a Gaussian pulse with $\sigma = 0.471$ ns.

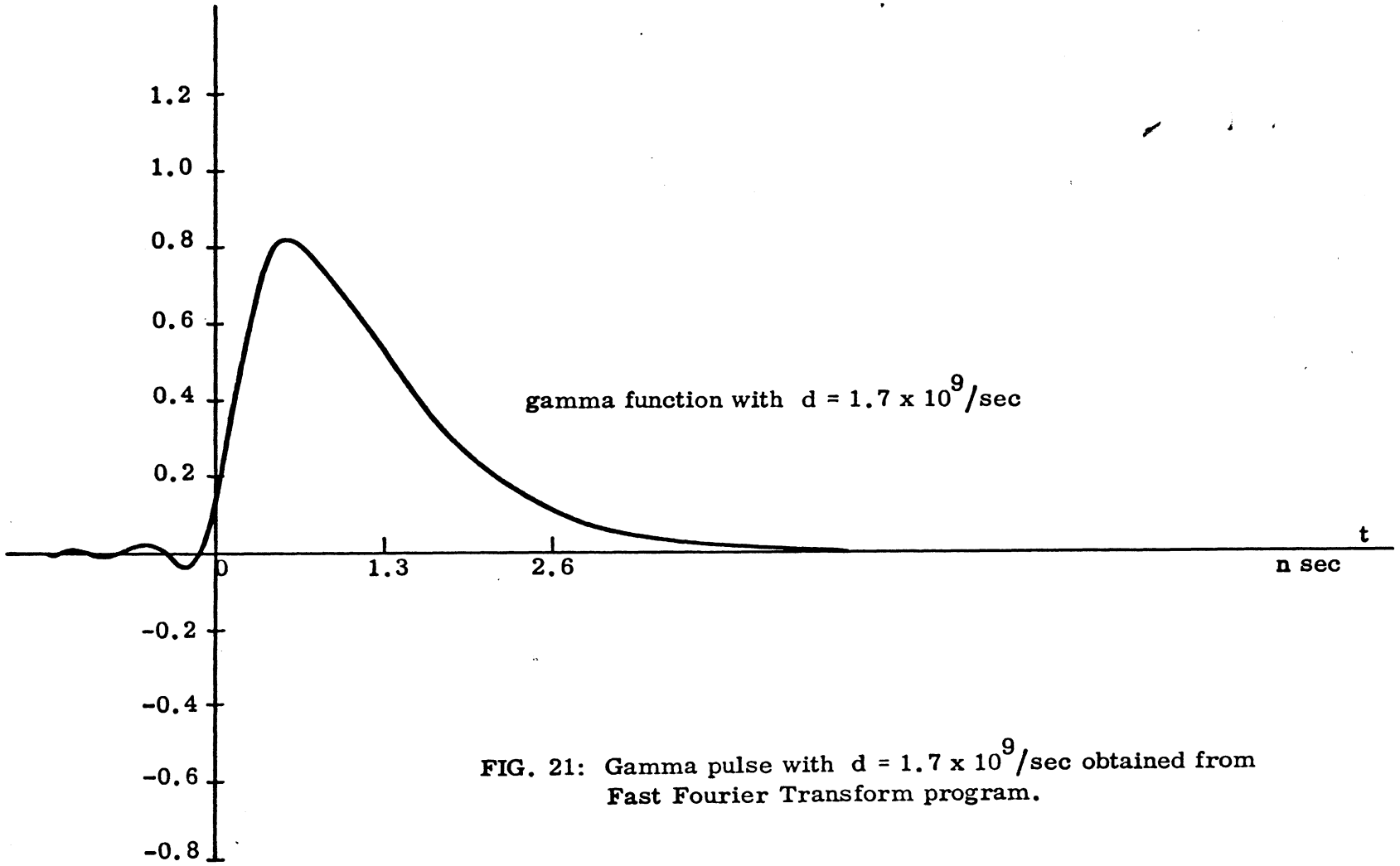

FIG. 21: Gamma pulse with $d = 1.7 \times 10^9$/sec obtained from Fast Fourier Transform program.

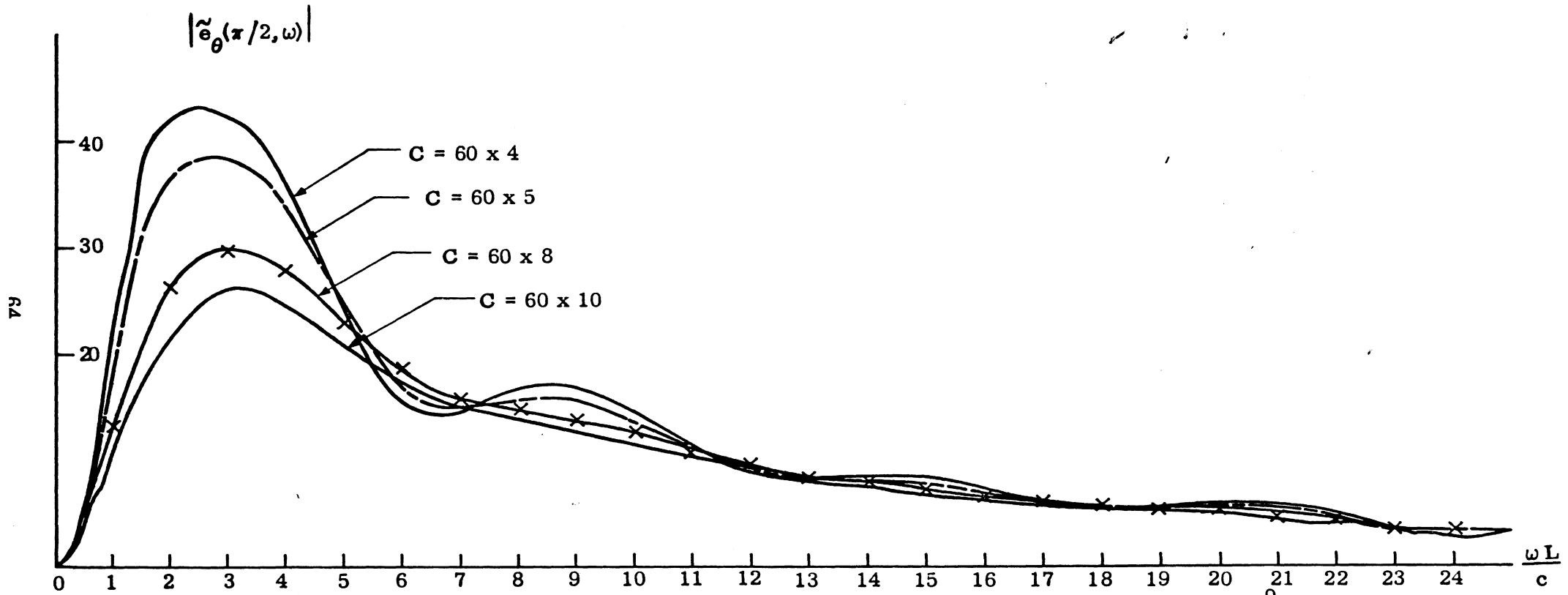

FIG. 22a: $|\tilde{e}_\theta(\pi/2,\omega)|$ vs $\omega L/c$ for the loaded antenna excited by a gamma pulse with $d = 1.7 \times 10^9$/sec.

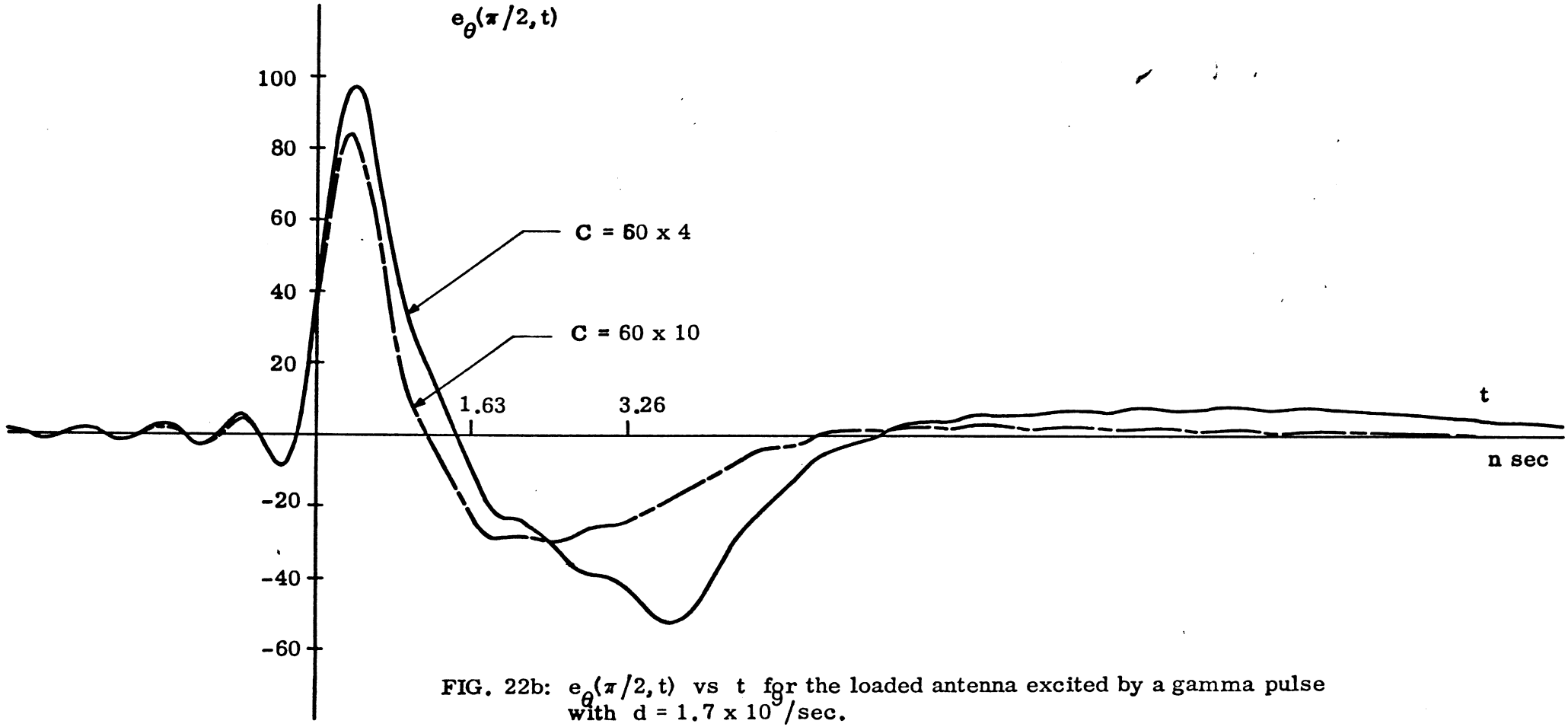

FIG. 22b: $e_\theta(\pi/2, t)$ vs t for the loaded antenna excited by a gamma pulse with $d = 1.7 \times 10^9$/sec.

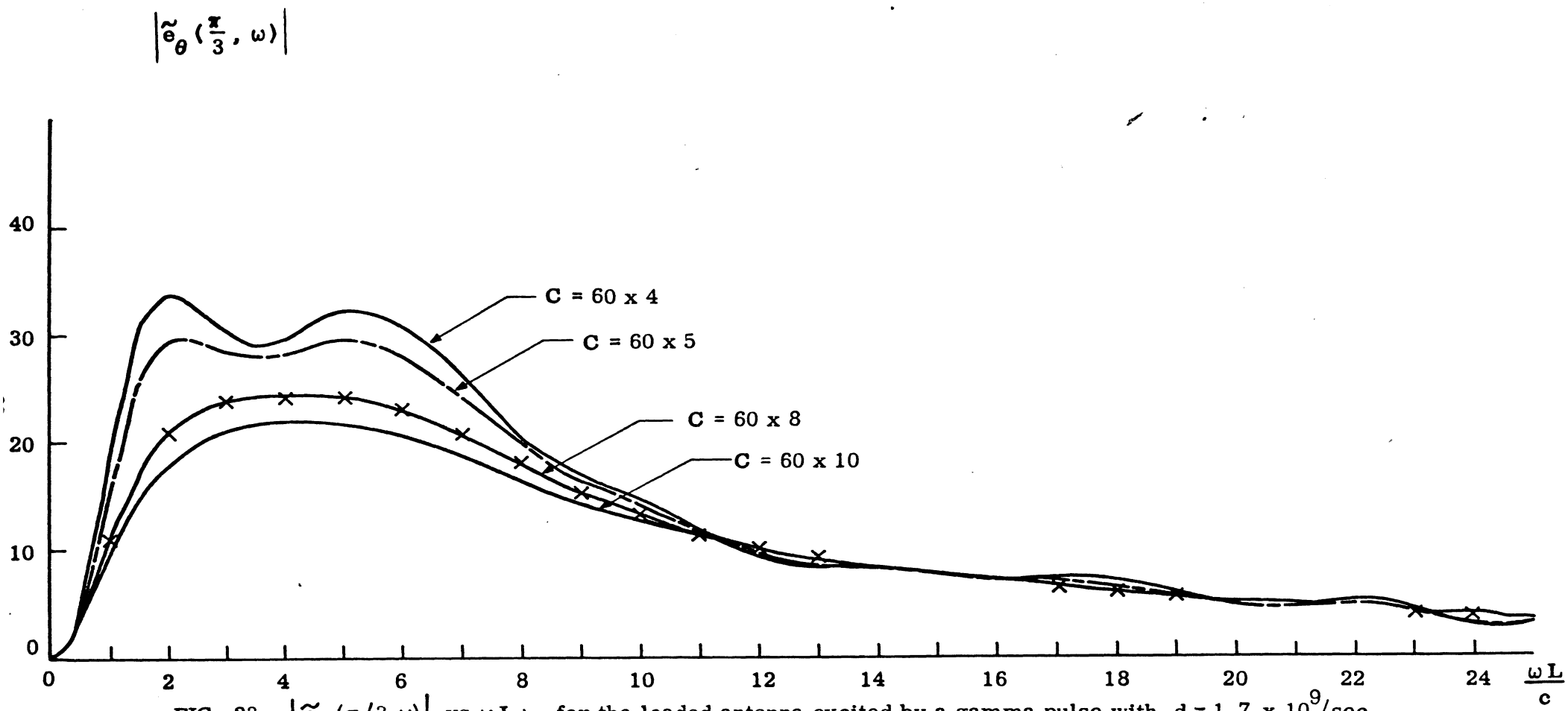

FIG. 23a: $\left|\tilde{e}_\theta(\pi/3, \omega)\right|$ vs $\omega L/c$ for the loaded antenna excited by a gamma pulse with $d = 1.7 \times 10^9$/sec.

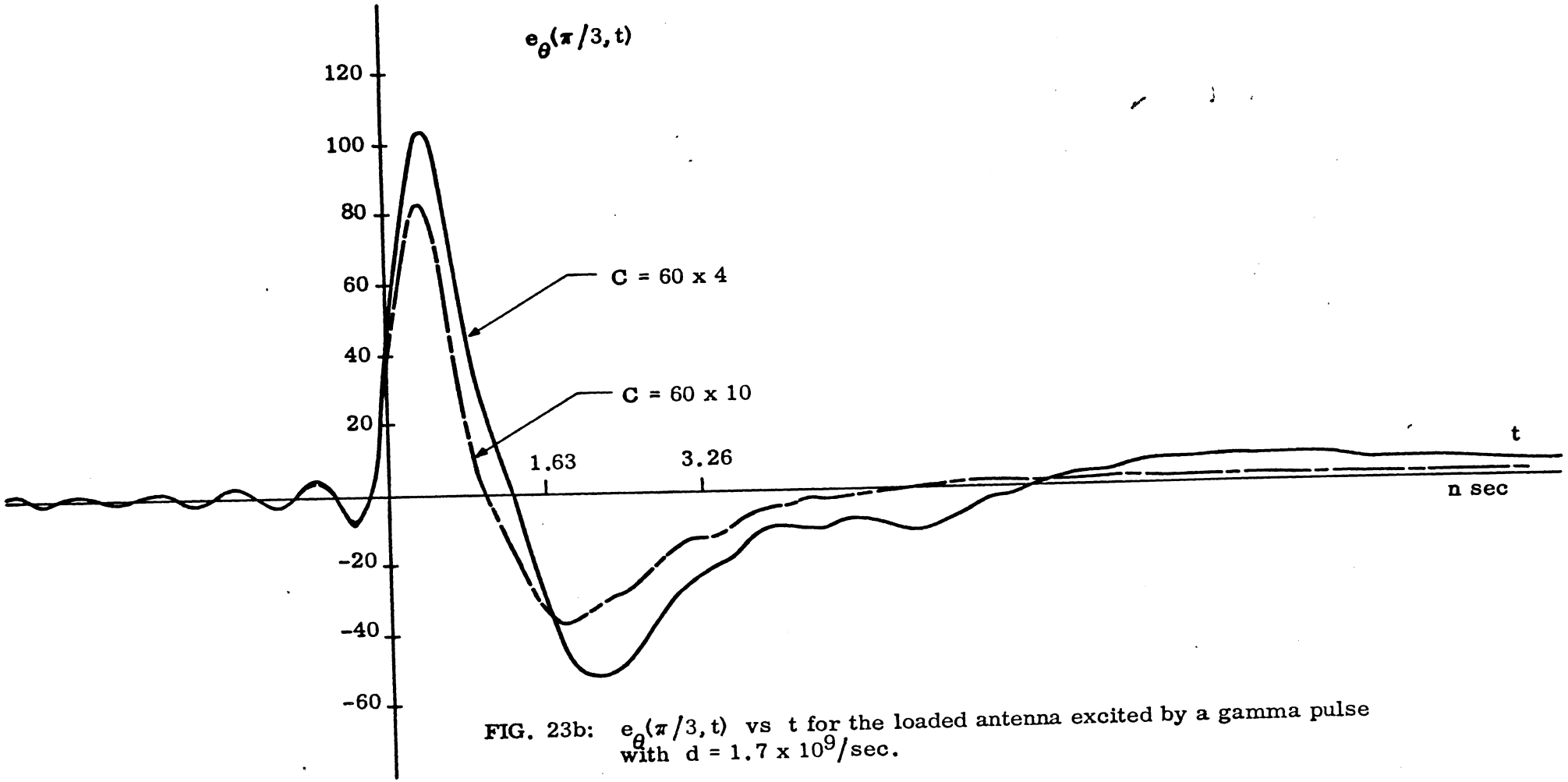

FIG. 23b: $e_\theta(\pi/3, t)$ vs t for the loaded antenna excited by a gamma pulse with $d = 1.7 \times 10^9$/sec.

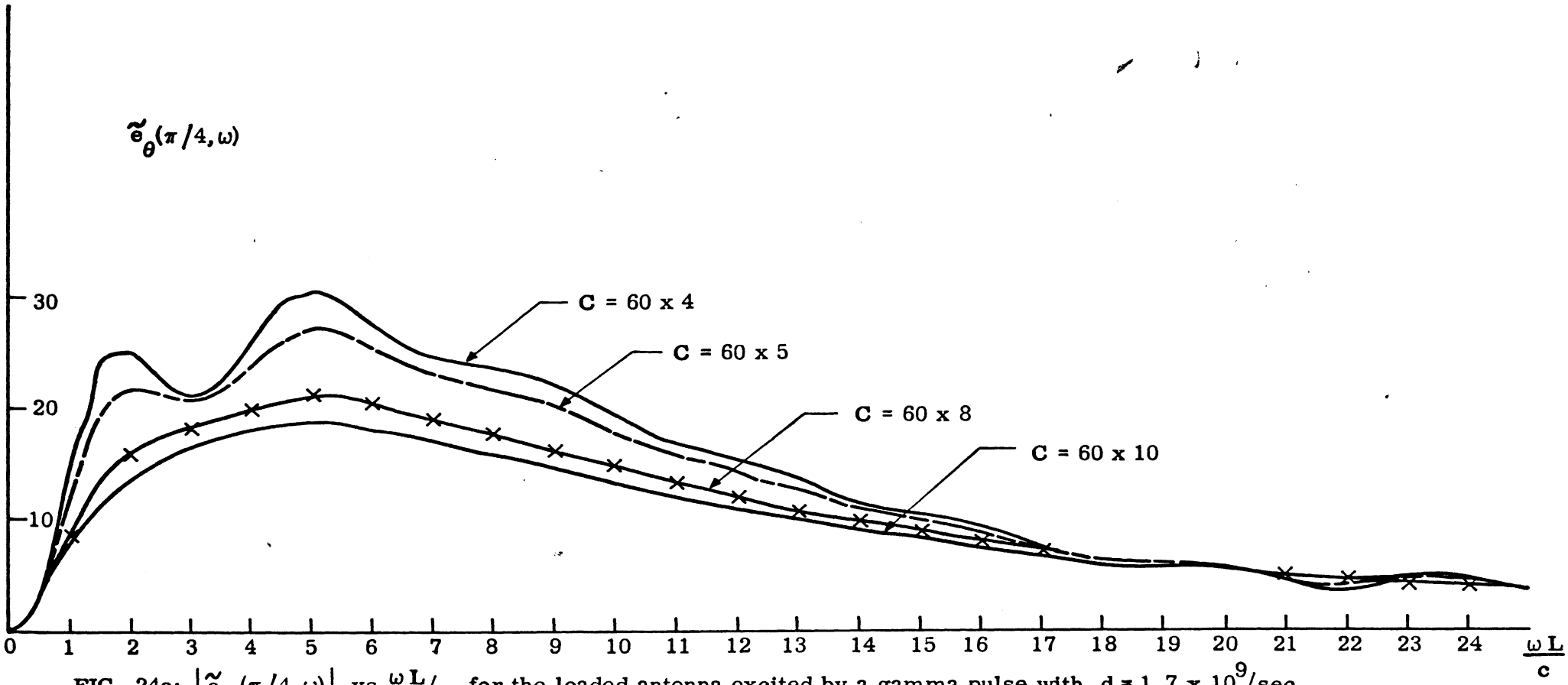

FIG. 24a: $\left|\tilde{e}_\theta(\pi/4,\omega)\right|$ vs $\omega L/c$ for the loaded antenna excited by a gamma pulse with $d = 1.7 \times 10^9$/sec.

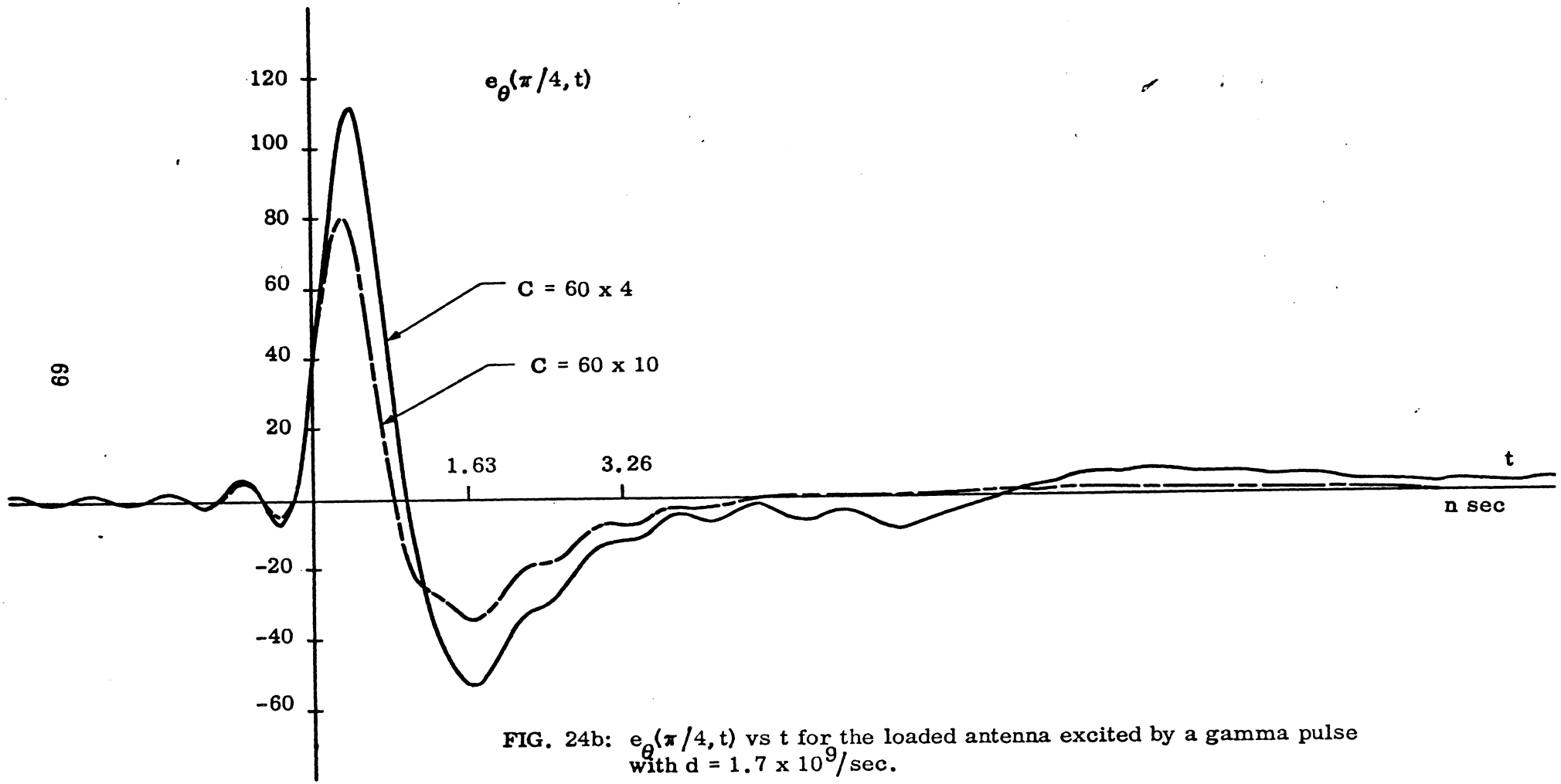

FIG. 24b: $e_\theta(\pi/4, t)$ vs t for the loaded antenna excited by a gamma pulse with d = 1.7×10^9/sec.

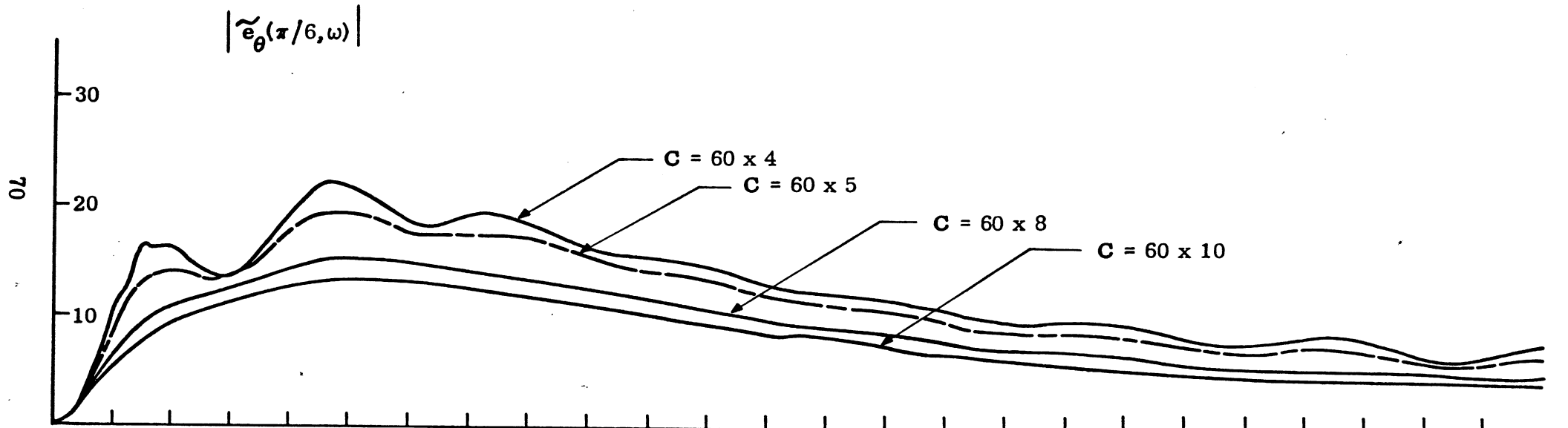

FIG. 25a: $|\tilde{e}_\theta(\pi/6,\omega)|$ vs $\omega L/c$ for the loaded antenna excited by a gamma pulse C = 60 x 4, d = 1.7 x 10^9/sec.

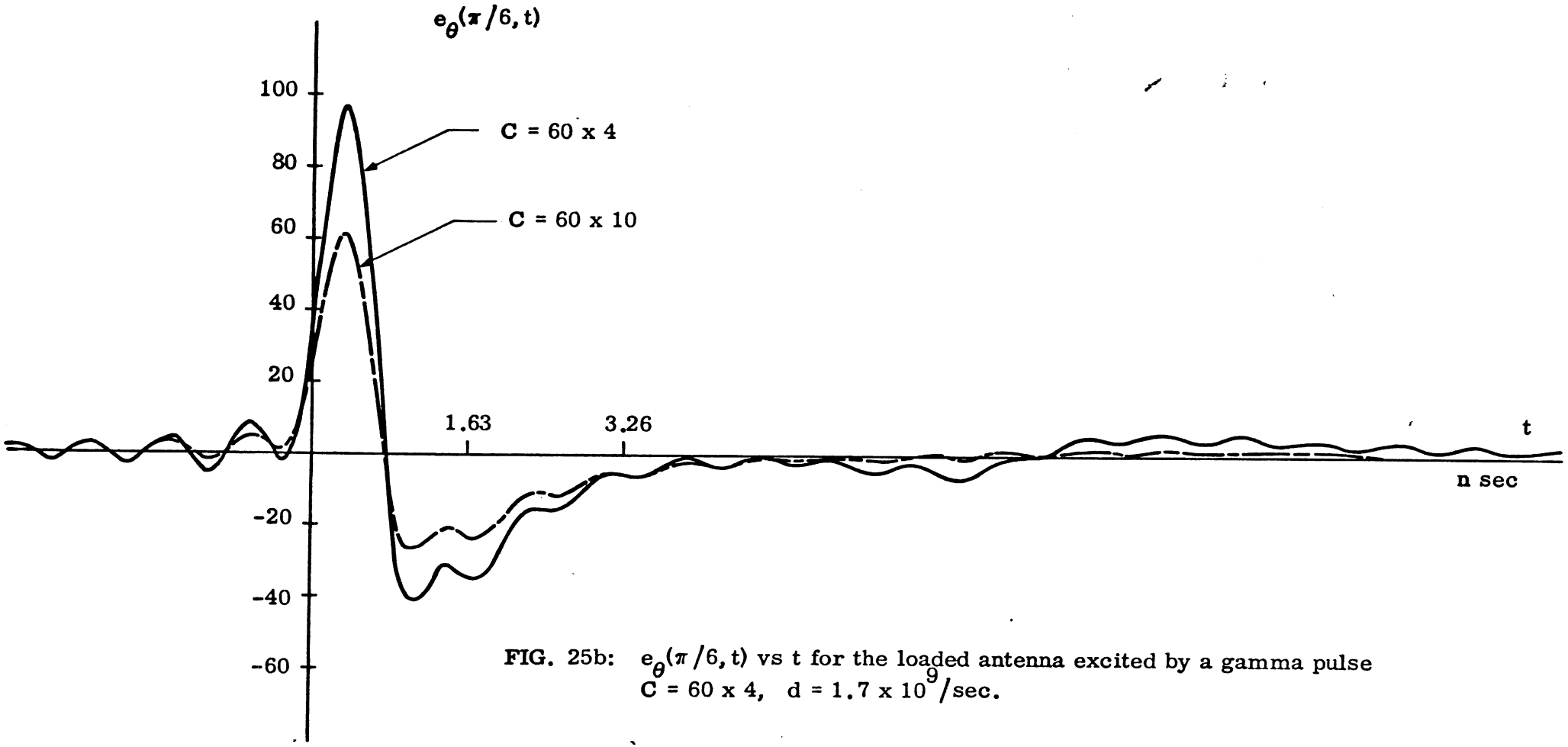

FIG. 25b: $e_\theta(\pi/6, t)$ vs t for the loaded antenna excited by a gamma pulse
C = 60 x 4, d = 1.7×10^9/sec.

at four different directions. For each direction in space, four values of loading have been considered. The width d of the gamma pulse is chosen to be 1.7×10^9 / sec. which approximates the same width as that of a Gaussian pulse with $\sigma = 0.47$. Fig. 21 shows the input gamma pulse reproduced by using the Fast Fourier inversion program. This computation is to show the round-off error involved in the F. F. T. program for sharply rising pulse. The truncation of the high frequency portion of the spectrum also induces error. The error results in the oscillating portion for negative value of t and the shift of the starting point to the left instead of at zero. Similar error would be introduced in computing the time domain solutions based on Gamma pulse input.

Since gamma pulse does not converge to zero as fast as Gaussian pulse, the spectral density shows small oscillation at high frequencies as shown in Figs. 22-25. The truncation of a Gamma pulse also introduces a larger error than that of a Gaussian at the same truncation frequency. Except for these minor variations, the general behavior of the time domain solution presented previously for the Gaussian pulse also applies to the Gamma pulse.

11. CONCLUSION

The waveform of the far-zone field radiated by a non-uniform resistively loaded linear antenna excited by a voltage pulse has been investigated by numerical means. Results have been obtained for a Gaussian pulse with three different pulse width and for one particular Gamma pulse at four directions of observation. Various values of the loading parameter have been considered.

In general, the resultant waveform corresponds to the convolution of the harmonic response and the input signal. The initial portion of the resultant wave however, appears to be proportional to time derivative of the input signal.

The result shows that the amplitude of the current distribution on the harmonically excited antenna is almost linear, being independent of the loading resis-

tance when the latter exceeds certain value. The phase of the current represents the characteristics of a traveling wave. Thus, the analysis of Baum[1] based on the transmission line model appears to be a valid description of the current for a resistively loaded antenna too. Our study also verifies the work of Wu and King[9] who examined the problem only for one particular loading at a single frequency. In the broadside direction, the waveform exhibits a compression in pulse width as the loading resistance is increased. No general trend is observed in other directions.

For a Gaussian pulse, our numerical results check very well with the analytical solution which indicates that the computing program has been properly executed. To simulate practical problems, we have considered the excitation to be presented by Gamma pulse. In general, much of the result obtained using the Gaussian pulse also applies to the Gamma pulse. One significant difference concerns the computing error involved in the two cases. For a Gamma pulse, the truncation error appears to be prominent. As a whole, it appears that a "critical" damping can be achieved when the loading resistance attains a certain sufficiently high value, corresponding to $C \geq 60 \times 10$.

In the Appendix, we have attached a computing program used in this work. The program with some minor changes can be applied to any loading.

12. REFERENCES

1. Baum, Carl E., (1970), Resistively Loaded Radiating Dipole Based on a Transmission-Line Model for the Antenna, AFWL EMP 1-6, Vol. 6, Note 81, pp. 81-1 - 81-27.

2. Latham, R.W. and K.S.H. Lee, (1969), Pulse Raidation Synthesis by an Infinite Cylindrical Antenna, AFWL EMP 1-5, Vol. 5, Note 73.

3. Latham, R.W. and K.S.H. Lee, (1970), Radiation of an Inffnite Cylindrical Antenna with Uniform Resistive Loading, AFWL EMP 1-6, Vol. 6, Note 83.

4. Bennett, C.L. and A.M. Auckenthaler, (1971), Transient and Time Domain Solutions for Antennas and Scatterers, SRRC-RR-70-61, Sperry Rand Research Center, Sudbury, Massachusetts.

5. Sayre, Edward Paul, (1969), Transient Response of Wire Antennas and Scatterers, Technical Report TR-69-4, Electrical Engineering Department, Syracuse, New York.

6. Taylor, C.D. and T.H. Shumpert, (1971), Electromagnetic Pulse Generation by an Impedance Loaded Dipole Antenna, AFWL EMP 1-8, Vol. 8, Note 104,

7. Shumpert, T.H., (1971), Some Theoretical-Numerical Procedures for the Study of the Impedance Loaded Dipole Antenna, AFWL EMP 1-8, Vol. 8, Note 105.

8. Sengupta, D.L., Y.P. Liu and C.T. Tai, (1972), Waveforms Radiated by a Non-Uniformly Loaded Linear Antenna Excited by Gaussian Pulses, The University of Michigan Radiation Laboratory Report No. 010748-3-T (in preparation).

9. Wu, T.T. and R.W.P. King, (1964), The Cylindrical Antenna with Non-Reflecting Resistive Loading, IEEE Trans., AP-13, No. 3, pp. 369-373.

10. Mei, K.K., (1965), On the Integral Equations of Thin Wire Antennas, IEEE Trans., AP-14, No. 3, pp. 374-378.

11. Harrington, R.F., (1968), Field Computation by Moment Methods, The Macmillan Company, New York.

12. King, R.W.P., C.W. Harrison and E.A. Aransen, (1966), The Imperfectly Conducting Cylindrical Transmitting Antenna: Numerical Results, IEEE Trans., AP-14, No. 5, pp. 535-542.

13. Taylor, C.D., (1968), Cylindrical Transmitting Antenna: Tapered Resistivity and Multiple Impedance Loadings, IEEE Trans., AP-16, No. 2, pp. 176-179.

14. Shen, L.C., (1967), An Experimental Study of the Antenna with Non-Reflecting Resistive Loading, IEEE Trans., AP-15, No. 5, pp. 606-611.

13. APPENDIX

COMPUTER PROGRAMS (FORTRAN IV)

1. Programs for $I(z, \omega)$, $\tilde{f}_\theta(\theta, \omega)$, $\tilde{e}_\theta(\theta, \omega)$.

2. Fast Fourier Transform Program for $e_\theta(\theta, t)$.